

# UAV-assisted Online Machine Learning over Multi-Tiered Networks: A Hierarchical Nested Personalized Federated Learning Approach

Su Wang, *Student Member, IEEE*, Seyyedali Hosseinalipour, *Member, IEEE*, Maria Gorlatova, *Member, IEEE*, Christopher G. Brinton, *Senior Member, IEEE*, and Mung Chiang, *Fellow, IEEE*

**Abstract**—We investigate training machine learning (ML) models across a set of geo-distributed, resource-constrained clusters of devices through unmanned aerial vehicles (UAV) swarms. The presence of time-varying data heterogeneity and computational resource inadequacy among device clusters motivate four key parts of our methodology: (i) *stratified UAV swarms* of leader, worker, and coordinator UAVs, (ii) *hierarchical nested personalized federated learning* (HN-PFL), a distributed ML framework for personalized model training across the worker-leader-core network hierarchy, (iii) *cooperative UAV resource pooling* to address computational inadequacy of devices by conducting model training among the UAV swarms, and (iv) *model/concept drift* to model time-varying data distributions. In doing so, we consider both *micro* (i.e., UAV-level) and *macro* (i.e., swarm-level) system design. At the micro-level, we propose network-aware HN-PFL, where we distributively orchestrate UAVs inside swarms to optimize energy consumption and ML model performance with performance guarantees. At the macro-level, we focus on swarm trajectory and learning duration design, which we formulate as a sequential decision making problem tackled via deep reinforcement learning. Our simulations demonstrate the improvements achieved by our methodology in terms of ML performance, network resource savings, and swarm trajectory efficiency.

**Index Terms**—UAVs, personalized federated learning, distributed model training, network optimization, model drift.

## I. INTRODUCTION

The benefits that machine learning (ML) techniques have provided in a plethora of applications are motivating attempts to push this intelligence towards the network edge. Several use cases in the Internet of Things (IoT), e.g., autonomous driving, smart manufacturing, and object tracking have inspired the development of distributed ML techniques, in particular federated learning, for conducting model training on the device side [1]–[3]. Concurrently, unmanned aerial vehicles (UAVs) have been recently incorporated into IoT networks to service applications such as surveillance, aerial base stations, smart agriculture, and search and rescue [4], [5]. Given that UAVs tend to be more powerful than other IoT edge devices, current literature is taking initial steps toward integrating UAVs into distributed ML [6]–[10]. However, these works have mostly focused on implementing the classic federated learning

architecture using UAVs, where either (i) the data is assumed to already be stored on the UAVs [6]–[9] or (ii) the UAVs replace cellular base stations as the model aggregators [10]. By contrast, in many IoT settings, the data of interest is collected across computationally-constrained, geo-distributed devices. To address this, there is a need for a holistic paradigm that integrates UAVs into the intelligent IoT ecosystem, where the UAVs must both efficiently collect data from devices and perform ML model training, which motivates our work.

Specifically, a UAV-assisted distributed ML paradigm must account for several factors. Online data variations across geo-distributed devices, as well as heterogeneity across the UAVs and devices in terms of data distributions and computation/communication resources, can each have a large impact on performance. On the infrastructure side, device-UAV-core network interfacing and the locations of recharging stations become important, especially across a large geographic region. To address these challenges, the methodology we propose consists of four interrelated parts: (i) a new model for UAV swarms, called *stratified swarms*, suitable for distributed ML data collection and model training; (ii) *hierarchical nested personalized federated learning* (HN-PFL) to account for data heterogeneity in model updates; (iii) cooperative data processing across the UAVs via *resource pooling*; and (iv) *model/concept drift* tracking, which is tied to the model performance at devices and UAV movement patterns. We will develop and solve both UAV-level and swarm-level system optimizations: (a) HN-PFL model performance is optimized via efficient orchestration of the UAVs, taking into account the heterogeneity of the network elements, while (b) the swarm trajectories are optimized to account for anticipated model drifts across device clusters that will maximize training performance.

### A. Motivations and Applications

The following scenarios will further motivate our system model for UAV-enabled online ML model training, where the UAVs perform both data collection and model training.

**Community Service Systems via Amazon Sidewalk:** Amazon proposes *Sidewalk* [11] to integrate community networks of IoT devices for household appliance diagnostics (e.g., garage system maintenance, pet finding, smart lighting) in the absence of consistent wi-fi connectivity [12], [13] by leveraging device-to-device (D2D) communications. However, efficient training of ML models on IoT devices and sharing them among distant

S. Wang, S. Hosseinalipour, C. Brinton, and M. Chiang are with Purdue University, IN, USA e-mail: {wang2506,hosseina,cgb,chiang}@purdue.edu.

M. Gorlatova is with Duke University, Durham, NC, USA e-mail: maria.gorlatova@duke.edu.

neighborhoods faces four non-trivial challenges: (i) IoT devices may not be idle, plugged into power, or have direct access to a cellular base station (i.e., the core-network), preventing them from performing computationally intensive ML training, (ii) distant neighborhoods may not be reachable through D2D, (iii) neighborhoods' collected data may be time varying, and (iv) the neighborhoods may have extremely heterogeneous data distributions. We address the first two limitations by introducing UAV resource pooling and transferring model training vertically onto UAV swarms (e.g., the Amazon Prime Air delivery system [14]), the third via model/concept drift at different neighborhoods, and the fourth through model personalization.

**Distributed Surveillance in Smart Cities:** Our proposed method has natural applications to smart city surveillance systems. For instance, multiple UAV swarms can be spread throughout a city, extracting data from sensors and cameras as well as those devices in rural areas without direct access to the closed-circuit cellular network to train an ML model [15]–[17]. Additionally, these swarms can travel to diverse neighborhoods (e.g., industrial parks vs. academic campuses) within a city, allowing for model recalibration in the presence of dynamic environments and improving the quality of personalized models through exploiting data commonality.

**Machine Learning on Wireless Sensor Networks:** ML techniques have been adapted for wireless sensor networks (WSN) with respect to a wide variety of tasks, e.g., object targeting and event detection [18]. Our model can be contextualized, as an example, for integrated-WSN-UAV response systems, wherein wireless sensors collect data, e.g., water level or seismic energy, and offload it to UAVs, which then train ML models [19]. The UAV swarms can travel to distant and disconnected WSNs, e.g., across a beach/coast, to gather heterogeneous and time-varying data, e.g., day vs. night tidal measurements, and train ML models for each WSN cluster, thus integrating the system together.

## B. Related Work

This paper contributes to both literature in distributed ML over wireless networks and ML for UAV networks. Below, we provide a summary of related works and highlight the main contributions of our methodology.

**Distributed ML over wireless networks:** Recent literature concerning ML by wireless networks has shifted towards federated learning [20], [21], and is mostly focused on studying the convergence and behavior of federated learning over wireless networks [7], [8], [10], [22]–[30]. Conventional federated learning assumes training a single ML model for all the engaged devices. However, upon having extreme data heterogeneity across the devices, training a single model may result in poor model performance for a portion of devices. This has motivated a new trend of research in ML that aims to train user-specific ML models, referred to as multi-task learning [31], [32] or personalized federated learning [33], in the latter of which meta-gradient updates are introduced to enhance the training efficiency. As compared to this literature, we develop and investigate a new distributed ML paradigm over wireless networks called *hierarchical nested personalized federated learning* (HN-PFL) inspired by meta-gradient updates, which

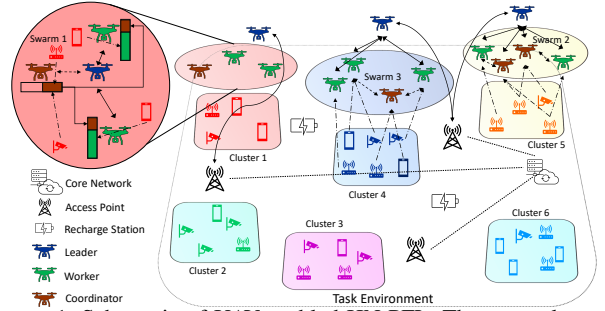


FIGURE 1: Schematic of UAV-enabled HN-PFL. The network consists of multiple IoT device clusters, stratified UAV swarms, access points, and recharging stations. UAV swarm leaders orchestrate intra-swarm ML training by workers, and manage the data collection/transfer at workers and coordinator UAVs. Periodically, leaders travel to access points for the core network, and perform a global model aggregation.

is different than hierarchical FL architectures, e.g., [34], which rely on conventional gradient descent updates for local model training. Furthermore, we develop a new framework for network-aware HN-PFL over UAV-assisted wireless networks that considers model training under heterogeneity of resources in wireless networks. Our resulting optimization formulation balances the tradeoffs between ML model performance and network parameters such as data offloading, training batch sizes, and CPU cycles, and is also part of our contributions.

**ML for UAV-assisted networks:** Deep learning techniques have been utilized to enhance the efficiency of wireless networks [35] in problems such as beamforming [36] and user scheduling [37]. In UAV-assisted networks, especially when the UAVs are deployed as aerial base stations, reinforcement learning (RL) has been utilized to carry out a variety of tasks, such as trajectory and power control for UAVs [38], [39], communication under signal jamming [40], and UAV server quality [41]. A key observation from the aforementioned existing literature is that UAV-assisted networks are difficult to model using traditional closed form methodologies and, as such, benefit from intelligent and autonomous management via RL. As compared to current literature, we introduce a new system model for UAV swarms and use a RL method to manage only the macro-level (i.e., swarm trajectories and temporal parameters of ML model training) of our methodology.

## C. Outline and Summary of Contributions

Our contributions in this work can be summarized as follows:

- We introduce the framework of UAV-enabled online model training for a set of geo-distributed ground device clusters. We propose *stratified UAV swarms*, which presume different roles for the UAVs: (i) a *leader* that manages UAVs within the swarm (e.g., adjusting the CPU cycles and mini-batch sizes), and determines data transfer configurations, (ii) *workers* that conduct ML model training through *resource pooling*, and (iii) *coordinators* that enable data relaying between the devices and the worker UAVs.
- We develop hierarchical nested personalized federated learning (HN-PFL), which exploits the commonality among the data across the device clusters to produce personalized local models. Through the nesting of intra-swarm updates within inter-swarm aggregations, HN-PFL conducts ML model

TABLE I: Summary of Key Notations for Devices, UAVs, Network Optimization, Machine Learning, and Swarm Trajectory Design

Device Cluster, UAV Swarm, and Network		Data Processing/Offloading Optimization and Network Energy Consumption			
$\mathcal{C}$	Set of all device clusters	$\rho_{i,j}(t)$	Data transfer ratio from device $i$ to UAV $j$	$g_{i,j}(t)$	Data transfer ratio from UAV $i$ to $j$
$\mathcal{R}$	Set of recharging stations	$g_j(t)$	Adjustable CPU cycle frequency at UAV $j$	$\zeta_j^G(k)$	Time used by UAV $j$ to gather data
$\mathcal{A}$	Set of access points	$\zeta_j^P(k)$	Time used by UAV $j$ to process data	$E_j^{\text{Ba}}(s)$	Starting battery of UAV $j$ at the $s$ -th sequence
$U(s)$	Number of active swarms at $s$ -th sequence	$M$	Number of bits per datapoint	$\bar{M}$	Number of bits used for model parameters
$\mathcal{U}(s)$	Set of active swarms at $s$ -th sequence	<b>Machine Learning Notation</b>			
$\ell_u$	Leader UAV of $u$ -th swarm	$F_j$	Meta loss function at UAV $j$	$f_j$	ML loss over all data in $\mathcal{D}_j$
$\mathcal{W}_u$	Worker UAVs in the $u$ -th swarm	$\hat{f}_j$	ML loss over a datapoint in $\mathcal{D}_j$	$\mathbf{w}_j(t)$	Model parameters at UAV $j$
$\hat{u}$	Non-leader UAVs in $u$ -th swarm	$\alpha_{j,1}(t)$	Inner mini-batch ratio for UAV $j$	$\alpha_{j,2}(t)$	Outer mini-batch ratio for UAV $j$
$\widehat{\mathcal{W}}_u$	Coordinator UAVs in the $u$ -th swarm	$\alpha_{j,3}(t)$	Hessian mini-batch ratio for UAV $j$	$t_s$	Starting time for the $s$ -th sequence
$\widehat{\mathcal{D}}_i(t)$	Dataset of $i$ -th device	$\tau_s^L$	Local aggregation period for $s$ -th sequence	$\tau_s^G$	Global aggregation period for $s$ -th sequence
$\mathcal{D}_j(t)$	Dataset of $j$ -th UAV	$k$	Local aggregation index	$k^G$	Global aggregation index
$\widehat{\mathcal{D}}_c(t)$	Union of datasets at cluster $c$	<b>Swarm Trajectory Optimization</b>			
$B_j^D(t)$	Max dataset size for UAV $j$	$\mathcal{X}(s)$	Swarm positions at $s$ -th sequence	$G_c(s)$	Online gradient as a result of model drift
$T_s$	Duration of the $s$ -th sequence	$\mathcal{Z}(s)$	Network state encoding at $s$ -th sequence	$\mathcal{H}(s)$	DRL agent action at the end of the $s$ -th sequence
$\Lambda_c$	Model drift of cluster $c$	$V(s)$	Reward of the $s$ -th sequence	$Q_\theta$	Q-network for trajectory design

training across the *worker-leader-core* network hierarchy. We analytically characterize the convergence behavior of HN-PFL, which leads us to new convergence bounds for distributed ML.

- We integrate network-characteristics into ML training/performance by formulating a joint energy and ML performance optimization problem, which aims to configure the data offloading among devices-UAVs and UAVs-UAVs, adjust the CPU cycles of the UAVs, and obtain the mini-batch sizes used at the worker UAVs. This holistic formulation is among the first in literature to consider all these design variables together. We demonstrate that the problem belongs to the category of *complementary geometric programming* problems which are highly non-convex and NP-Hard. We then develop a distributed method, with performance guarantee, based on posynomial condensation to solve the problem for all UAV swarms in parallel.
- We formulate the problem of UAV swarm trajectory design, alongside of which we also optimize the learning duration of HN-PFL. In the formulation, we consider *online model training* under temporal data distribution variations, which is quantified via *model/concept drift*. We demonstrate that the problem solution is intractable and then cast the problem as a sequential decision making problem tackled via a deep reinforcement learning-based method.

## II. SYSTEM MODEL

In this section, we introduce the system components, which include IoT device clusters (Sec. II-A), UAV swarms, recharging stations, and access points (Sec. II-B). We also provide an overview of our entire methodology, including the macro- and micro-level design in Sec. II-C.

### A. Device Clusters and Data Distributions

We consider a set of geo-distributed devices collected into into  $C$  clusters, denoted by  $\mathcal{C} = \{\mathcal{C}_1, \dots, \mathcal{C}_C\}$ , based on geographic proximity. Hereafter, we will refer to an arbitrary cluster via  $c$  for brevity. At time instance  $t \in \mathcal{T} \triangleq \{1, 2, \dots\}$ , we denote  $\widehat{\mathcal{D}}_i(t)$  as the set of datapoints device  $i \in c$  has collected at that time. Each  $x \in \widehat{\mathcal{D}}_i(t)$  is a data sample containing model features and (possibly) a target variable.

Motivated by the real-world applications in Sec. I-A, wherein data distributions are expected to change temporally (e.g., at environmental sensors), we focus on *online/dynamic* model training and deployment, which is different from current literature that mainly consider static data at the devices

(e.g., [22], [23], [25], [27], [28], [30]). Our goal is to obtain and periodically update a personalized ML model for each cluster  $c$  to use for real-time inference. However, due to significant computation/communication constraints the devices may be unable to train high-dimensional ML models (e.g., surveillance cameras as described in Sec. I-A). We thus transpose the ML model training to UAV swarms via data offloading from the devices. We assume that each device  $i \in c$  collects data in its buffer  $\widehat{\mathcal{B}}_i$  of finite size, and that each device is capable of transmitting data to nearby UAVs to perform model training. We consider  $\widehat{\mathcal{B}}_i$  as a double-ended queue (i.e., deque) so that, when filled, new datapoints will displace the oldest ones.<sup>1</sup>

### B. Swarms, Recharging Stations, and Access Points

To conduct efficient ML model training at the UAVs, we introduce stratified UAV swarms, where UAVs have different roles for data collection and data processing (Sec. II-B1). Since the battery-limited UAVs perform energy-intensive ML model training, we also integrate a recharging methodology via recharging stations in our model (Sec. II-B2). Also, to synchronize the ML model training and UAV orchestration, we consider a set of access points in the network (Sec. II-B3). In the following, we explain each of these components. A schematic of our model is depicted in Fig. 1.

1) *UAV Swarms and Stratification*: We consider a set of  $U$  UAV swarms  $\mathcal{U} = \{\mathcal{U}_1, \dots, \mathcal{U}_U\}$ , and assume that  $U < C$ . We denote an arbitrary UAV swarm as  $u$  for brevity. We assume that each UAV swarm  $u$  is composed of UAVs with heterogeneous capabilities, e.g., from micro-drones weighing under 200grams that have data storage capabilities [42] to medium-sized fixed/rotatory wing UAVs that have more advanced computational capabilities [43]. Subsequently, to maximize the performance of each swarm, we propose a new *swarm stratification* model, which compared to current literature on UAV trajectory design [38], [44] is tailored specifically for ML training tasks. In our swarm stratification, there are three types of UAVs: (i) a leader  $\ell_u$  of each swarm  $u$ , with the set of leaders across swarms denoted by  $\mathcal{L} = \cup_{u \in \mathcal{U}} \ell_u$ , (ii) a set of workers  $\mathcal{W}_u$  in swarm  $u$ , with the set across swarms denoted by  $\mathcal{W} = \cup_{u \in \mathcal{U}} \mathcal{W}_u$ , and (iii) a set of coordinators  $\widehat{\mathcal{W}}_u$  in  $u$ , gathered via the set  $\widehat{\mathcal{W}} = \cup_{u \in \mathcal{U}} \widehat{\mathcal{W}}_u$ . For convenience, we refer to the workers and coordinators together as  $\widehat{u} = \mathcal{W}_u \cup \widehat{\mathcal{W}}_u = u \setminus \{\ell_u\}$ . UAVs in  $\widehat{u}$  collect data from

<sup>1</sup>Henceforth, we use calligraphic (e.g.,  $\widehat{\mathcal{D}}_i(t)$ ) to denote a set, and non-calligraphic (e.g.,  $\widehat{D}_i(t)$ ) to denote its cardinality.

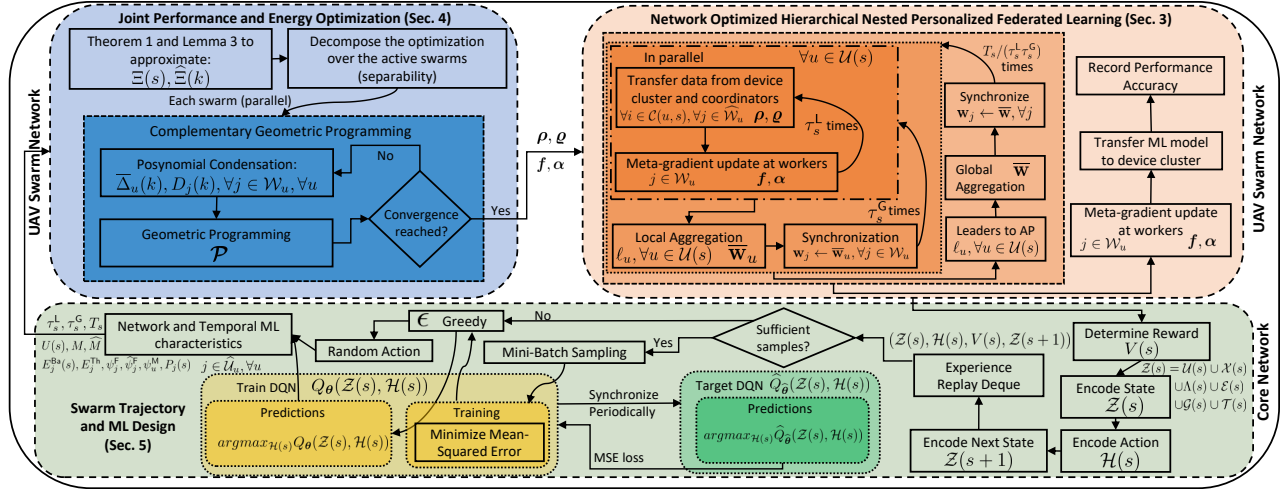


FIGURE 2: Our methodology consists of three components - the HN-PFL architecture (Sec. III), the data transfer and processing optimization (Sec. IV), and the swarm trajectory design (Sec. V). Our three components effectively reduce the problem into two layers: a *micro*-level wherein ML model training is optimized and subsequently performed via HN-PFL and a *macro*-level wherein the optimality of the macro-system (i.e. the holistic network-wide consideration of all separate device clusters) is achieved. We additionally emphasize that a sole reinforcement learning based architecture would struggle greatly from the large and dynamic state-space of energy-efficient swarm trajectory design, HN-PFL performance and energy maximization, coordinator UAV transmissions, online model drifts, and meta-training convergence determination.

nearby IoT devices, with the workers  $\mathcal{W}_u$  conducting model training based on their gathered data, and the coordinators  $\widehat{\mathcal{W}}_u$  relaying data to other UAVs in  $\widehat{u}$  and building a data profile of the device cluster under visit.

When swarm  $u$  arrives at some device cluster  $c$ , the leader  $\ell_u$  scatters the UAVs  $\widehat{u}$  throughout predetermined locations in  $c$  (e.g., using Voronoi diagrams [45]). All UAVs in  $\widehat{u}$  gather data from devices  $i \in c$  through a “wake up and sleep” paradigm, where the UAV notifies nearby IoT devices and prompts them to upload data. We denote  $\mathcal{D}_j(t)$  as the dataset UAV  $j \in \widehat{u}$ , with buffer size  $B_j^D(t)$ , obtains at time  $t$ . Workers  $\mathcal{W}_u$  form a pool of computational resources above the device cluster and use their gathered data for cooperative ML training, in which they engage in periodic communication with the leader  $\ell_u$  regarding their training results. On the other hand, coordinators  $\widehat{\mathcal{W}}_u$  act as *aerial data caches* to relay data to other UAVs in  $\widehat{u}$ . This arrangement allows more energy-efficient data transfer from IoT devices to worker UAVs via coordinator relaying. We formalize  $\mathcal{D}_j(t), \forall j$ , through our optimization in Sec. IV-A.

2) *Recharging Stations*: We consider a set of geo-distributed recharging stations  $\mathcal{R}$  in the network [46], [47]. We assume that when any UAV  $j \in u$  reaches a minimum battery threshold, the entire swarm  $u$  must travel to a recharging station  $r \in \mathcal{R}$ .

3) *Access Points (AP)*: We consider a set of gateway APs  $\mathcal{A}$ , which can be interpreted for example as cellular base stations. All APs  $a \in \mathcal{A}$  are connected through the core network. The APs are used by the leader UAVs  $\mathcal{L}$  to communicate with the core network, which determines swarm trajectories and synchronizes ML training among the swarms.

### C. Components of Our Methodology and Roadmap

We break down our methodology for conducting geo-distributed ML using UAVs into three parts: (i) ML model training through the worker-leader-core network hierarchy, (ii) efficient orchestration of the UAVs inside each swarm, and (iii) energy and performance-driven design of the UAV swarm trajectories across device clusters. For (i), we develop

hierarchical nested personalized federated learning (HN-PFL) and subsequently derive its performance through theoretical bounds in Sec. III. For (ii), we formulate a network-aware ML performance and swarm-wide energy consumption optimization problem, and then develop a distributed solver in Sec. IV. For (iii), we capture the temporal variation of data across the clusters and obtain the sequence of cluster visits for the UAV swarms (i.e., swarm trajectories) via integrating a deep reinforcement learning architecture in Sec. V. The interactions between these three components and an overview of their functionality is depicted in Fig. 2. From a high-level standpoint, the swarm-wide optimization (blue block) is used to determine HN-PFL’s runtime characteristics, and the performance results of HN-PFL (orange block) are used to obtain the sequence of cluster visits (green block), which are carried out cyclically. We will explain the details of the processes of each block of Fig. 2 in Sec. III, IV, and V, respectively.

### D. Metrics of Interest

The evaluation of our methodology requires several primary metrics: classification loss at the UAVs (Thm. 1), the mismatch between the model performance at the UAVs vs. at the device clusters (Prop. 1), and energy consumption (Sec. IV). We will further demonstrate that our learning method provides substantial improvements compared to baselines in terms of convergence rate (Sec. VI-A), network resource savings (Sec. VI-B), and trajectory design efficiency (Sec. VI-C).

## III. HIERARCHICAL NESTED PERSONALIZED FEDERATED LEARNING (HN-PFL)

In this section, we develop our UAV-enabled methodology for personalized federated learning (PFL). We begin with the rationale (Sec. III-A), and then present the HN-PFL algorithm (Sec. III-B). Finally, we theoretically analyze the convergence of our distributed ML method (Sec. III-C).

### A. Overview and Rationale

Conventional federated learning (FL) trains a single ML model suitable for all devices [48]. As devices may exhibit

significant heterogeneity in their data distributions, training a global model used for all the devices may lead to poor overall performance. This has motivated personalized federated learning (PFL) [33], which trains device-specific ML models by leveraging the *commonality* across the devices' data. Conventional FL and PFL both assume a "star" learning topology, where a set of workers/devices are connected to a main server [3], which requires direct communication between the devices and the server.

In our setting, the star topology assumed in FL/PFL applies poorly as the IoT device clusters are geo-distributed, and UAVs visiting the clusters may not have direct access to an AP. On the other hand, UAV-to-UAV communications within a swarm is comparatively low in resource consumption, which motivates *local model aggregations* inside the swarms enabled by the leader UAV. The leaders can then occasionally visit their nearest AP for global aggregation of their associated swarm ML model parameters. By *nesting* intra-swarm (local) aggregations within inter-swarm (global) aggregations, we develop a new methodology to generalize the star topology in conventional FL/PFL to that of a *hierarchical* tree, called HN-PFL where the ML model training is segmented into two layers: (i) swarm-level between leaders and their constituents, and (ii) global-level between access points/core-network and swarm leaders. To the best of our knowledge, HN-PFL is the first hierarchical personalized federated learning architecture in literature.

### B. HN-PFL Algorithm

HN-PFL breaks down the model training problem into two layers: (i) *workers-leaders*, in which the worker UAVs carry out the ML model training and the leader UAVs perform swarm-wide (local) aggregations; and (ii) *leaders-APs*, in which the leader UAVs engage in global aggregations.

Since our problem requires the swarms  $\mathcal{U}$  to travel between IoT device clusters, HN-PFL carries out the model learning through consecutive *training sequences*. Each training sequence starts when all active UAV swarms (i.e., non-recharging swarms) arrive at their designated device clusters, and concludes when the swarms finish the model training and begin travelling to their next destination. We denote the start of the  $s$ -th training sequence,  $s = 1, 2, \dots$ , by  $t_s \in \mathcal{T}$ , its scheduled interval as  $\mathcal{T}_s = \{t_s, \dots, t_s + T_s - 1\}$ , and the active swarms for the  $s$ -th sequence as  $\mathcal{U}(s) \subseteq \mathcal{U}$ . Defining the active swarms  $\mathcal{U}(s)$  with respect to the training sequence encompasses the cases where a portion of UAV swarms recharge their batteries and thus are not engaged in ML model training during  $\mathcal{T}_s$ .

At each time  $t \in \mathcal{T}_s$ , each worker UAV  $j \in \mathcal{W}_u$ ,  $u \in \mathcal{U}(s)$  conducts a *local model update*. This consists of computing its next ML model parameter vector  $\mathbf{w}_j(t+1)$  using a meta-gradient update [49] defined as:

$$\mathbf{w}_j(t+1) = \mathbf{w}_j(t) - \eta_2 \nabla \tilde{F}_j(\mathbf{w}_j(t)), \quad t+1 \in \mathcal{T}_s, \quad (1)$$

where  $\eta_2 > 0$  is the meta-update step-size, and  $\nabla \tilde{F}_j(\mathbf{w}_j(t))$  is the mini-batch approximation of the meta-gradient  $\nabla F_j(\mathbf{w}_j(t))$ .  $\nabla F_j(\mathbf{w}_j(t))$  is the gradient of the meta-function  $F_j$ , defined as the loss of the gradient descent procedure:

$$F_j(\mathbf{w}_j(t)) = f_j(\underbrace{\mathbf{w}_j(t) - \eta_1 \nabla f_j(\mathbf{w}_j(t))}_{(a)}), \quad (2)$$

where  $\eta_1 > 0$  is the step size for gradient descent and  $f_j$  is the local loss function over the local dataset  $\mathcal{D}_j(t)$  at UAV  $j$ :

$$f_j(\mathbf{w}_j(t)) = \frac{\sum_{x \in \mathcal{D}_j(t)} \hat{f}(\mathbf{w}_j(t); x)}{D_j(t)}, \quad (3)$$

and  $\hat{f}(\mathbf{w}_j(t); x)$  is the loss per datum  $x$ . This meta-gradient procedure effectively updates the parameters on the loss of the update rule. In particular, based on (2), it *results in a set of global parameters that can be better adapted/personalized to local data distributions with an additional gradient descent step (term (a))*. We approximate the gradient  $\nabla F_j$  by mini-batch methods [48], [50], obtaining

$$\nabla \tilde{F}_j(\mathbf{w}_j(t)) = \nabla \tilde{f}_j \left( \mathbf{w}_j(t) - \eta_1 \nabla \tilde{f}_j(\mathbf{w}_j(t) | \mathcal{D}_{j,1}(t)) \Big|_{\mathcal{D}_{j,2}(t)} \right) \cdot \left( \mathbf{I} - \eta_1 \nabla^2 \tilde{f}_j(\mathbf{w}_j(t) | \mathcal{D}_{j,3}(t)) \right), \quad (4)$$

where  $\tilde{f}_j$  is the mini-batch loss defined similarly to (3) over a specific data batch<sup>2</sup>,  $\nabla^2$  is the Hessian operator, and  $\mathcal{D}_{j,1}(t)$ ,  $\mathcal{D}_{j,2}(t)$ ,  $\mathcal{D}_{j,3}(t)$  are three independent mini-batches sampled with replacement from  $\mathcal{D}_j(t)$ . We denote the mini-batch sampling ratios as  $\alpha_{j,1}(t)$ ,  $\alpha_{j,2}(t)$ , and  $\alpha_{j,3}(t) \in (0, 1)$ , i.e.,  $D_{j,i}(t) = \alpha_{j,i}(t) D_j(t)$ ,  $i = 1, 2, 3$ , and the total ratio of data at time  $t$  used for processing by worker  $j \in \mathcal{W}_u$ ,  $u \in \mathcal{U}(s)$  is denoted by  $\alpha_j(t) = \alpha_{j,1}(t) + \alpha_{j,2}(t) + \alpha_{j,3}(t)$ .

**Remark 1.** *The computational burden of the Hessian-based gradient descent in (4) can be alleviated by substituting it with approximate methods such as first order or hessian free model agnostic training [33], [49], which have been shown to attain a similar performance to that of exact Hessian computation.*

HN-PFL performs a series of local and global aggregations during each training sequence  $\mathcal{T}_s$ . We conduct local aggregations with period of  $\tau_s^L$  (i.e.,  $\tau_s^L$  local meta-gradient updates prior to each local aggregation), and global aggregations with period of  $\tau_s^L \tau_s^G$ , defined such that  $T_s \triangleq \tau_s^L K_s^L \equiv \tau_s^L \tau_s^G K_s^G$ , where  $K_s^L$  is the total number of local aggregations, and  $K_s^G$  is the total number of global aggregations conducted in  $\mathcal{T}_s$ . Using  $k$  for the local aggregation index,  $t_s^L(k) = t_s + k\tau_s^L$  is the time of the  $k$ -th local aggregation in  $\mathcal{T}_s$ . Using  $k'$  as the global aggregation index,  $t_s^G(k') = t_s + k'\tau_s^L \tau_s^G$  will denote the time of the  $k'$ -th global aggregation in  $\mathcal{T}_s$ .

At the  $k$ -th *local aggregation*, when  $t = t_s^L(k)$ , HN-PFL performs a weighted average at each leader  $\ell_u$ ,  $u \in \mathcal{U}(s)$ :

$$\bar{\mathbf{w}}_u(t) = \frac{\sum_{j \in \mathcal{W}_u} \mathbf{w}_j(t) \sum_{t'=t_s^L(k-1)+1}^t \alpha_j(t') D_j(t')}{\sum_{j \in \mathcal{W}_u} \sum_{t'=t_s^L(k-1)+1}^t \alpha_j(t') D_j(t')}. \quad (5)$$

Leader  $\ell_u$  then broadcasts  $\bar{\mathbf{w}}_u(t_s^L(k))$  to all worker UAVs  $\mathcal{W}_u$ . This completes our *swarm-wide aggregation*, and we define the swarm-wide/local meta-function  $F_u$  for  $t = t_s^L(k)$  as follows:

$$\bar{F}_u(\bar{\mathbf{w}}_u(t)) = \frac{\sum_{j \in \mathcal{W}_u} F_j(\bar{\mathbf{w}}_u(t)) \sum_{t'=t_s^L(k-1)+1}^t \alpha_j(t') D_j(t')}{\sum_{j \in \mathcal{W}_u} \sum_{t'=t_s^L(k-1)+1}^t \alpha_j(t') D_j(t')}. \quad (6)$$

After  $\tau_s^L$  swarm-wide aggregations at the active swarms, the leaders  $\ell_u$ ,  $u \in \mathcal{U}(s)$ , travel to their nearest AP, and transmit

<sup>2</sup>The second argument in  $\tilde{f}_j(\cdot)$  denotes the data batch used to compute the respective function.

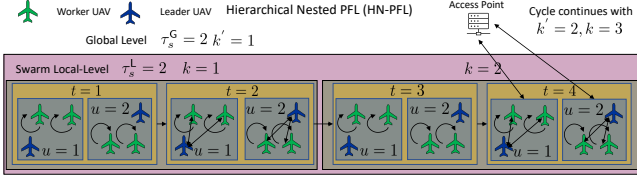


FIGURE 3: Behavior of workers, leaders, and APs in HN-PFL. Workers perform local meta-updates, and leaders aggregate their workers' model parameters with period  $\tau_s^L$ . After  $\tau_s^G$  local aggregations, the core network performs a global aggregation, wherein leaders' parameters are re-synchronized.

their swarm-wide parameters to the core network. At the  $k'$ -th *global aggregation*, when  $t = t_s^G(k')$ , the core network determines the global model parameters as:

$$\bar{\mathbf{w}}(t) = \frac{1}{U(s)} \sum_{u \in \mathcal{U}(s)} \bar{\mathbf{w}}_u(t), \quad (7)$$

with global meta-function  $\bar{F}$  for  $t = t_s^G(k')$  as:

$$\bar{F}(\bar{\mathbf{w}}(t)) = \frac{1}{U(s)} \sum_{u \in \mathcal{U}(s)} \bar{F}_u(\bar{\mathbf{w}}(t)). \quad (8)$$

We use an *unweighted* aggregation across swarms in (7) and (8), and weigh swarms equally. This allows for using the commonality of the data across the clients while avoiding the bias towards specific cluster data distribution, which in turn enables efficient model personalization. The access points  $\mathcal{A}$  then broadcast  $\bar{\mathbf{w}}(t_s^G(k'))$  to the leaders, which return to their swarms to synchronize parameters across their workers.

At the final global aggregation of training sequence  $s$ , i.e.,  $t = t_s + T_s - 1$ , swarms in  $\mathcal{U}(s)$  *personalize* the global model to their respective visiting device cluster data distribution by performing a *single* stochastic gradient update (accounting for term (a) in (2)) followed by a swarm-wide aggregation as in (5), and then swarm leaders transfer the resulting ML model to the devices. Next, active swarms from both  $s$  and  $s + 1$  initialize the next sequence. For each  $u \in \mathcal{U}(s) \cup \mathcal{U}(s + 1)$ , leader  $\ell_u$  will receive (i) final global parameters  $\bar{\mathbf{w}}(t_s + T_s - 1)$ , and (ii) trajectory decisions from the APs. Swarms then travel to their next cluster (for swarms  $u \in \mathcal{U}(s) \setminus \mathcal{U}(s + 1)$ , this would be a recharging station). Upon arrival, swarm leaders  $\ell_u$ ,  $u \in \mathcal{U}(s + 1)$ , will begin training sequence  $s + 1$  by synchronizing workers with the latest global parameters. Our developed HN-PFL algorithm is summarized in Fig. 3.

We assume that data distributions at the IoT devices are stationary during training sequences, although they may vary between training sequences. Data distribution changes may lead to decreasing the ML inference performance (i.e., a weaker ML model) at some clusters over time, which incentivizes swarms to re-visit them and re-calibrate their ML models. We capture the time-varying data distributions at clusters by introducing heterogeneous *model/concept drift*, which will in turn affect the UAV trajectories (see Sec. V-A). We next obtain the convergence bound of HN-PFL, which will be employed in the optimization formulation in Sec. IV.

### C. Convergence Analysis of HN-PFL

In the following, we derive the performance bound of HN-PFL for non-convex loss functions. To this end, in addition

to the meta functions defined in (6) and (8), we define the swarm-average loss function  $\bar{f}_u(\mathbf{w})$  at  $t \in \mathcal{T}_s$  as:

$$\bar{f}_u(\mathbf{w}(t)) = \sum_{j \in \mathcal{W}_u} \frac{\Delta_j(k)}{\Delta_u(k)} f_j(\mathbf{w}(t)), \quad (9)$$

where  $f_j$  is defined as in (3),  $k$  is the most recent local aggregation index,  $\Delta_j(k) = \sum_{t'=t_s^L(k-1)+1}^t \alpha_j(t') D_j(t')$ , and  $\Delta_u(k) = \sum_{j \in \mathcal{W}_u} \Delta_j(k)$ . Also, we define the global average loss function  $\bar{f}(\mathbf{w})$  at time  $t \in \mathcal{T}_s$  as:

$$\bar{f}(\mathbf{w}(t)) = \frac{1}{U} \sum_{u \in \mathcal{U}} \bar{f}_u(\mathbf{w}(t)). \quad (10)$$

While (5),(6),(9) are only realized by HN-PFL at a local aggregation,  $t = t_s^L(k)$ , and (7),(8),(10) are only realized at a global aggregation,  $t = t_s^G(k')$ , defining them for each  $t \in \mathcal{T}_s$  will be useful in our theoretical analysis.

Our convergence analysis employs some standard assumptions [51], [52] on non-convex loss functions:

**Assumption 1** (Loss function characteristics). *We make the following assumptions on  $f_j$  at worker  $j \in \mathcal{W}_u$ ,  $\forall u \in \mathcal{U}$ :*

- 1)  $f_j$  is bounded below:  $f_j(\mathbf{w}) > -\infty, \forall \mathbf{w}$ .
- 2)  $f_j$  is twice continuously differentiable and its gradient is  $\mu_j^G$ -Lipschitz and bounded by  $B_j$ : (i)  $\|\nabla f_j(\mathbf{w}) - \nabla f_j(\mathbf{w}')\| \leq \mu_j^G \|\mathbf{w} - \mathbf{w}'\|, \forall \mathbf{w}, \mathbf{w}'$ , (ii)  $\|\nabla f_j(\mathbf{w})\| \leq B_j$ .
- 3) The Hessian of  $f_j$  is  $\mu_j^H$ -Lipschitz continuous:  $\|\nabla^2 f_j(\mathbf{w}) - \nabla^2 f_j(\mathbf{w}')\| \leq \mu_j^H \|\mathbf{w} - \mathbf{w}'\|, \forall \mathbf{w}, \mathbf{w}'$ .
- 4) Bounded local data variability:  $\mathbb{E}[\|\nabla \hat{f}(x, \mathbf{w}) - \nabla f_j(\mathbf{w})\|^2] \leq \sigma_j^G$  and  $\mathbb{E}[\|\nabla^2 \hat{f}(x, \mathbf{w}) - \nabla^2 f_j(\mathbf{w})\|^2] \leq \sigma_j^H, \forall \mathbf{w}, x$ .
- 5) The variance of the gradient and Hessian of  $f_j(\mathbf{w})$  are bounded:  $\sum_{j \in \mathcal{W}_u} \frac{\Delta_j(k)}{\Delta_u(k)} \|\nabla f_j(\mathbf{w}) - \nabla \bar{f}_u(\mathbf{w})\|^2 \leq \gamma_u^G$ ,  $\sum_{j \in \mathcal{W}_u} \frac{\Delta_j(k)}{\Delta_u(k)} \|\nabla^2 f_j(\mathbf{w}) - \nabla^2 \bar{f}_u(\mathbf{w})\|^2 \leq \gamma_u^H, \forall \mathbf{w}, k$ .
- 6) The variance of the gradient and Hessian of  $\bar{f}_u(\mathbf{w})$  are bounded:  $\frac{1}{U} \sum_{u \in \mathcal{U}} \|\nabla \bar{f}_u(\mathbf{w}) - \nabla \bar{f}(\mathbf{w})\|^2 \leq \gamma^G$ ,  $\frac{1}{U} \sum_{u \in \mathcal{U}} \|\nabla^2 \bar{f}_u(\mathbf{w}) - \nabla^2 \bar{f}(\mathbf{w})\|^2 \leq \gamma^H, \forall \mathbf{w}$ .

We also require an assumption to characterize the loss function behavior at the device clusters:

**Assumption 2** (Device cluster loss function characteristics). *For device cluster  $c$  and a model parameter  $\mathbf{w}$ , let  $f_c^D(\mathbf{w}) = \sum_{x \in \bar{\mathcal{D}}_c(t)} \hat{f}(x; \mathbf{w}) / \bar{D}_c(t)$ , where  $\bar{\mathcal{D}}_c(t) \triangleq \cup_{i \in c} \bar{\mathcal{D}}_i(t)$ , denote the local loss at time  $t$ . We assume that (i) the gradient of the loss function is  $\mu_c^G$ -Lipschitz continuous, (ii) the Hessian is  $\mu_c^H$ -Lipschitz continuous, (iii)  $\mathbb{E}[\|\nabla \hat{f}(x, \mathbf{w}) - \nabla f_c^D(\mathbf{w})\|^2] \leq \sigma_c^G \forall x, \mathbf{w}$ , and (iv)  $\mathbb{E}[\|\nabla^2 \hat{f}(x, \mathbf{w}) - \nabla^2 f_c^D(\mathbf{w})\|^2] \leq \sigma_c^H \forall x, \mathbf{w}$ .*

The loss functions of many common ML models (e.g., neural networks with continuous activation functions [25]) will satisfy these assumptions. In the following analysis, we let  $B = \max_j \{B_j\}$ ,  $\mu^G = \max_j \{\mu_j^G\}$ , and  $\mu^H = \max_j \{\mu_j^H\}$ .

Our main result in this section will be the convergence behavior of the global meta-function  $\bar{F}$  in HN-PFL (Theorem 1). To obtain this, we first derive bounds on the expected error of the meta-gradient approximations at worker UAVs (Lemma 1), and on the meta-gradient variability between workers, leaders, and the core network (Lemma 2).

**Lemma 1** (Mini-batch versus full batch meta-gradients). *During each training interval  $\mathcal{T}_s$ , the expected error of the mini-batch approximation  $\nabla \tilde{F}_j(\mathbf{w}(t))$  of the true meta-gradient  $\nabla F_j(\mathbf{w}(t))$  at each worker UAV  $j \in \mathcal{W}_u$ ,  $\forall u \in \mathcal{U}(s)$  satisfies:*

$$\mathbb{E}[\|\nabla \tilde{F}_j(\mathbf{w}(t)) - \nabla F_j(\mathbf{w}(t))\|^2] \leq \sigma_j^F(t), \quad (11)$$

where

$$\begin{aligned} \sigma_j^F(t) = & \underbrace{\frac{3\eta_1^2 \sigma_j^H}{\alpha_{j,3}(t) D_j(t)}}_{(a)} \underbrace{\left[ B^2 + \frac{\sigma_j^G (\alpha_{j,1}(t) + (\mu^G \eta_1)^2 \alpha_{j,2}(t))}{\alpha_{j,1}(t) \alpha_{j,2}(t) D_j(t)} \right]}_{(b)} \\ & + \underbrace{\frac{12\sigma_j^G (\alpha_{j,1}(t) + (\mu^G \eta_1)^2 \alpha_{j,2}(t))}{\alpha_{j,1}(t) \alpha_{j,2}(t) D_j(t)}}_{(c)}. \end{aligned} \quad (12)$$

*Sketch of Proof:* The proof uses similar techniques to those found in Lemma 4.3 in [33]. We use our defined data processing ratios  $\alpha_{j,1}, \alpha_{j,2}, \alpha_{j,3}$  in place for batch sizes within the data variability component of Assumption 1. ■

We make a few observations from Lemma 1 regarding the mini-batch ratios  $\alpha_{j,1}(t)$ ,  $\alpha_{j,2}(t)$ , and  $\alpha_{j,3}(t)$ . Intuitively, if any of these are 0, then the upper bound in (11) should diverge, which is what we observe in (12). Next, the groups (a), (b), and (c) in (12) show that each mini-batch ratio has a unique impact on the bound. In particular,  $\alpha_{j,3}(t)$  weighs the Hessian data variability  $\sigma_j^H$  in (a), while  $\alpha_{j,1}(t)$  and  $\alpha_{j,2}(t)$  scale the gradient data variability  $\sigma_j^G$  in (b) and (c). Due to the multiplicative effect of the Hessian and gradient in the meta-gradient computation (see (4)), the effects of the mini-batch ratios are coupled between (a) and (b), through which  $\alpha_{j,3}(t)$  also weights the impact of  $\sigma_j^G$ . Hence, when we are faced with a limited budget for data processing in a UAV swarm, the mini-batch ratios must be allocated carefully, which we will address through our optimization problem in Sec. IV-A.

**Lemma 2** (Intra- and inter-swarm meta-gradient variability). *During each training interval  $\mathcal{T}_s$ , the intra-swarm meta-gradient variability at each UAV swarm  $u \in \mathcal{U}(s)$  obeys the following upper bound at local aggregation  $k$ :*

$$\sum_{j \in \mathcal{W}_u} \frac{\Delta_j(k)}{\Delta_u(k)} \|\nabla F_j(\mathbf{w}) - \nabla \bar{F}_u(\mathbf{w})\|^2 \leq \gamma_u^F, \quad (13)$$

where  $\gamma_u^F = 3B^2\eta_1^2\gamma_u^H + 192\gamma_u^G$ . Also, the variability of inter-swarm meta-gradients is upper bounded as follows:

$$\frac{1}{U(s)} \sum_{u \in \mathcal{U}(s)} \|\nabla \bar{F}_u(\mathbf{w}) - \nabla F(\mathbf{w})\|^2 \leq \gamma^F, \quad (14)$$

where  $\gamma^F = 3B^2\eta_1^2\gamma^H + 192\gamma^G$ .

*Sketch of Proof:* The proof uses similar techniques to those found in Lemma 4.4 in [33]. The difference is that we use the weighted aggregation definition for the meta function in (6) before applying Assumption 1 and Jensen's inequality. ■

Using Lemmas 1 and 2, we can bound the variance of HN-PFL model parameters across worker UAVs after a given global aggregation, which is one of our key theoretical results. For brevity, all proofs are given as sketches, with the key steps emphasized. The full proofs are provided in the appendices.

**Proposition 1** (Parameter variability across UAVs). *During interval  $\mathcal{T}_s$ , the variance in model parameters across the active*

*worker UAVs in the network at the  $k'$ -th global aggregation, i.e.,  $t = t_s^G(k')$ , satisfies the following upper bound:*

$$\mathbb{E} \left[ \left\| \frac{1}{U(s)} \sum_{u \in \mathcal{U}(s)} \sum_{j \in \mathcal{W}_u} \frac{\Delta_j(k' \tau_s^G)}{\Delta_u(k' \tau_s^G)} (\mathbf{w}_j(t) - \bar{\mathbf{w}}(t)) \right\|^2 \right] \leq \Upsilon(t) \quad (15)$$

where  $\Upsilon(t)$  is defined in (16) with  $\mu^F \triangleq 4\mu^G + \eta_1\mu^H B$ , and  $\sigma_u^F(t) = \sum_{j \in \mathcal{W}_u} \frac{\Delta_j(k' \tau_s^G)}{\Delta_u(k' \tau_s^G)} \sigma_j^F(t)$ .

*Sketch of Proof:* The complete proof is contained in Appendix A, where we split (15) into local and global relationships and then bound each separately using different techniques. The local relationships  $\mathbb{E}[\|\sum_{j \in \mathcal{W}_u} \frac{\Delta_j(k' \tau_s^G)}{\Delta_u(k' \tau_s^G)} \mathbf{w}_j(t) - \bar{\mathbf{w}}_u(t)\|^2]$  are expanded via (1), after which approximated gradients  $\nabla \tilde{F}_j$  are introduced and the result simplified using Jensen's inequality. Next, applying Assumption 1 for  $\sigma_j^F$  and using recursive techniques over  $\tau_s^L$  yields an upper bound for the local aggregation relationships. The global term  $\mathbb{E}[\|\frac{1}{U(s)} \sum_{u \in \mathcal{U}(s)} \sum_{j \in \mathcal{W}_u} \frac{\Delta_j(k' \tau_s^G)}{\Delta_u(k' \tau_s^G)} \bar{\mathbf{w}}_u(t) - \bar{\mathbf{w}}(t)\|^2]$  requires separate techniques, such as approximated aggregated gradients  $\nabla \bar{F}_u$  and recursion over  $\tau_s^G$ . ■

Considering the two terms in (16), term (a) captures the impact of the local aggregation frequency  $\tau_s^L$  while term (b) captures the *nested* impact of the local-global aggregation frequency  $\tau_s^L \tau_s^G$ . It can be seen that, to reduce the variance of ML models  $\mathbf{w}_j$  across workers  $j \in \mathcal{W}_u \forall u \in \mathcal{U}(s)$ , which is desirable as we will show in Theorem 1, the local or global aggregation periods  $\tau_s^L, \tau_s^G$  need to be reduced, i.e., more frequent aggregations. Proposition 1 suggests that the improvement is exponential. However, global aggregations consume more network resources than local aggregations in HN-PFL - they require bidirectional communications between worker and leader UAVs, and between leaders and APs during which non-leader UAVs continue to consume energy by remaining idle in the air. We balance this trade-off by obtaining the optimal UAV orchestration for a choice of  $\tau_s^L$  and  $\tau_s^G$  (Sec. IV), and then jointly optimizing  $\tau_s^L$  and  $\tau_s^G$  and UAV trajectories under optimal UAV orchestration (Sec. V).

Finally, we apply Proposition 1 to obtain our main result, which characterizes the decreasing magnitude of the gradient of (8), i.e., the global meta-function in HN-PFL, over training sequences. Since we consider non-convex ML models, the main metric of interest for learning performance is the norm squared of the meta-gradient.

**Theorem 1.** *[Global meta-gradient over training sequences] For training sequence  $\mathcal{T}_s$ , if  $\eta_2 < \frac{1}{6\mu^F}$ , we have the following upper bound on the expected cumulative average magnitude of the global meta-gradient across the active UAV swarms:*

$$\frac{1}{T_s} \sum_{t=t_{s-1}}^{t_s-1} \mathbb{E} \left[ \|\nabla \bar{F}(\mathbf{w}(t))\|^2 \right] \leq \Xi(s), \quad (17)$$

where  $\Xi(s)$  is given in (18).

*Sketch of Proof:* It can be verified that the gradient of meta-functions is  $\mu^F$ -Lipschitz continuous. Using this property for the global meta-function  $\bar{F}$ , and decomposing  $\bar{F}$  into its weighted average of constituent  $F_j$  using (6) and (8), allows us to segment the bound into two

$$\begin{aligned} \Upsilon(t) = & \underbrace{\left( \frac{16\eta_2^2}{U(s)} \sum_{u \in \mathcal{U}(s)} \sum_{j \in \mathcal{W}_u} \frac{\Delta_j(k' \tau_s^G)}{\Delta_u(k' \tau_s^G)} \sum_{y=1}^{\tau_s^L} \sigma_j^F(t-y) + \frac{24\eta_2^2}{U(s)} \sum_{u \in \mathcal{U}(s)} \gamma_u^F \right)}_{(a)} \frac{1 - (8 + 48(\eta_2 \mu^F)^2)^{\tau_s^L}}{1 - (8 + 48(\eta_2 \mu^F)^2)} \\ & + \underbrace{\left( \frac{16\eta_2^2}{U(s)} \sum_{u \in \mathcal{U}(s)} \sum_{y=1}^{\tau_s^L \tau_s^G} \sigma_u^F(t-y) + 24\eta_2^2 \gamma^F \right)}_{(b)} \frac{1 - (8 + 48(\eta_2 \mu^F)^2)^{\tau_s^L \tau_s^G}}{1 - (8 + 48(\eta_2 \mu^F)^2)} \end{aligned} \quad (16)$$

$$\begin{aligned} \Xi(s) \triangleq & \frac{1}{\frac{\eta_2}{2} - 6\eta_2^2 \frac{\mu^F}{2}} \left[ \frac{F^U(\mathbf{w}(t_{s-1})) - (F^U)^*}{T_s} + \frac{1}{T_s} \sum_{k'=1}^{K_s^G} \sum_{k=(k'-1)\tau_s^G+1}^{\tau_s^G k'} \sum_{t=(k-1)\tau_s^L}^{\tau_s^L k-1} \left[ \left( 3\eta_2^2 \frac{\mu^F}{2} + \eta_2 \right) \right. \right. \\ & \left. \left. \times \left( \frac{1}{U(s)} \sum_{u \in \mathcal{U}(s)} \sum_{j \in \mathcal{W}_u} \frac{\Delta_j(k' \tau_s^G)}{\Delta_u(k' \tau_s^G)} \sigma_j^F(t) + (\mu^F)^2 \Upsilon(t_s^G(k')) \right) + 3\eta_2^2 \mu^F \frac{1}{U(s)} \sum_{u \in \mathcal{U}(s)} \gamma_u^F \right] \right] \end{aligned} \quad (18)$$

terms: (i)  $\frac{1}{U(s)} \sum_{u \in \mathcal{U}(s)} \sum_{j \in \mathcal{W}_u} \frac{\Delta_j(k' \tau_s^G)}{\Delta_u(k' \tau_s^G)} \left[ \nabla \tilde{F}_j(\mathbf{w}_j(\tau_s^L \tau_s^G k' - 1)) - \nabla F_j(\mathbf{w}_j(\tau_s^L \tau_s^G k' - 1)) \right]$ , which is then bounded by successively applying Jensen's inequality and Lemma 1, and (ii)  $\frac{1}{U(s)} \sum_{u \in \mathcal{U}(s)} \sum_{j \in \mathcal{W}_u} \frac{\Delta_j(k' \tau_s^G)}{\Delta_u(k' \tau_s^G)} \left[ \nabla F_j(\mathbf{w}_j(\tau_s^L \tau_s^G k' - 1)) - \nabla F_j(\bar{\mathbf{w}}(\tau_s^L \tau_s^G k' - 1)) \right]$ , which is bounded by Proposition 1, Lemma 1, and Lemma 2. The results are then recursively expanded to get (17). The expressions are lengthy and thus omitted. The full proof is provided in Appendix B. ■

**Main takeaways.** Theorem 1 yields a general bound on the average gradient for HN-PFL with time-varying mini-batch sizes. Smaller values of the bound are desired, as it indicates closeness to a stationary point. This bound quantifies how several parameters (some controllable and others a factor of the environment) affect training performance. Specifically, the bound in (18) is dependent on the mini-batch ratios and processed data sizes at the UAVs (embedded in  $\Delta_j$ , and  $\Delta_u$ ), the initial performance of the ML model for the  $s$ -th training sequence (embedded in  $F^U(\mathbf{w}(t_{s-1}))$ ), the data variability (embedded in  $\sigma_j^F$ ,  $\sigma_u^F$ , and  $\Upsilon$ ), the gradient/Hessian characteristics (embedded in  $\mu^F$ ,  $\gamma_u^F$ , and  $\gamma^F$ ), the local/global aggregation periods (through the nested sums), and the inner and outer step-sizes ( $\eta_1$ ,  $\eta_2$ ).

Since HN-PFL conducts ML model training at the UAVs, the bound in Theorem 1 is based on the meta-functions defined at the UAVs. However, as the ML model is used by the devices and UAVs train on a subset of the cluster's total data, we need to bound the difference between the ML model performance at the UAVs and the devices. Henceforth, since the data at UAVs is assumed to be constant within a local aggregation period  $k$ , we refer to  $D_j(t) \forall j$  as  $D_j(k)$ .

**Lemma 3** (Meta-gradient mismatch between clusters and swarms). *Let  $F_c^D$  denote the meta-function defined based on  $f_c^D$  in Assumption 2,  $\mathcal{C}(s)$  denote the set of actively trained device clusters for training sequence  $s$ , and  $\bar{F}^D(\mathbf{w}(t)) = \frac{1}{|\mathcal{C}(s)|} \sum_{c \in \mathcal{C}(s)} F_c^D(\mathbf{w}(t))$ ,  $t \in \mathcal{T}_s$ , be the average meta-function for all actively trained device clusters for sequence  $s$  for a given parameter  $\mathbf{w}(t)$  at time  $t$ . The difference between the meta-gradient computed at the UAVs vs. those of their respective device clusters for local aggregation  $k$  is bounded by:*

$$\mathbb{E} \left[ \left\| \nabla \bar{F}(\mathbf{w}(t)) - \nabla \bar{F}^D(\mathbf{w}(t)) \right\|^2 \right] \leq \hat{\Xi}(k), \quad t = \tau_s^L(k), \quad (19)$$

where  $\hat{\Xi}(k)$  is given by:

$$\begin{aligned} \hat{\Xi}(k) \triangleq & \frac{1}{U(s)} \sum_{u \in \mathcal{U}(s)} \sum_{j \in \mathcal{W}_u} \frac{\Delta_j(k)}{\Delta_u(k)} \left[ \frac{3\eta_1^2 \sigma_{C(u,s)}^H}{D_j(k)} \left[ B^2 \right. \right. \\ & \left. \left. + \frac{\sigma_{C(u,s)}^G (1 + \mu^2 \eta_1^2)}{D_j(k)} \right] + \frac{12\sigma_{C(u,s)}^G (1 + \mu^2 \eta_1^2)}{D_j(k)} \right], \end{aligned} \quad (20)$$

where  $C(u, s)$  denotes the cluster which UAV swarm  $u$  trains during  $s$  and  $\sigma^H$  and  $\sigma^G$  are defined in Assumption 2.

*Proof.* Expanding the left hand side of (19) using the definitions of  $\nabla \bar{F}$  and  $\nabla \bar{F}^D$ , and upper bounding it using the Jensen's inequality yields  $\frac{1}{U(s)} \sum_{u \in \mathcal{U}(s)} \mathbb{E} [\| \nabla \bar{F}_u(\mathbf{w}(t)) - \nabla F_{C(u,s)}^D(\mathbf{w}(t)) \|^2]$ , where we substitute  $C(u, s)$  for  $c$  as the coupling of active UAV swarm to actively trained device cluster allows us to apply (6) onto  $\nabla \bar{F}_u$  and obtain:  $\frac{1}{U(s)} \sum_{u \in \mathcal{U}(s)} \sum_{j \in \mathcal{W}_u} \frac{\Delta_j(k)}{\Delta_u(k)} \mathbb{E} [\| \nabla F_j(\mathbf{w}(t)) - \nabla F_{C(u,s)}^D(\mathbf{w}(t)) \|^2]$  by applying of Jensen's inequality. Similar techniques used in Lemma 1 then yield the result. ■

The bound in Lemma 3 captures the effect of total data at the worker UAVs on the mismatch between the cluster and UAV swarm meta-gradients. In particular, as more data from the devices are transferred to the UAVs (increasing  $D_j(k)$ ), the error in (20) due to sampling decreases.

#### IV. DATA PROCESSING OPTIMIZATION FOR HN-PFL

Given our HN-PFL algorithm and its convergence behavior in Sec. III-B, we next aim to develop efficient ML model training for our system. To this end, we need to obtain the optimal orchestration of UAVs once they engage in model training (micro-level design) and the swarm trajectories (macro-level design). We break these down into two main components: (i) data transfer and processing configurations at UAVs during the training sequences (the blue block in Fig. 2) and (ii) learning sequence duration and UAV swarm trajectory/movement patterns in-between training sequences (the green block in Fig. 2). These two parts are intertwined, i.e., the model training performance at clusters affects the UAV trajectory design, and vice versa.

In this section, we address the first component, by formulating the UAV data processing and transfer optimization problem, and subsequently develop the second component in Sec. V. Our formulation will optimize the trade-off between model performance and energy consumption by configuring

key network parameters (Sec. IV-A). Then, we show that the resulting optimization can be characterized as a complementary geometric program, and develop an iterative *distributed optimization* method for solving it (Sec. IV-B).

#### A. Data Processing/Offloading Configuration

1) *Offloading and processing models*: At each training sequence  $s$ , each active UAV swarm  $u \in \mathcal{U}(s)$  is located above a device cluster denoted by  $\mathcal{C}(u, s) \in \mathcal{C}$ . Let  $A(u, s) \in \mathcal{A}$  denote the nearest AP to UAV swarm  $u$ , which leader  $\ell_u$  will periodically visit during the model training to conduct global model aggregation. Also, let  $\psi_j^F$  denote the energy consumed per unit time by worker/coordinator UAV  $j \in \mathcal{W}_u$  for flying/hovering, and  $\psi_u^F$  that of leader UAV  $\ell_u$ . We denote the geographical distance between leader  $\ell_u$  and its nearest AP as  $d(\ell_u, A)$ , and denote the movement energy consumption of the leader UAV per unit distance as  $\psi_{\ell_u}^M$ .

Device-UAV and UAV-UAV data transfers are carried out at the beginning of local aggregation rounds, i.e., when  $t = t_s^L(k)$ . The data received by the worker UAVs is used throughout the local aggregation period. Upon engaging in data transmission, each device  $i \in \mathcal{C}(u, s)$  samples data points uniformly at random from its local buffer and transmits them to the UAVs. We let  $\rho_{i,j}(k) \in [0, 1]$  denote the fraction of datapoints in the local dataset  $\tilde{D}_i(k)$  of the device that is transmitted to worker/coordinator UAV  $j \in \hat{u}$ . Coordinator UAVs act as data caches that facilitate multi-hop data relaying between the devices to worker UAVs used for ML model training. We let  $\rho_{h,j}(k) \in [0, 1]$  denote the fraction of the datapoints in the local dataset of the coordinator UAV  $h \in \hat{\mathcal{W}}_u$  that is forwarded to another UAV  $j \in \mathcal{W}_u$ . Each worker UAV  $j \in \mathcal{W}_u$  is assumed to process data with CPU cycle frequency  $g_j(k) \in [g_j^{\min}, g_j^{\max}]$ .

For sequence  $s$ , we denote the transmit powers of device  $i$ , UAV  $j$ , and leader  $\ell_u$  by  $P_i(s)$ ,  $P_j(s)$ , and  $P_{\ell_u}(s)$ , respectively. Through transmissions, either data or model parameters are transferred. We denote the number of bits used to represent one data point as  $\tilde{M}$ , and the number of bits used to represent the one model parameter vector as  $M$ .

UAV-to-UAV data transmissions are carried out through air-to-air (A2A) channels, which are considered to be line-of-sight (LoS). Device-to-UAV and leader UAV-to-AP transmissions are performed through ground-to-air (G2A) and air-to-ground (A2G) channels, respectively, which are a mixture of LoS and non-line-of-sight (NLoS) links. Denoting  $d(a, b)$  as the geographical distance between two nodes  $a$  and  $b$  ( $a, b \in \mathcal{U} \cup \mathcal{C}$ ), the path-loss model for the LoS link between two nodes  $a$  and  $b$  is then given by [53]:

$$L_{a,b}^{\text{A2A}} = \eta^{\text{LoS}} (\mu^{\text{Tx}} d(a, b))^{\alpha^{\text{PL}}}, \quad (21)$$

where  $\eta^{\text{LoS}} > 1$  denotes the excessive path loss factor for the LoS link,  $\alpha^{\text{PL}}$  is the path-loss exponent, and  $\mu^{\text{Tx}} = 4\pi f^{\text{Tx}}/c^{\text{light}}$  with  $c^{\text{light}}$  denoting the speed of light and  $f^{\text{Tx}}$  denoting the carrier frequency. For the G2A/A2G channel, the probability of having an LoS link between two nodes  $a$  and  $b$  is given by [53], [54]:  $P_{a,b}^{\text{LoS}} = (1 + \psi^{\text{Tx}} \exp(-\beta^{\text{Tx}}[\theta_{ab} - \psi^{\text{Tx}}]))^{-1}$ , where  $\psi^{\text{Tx}}$  and  $\beta^{\text{Tx}}$  are constants depending on the carrier frequency and the conditions of the environment, and  $\theta_{a,b}$  is the elevation angle between the

respective nodes defined as:  $\theta_{a,b} = \frac{180}{\pi} \times \sin^{-1} \left( \frac{\Delta h_{a,b}}{d(a,b)} \right)$ , with  $\Delta h_{a,b}$  denoting the difference in altitude between nodes  $a$  and  $b$ . The probability of NLoS link is given by  $P_{a,b}^{\text{NLoS}} = 1 - P_{a,b}^{\text{LoS}}$ . With this, the path-loss of an A2G/G2A link from node  $a$  to node  $b$  can be obtained as:

$$L_{a,b}^{\text{A2G}} = (\mu^{\text{Tx}} d(a, b))^{\alpha^{\text{PL}}} [P_{a,b}^{\text{LoS}} \times \eta^{\text{LoS}} + P_{a,b}^{\text{NLoS}} \times \eta^{\text{NLoS}}], \quad (22)$$

where  $\eta^{\text{NLoS}} > \eta^{\text{LoS}}$  denotes the excessive path loss factor for the NLoS link. Finally, the data-rate between two nodes  $a$  and  $b$  is given by:

$$R_{a,b} = \bar{B}_{a,b} \log_2 \left( 1 + \frac{P_a/L_{a,b}}{\sigma^2} \right), \quad a, b \in \mathcal{U} \cup \mathcal{C}, \quad (23)$$

where  $\bar{B}_{a,b}$  denotes the bandwidth,  $\sigma^2 = N_0 \bar{B}_{a,b}$  denotes the noise power with  $N_0$  as the noise spectral density,  $P_a$  is the transmit power of node  $a$ , and  $L_{a,b}$  is the path-loss obtained through either (21) or (22). We also use  $R_{a,b}(s)$  as the data rate between nodes  $a$  and  $b$ , given their transmit powers and locations during training sequence  $s$ . We ignore interference from simultaneous transmissions to the UAVs as they are stationary and can use orthogonal frequency bands [55].

We denote the time used for data gathering at UAV  $j$  as  $\zeta_j^G(k)$ , and the time used for data processing as  $\zeta_j^P(k)$ . We also define  $\zeta^{\text{Local}}$  as the maximum allowable time for data gathering and local computation before each UAV transmits its parameters to the leader UAV for aggregation.

2) *Joint energy and performance optimization*: With the aforementioned models in hand, we formulate the following optimization problem for determining data offloading/processing configuration at training sequence  $s$ :

$$(\mathcal{P}) : \min_{\rho, \theta, \alpha, g} (1 - \theta) \underbrace{\left( \theta_1 \Xi(s) + \theta_2 \sum_{k=1}^{K_s^L} \hat{\Xi}(k) \right)}_{(a)} \quad (24)$$

$$+ \theta \underbrace{\sum_{k=1}^{K_s^L} \sum_{u \in \mathcal{U}(s)} \left[ \sum_{j \in \hat{\mathcal{W}}_u} E_j^{\text{Tx}, \text{U}}(k) + \sum_{j \in \mathcal{W}_u} E_j^{\text{P}}(k) + \sum_{i \in \mathcal{C}(u, s)} E_i^{\text{Tx}, \text{C}}(k) \right]}_{(b)}$$

s.t.

$$E_j^{\text{P}}(k) = \tau_s^L \frac{\alpha_j c_j}{2} (\alpha_j(k)) D_j(k) g_j^2(k), \quad j \in \mathcal{W}_u, \forall u \quad (25)$$

$$E_i^{\text{Tx}, \text{C}}(k) = \sum_{j \in \hat{u}} \frac{\rho_{i,j}(k) \tilde{D}_i(k) \tilde{M}}{R_{i,j}(s)} P_i(s), \quad i \in \mathcal{C}(u, s), \forall u \quad (26)$$

$$E_j^{\text{Tx}, \text{U}}(k) = \sum_{h \in \hat{\mathcal{W}}_u} \frac{\rho_{j,h}(k) D_j(k) \tilde{M}}{R_{j,h}(s)} P_j(s), \quad j \in \hat{\mathcal{W}}_u, \forall u \quad (27)$$

$$E_j^{\text{Tx}, \text{W}} = K_s^L P_j(s) M / R_{j, \ell_u}(s), \quad j \in \mathcal{W}_u, \forall u \quad (28)$$

$$E_{\ell_u}^{\text{Tx}, \text{L}} = K_s^L P_{\ell_u}(s) \max_{j \in \mathcal{W}_u} \left\{ M / R_{\ell_u, j}(s) \right\}, \quad \forall u \quad (29)$$

$$E_j^{\text{F}, \text{U}} = T_s \psi_j^{\text{F}}, \quad j \in \hat{u}, \forall \hat{u} \quad (30)$$

$$E_{\ell_u}^{\text{F}, \text{L}} = T_s \psi_u^{\text{F}} + 2K_s^G \psi_u^{\text{M}}(d(\ell_u, A)), \quad \forall u \quad (31)$$

$$\sum_{k=1}^{K_s^L} E_j^{\text{P}}(k) + E_j^{\text{Tx}, \text{W}} + E_j^{\text{F}, \text{U}} \leq E_j^{\text{Ba}}(s) - E_j^{\text{Th}}, \quad j \in \mathcal{W}_u, \forall u \quad (32)$$

$$\sum_{k=1}^{K_s^L} E_j^{\text{Tx}, \text{U}}(k) + E_j^{\text{F}, \text{U}} \leq E_j^{\text{Ba}}(s) - E_j^{\text{Th}}, \quad j \in \hat{\mathcal{W}}_u, \forall u \quad (33)$$

$$E_{\ell_u}^{\text{Tx,L}} + E_{\ell_u}^{\text{F,L}} \leq E_{\ell_u}^{\text{Ba}}(s) - E_{\ell_u}^{\text{Th}}, \forall u \quad (34)$$

$$\sum_{j \in \hat{u}} \rho_{i,j}(k) \leq 1, i \in \mathcal{C}(u, s), \forall u \quad (35)$$

$$\sum_{h \in \mathcal{W}_u} \varrho_{j,h}(k) \leq 1, j \in \widehat{\mathcal{W}}_u, \forall u \quad (36)$$

$$D_j(k) = \sum_{i \in \mathcal{C}(u, s)} \rho_{i,j}(k) \tilde{D}_i(k) + \sum_{h \in \widehat{\mathcal{W}}_u} \varrho_{h,j}(k) D_h(k) \leq B_j^{\text{D}}(k), j \in \mathcal{W}_u, \forall u \quad (37)$$

$$D_j(k) = \sum_{i \in \mathcal{C}(u, s)} \rho_{i,j}(k) \tilde{D}_i(k) \leq B_j^{\text{D}}(k), j \in \widehat{\mathcal{W}}_u, \forall u \quad (38)$$

$$\zeta_j^{\text{G}}(k) + \zeta_j^{\text{P}}(k) \leq \zeta^{\text{Local}}, j \in u, \forall u \quad (39)$$

$$\zeta_j^{\text{G}}(k) = \sum_{i \in \mathcal{C}(u, s)} \rho_{i,j}(k) \tilde{D}_i(k) \tilde{M} / R_{i,j}(s) + \sum_{h \in \widehat{\mathcal{W}}_u} \varrho_{h,j}(k) D_h(k) \tilde{M} / R_{h,j}(s), j \in \hat{u}, \forall u \quad (40)$$

$$\zeta_j^{\text{P}}(k) = \tau_s^{\text{L}} c_j \alpha_j(k) D_j(k) / g_j(k), j \in \mathcal{W}_u, \forall u \quad (41)$$

$$g_j^{\text{min}} \leq g_j(k) \leq g_j^{\text{max}}, j \in \mathcal{W}_u, \forall u \quad (42)$$

$$0 \leq \rho_{i,j}(k) \leq 1, i \in \mathcal{C}(u, s), j \in \hat{u}, \forall u \quad (43)$$

$$0 \leq \varrho_{h,j}(k) \leq 1, h \in \widehat{\mathcal{W}}_u, j \in \mathcal{W}_u \quad (44)$$

$$\alpha_j(k) = \alpha_{j,1}(k) + \alpha_{j,2}(k) + \alpha_{j,3}(k), j \in \mathcal{W}_u, \forall u \quad (45)$$

$$0 < \alpha_{j,1}(k), \alpha_{j,2}(k), \alpha_{j,3}(k) \leq 1, j \in \mathcal{W}_u, \forall u \quad (46)$$

**Objective and variables.** The objective function in (24) captures the tradeoff between the expected ML model performance (term (a)) and the energy consumption during the training sequence (term (b)). Term (a) encompasses both the ML performance at the active UAV swarms (through  $\Xi$ ) and the mismatch to the ML performance at the device cluster (through  $\hat{\Xi}$ ), which we quantified in Theorem 1 and Lemma 3. We weigh the importance of the two terms in (a) with normalized positive coefficients  $\theta_1$  and  $\theta_2$ . The coefficient  $\theta \in [0, 1]$  weighs the importance of the terms in the objective function. The variables in the problem are the device-to-UAV data transfer configurations  $\rho = \{\rho_{i,j}\}_{i \in \mathcal{C}(u, s), j \in \hat{u}, u \in \mathcal{U}(s)}$ , the UAV-to-UAV data transfer configurations  $\varrho = \{\varrho_{h,j}\}_{h \in \widehat{\mathcal{W}}_u, j \in \mathcal{W}_u, u \in \mathcal{U}(s)}$ , the mini-batch ratios  $\alpha = \{\alpha_{j,1}, \alpha_{j,2}, \alpha_{j,3}\}_{j \in \mathcal{W}_u, u \in \mathcal{U}(s)}$ , and the UAV CPU frequency cycles  $\mathbf{g} = \{g_j\}_{j \in \mathcal{W}_u, u \in \mathcal{U}(s)}$ .

For the energy objective terms,  $E_j^{\text{P}}(k)$  in (25) denotes the energy consumption used for processing data during each meta-gradient update at worker UAV  $j \in \mathcal{W}_u$ , where  $a_j$  is the effective capacitance coefficient of UAV  $j$ 's chipset [22], and  $c_j$  is the number of CPU cycles to process each datapoint. In (26),  $E_i^{\text{Tx,C}}(k)$  is the energy used for data transmission ( $\text{Tx}$ ) from device  $i$  in cluster  $\mathcal{C}(u, s)$  to the UAVs. In (27), we define  $E_j^{\text{Tx,U}}(k)$  as the energy used for data transmissions from coordinator UAV  $j \in \widehat{\mathcal{W}}_u$  to other UAVs. In (28),  $E_j^{\text{Tx,W}}$  denotes the total energy consumed for ML model parameter transmission from worker UAV  $j \in \mathcal{W}_u$  to its associated leader, which occurs  $K_s^{\text{L}}$  times during the training sequence. In (29),  $E_{\ell_u}^{\text{Tx,L}}$  captures the energy consumption used for parameter transmission through broadcasting from leader  $\ell_u$  to worker UAVs  $j \in \mathcal{W}_u$ . In (30),  $E_j^{\text{F,U}}$  represents the total energy used

for flying/hovering by UAV  $j \in \hat{u}$  for the  $s$ -th training sequence, which can be obtained using the result of [56] for fixed-wing UAVs, and the result of [57] for rotatory wing UAVs. Similarly, in (31),  $E_{\ell_u}^{\text{F,L}}$  captures the energy consumption for flying by leaders  $\ell_u$ , accounting for levitation and round-trips to the nearest APs at the global aggregation instances.

**Constraints.** Constraint (32) ensures that the total energy consumed by each worker UAV  $j$  for data processing, parameter transmission and flying is less than  $E_j^{\text{Ba}}(s) - E_j^{\text{Th}}$ , where  $E_j^{\text{Ba}}(s)$  represents the battery energy at  $j$  at the start of the  $s$ -th training sequence and  $E_j^{\text{Th}}$  encompasses both (i) surplus idle energy needed for extra hovering time caused by potential asynchronicity due to the heterogeneity of leader UAV to AP travel times, and (ii) the minimum energy threshold for  $j$  to reach the nearest recharging station after the conclusion of the training sequence. Constraint (33) imposed on the coordinator UAVs is similar to (32), except that coordinator UAVs only conduct data transmission while flying. Constraint (34) imposed on the leader UAVs guarantees that there is enough energy remaining after parameter broadcasting and flying to reach the nearest recharging station. Constraints (35) and (36) ensure that the total amount of data offloaded from each device  $i \in \mathcal{C}(u, s)$  and each coordinator UAV  $h \in \widehat{\mathcal{W}}_u$  is less than the size of the available data set. As a result of this offloading, (37) and (38) capture the total number of datapoints at the UAVs. Constraint (39) ensures that the accumulated time used for data gathering  $\zeta_j^{\text{G}}(k)$  and local data processing  $\zeta_j^{\text{P}}(k)$  at each worker UAV  $j$  during one local aggregation is lower than the maximum allowable time for parameter transfer to the corresponding leader UAV  $\zeta^{\text{Local}}$ . These two quantities are in turn defined in (40) and (41). Finally, constraints (42)-(46) ensure the feasibility of the optimization variables.

**Complementary geometric program.**  $\mathcal{P}$  is a non-convex problem, since products of the optimization variables are present in the objective. For instance, in the definition  $E_j^{\text{P}}(n)$  in (25), there are multiplications between all four variable types:  $\alpha$ ,  $g$ ,  $\rho$ , and  $\varrho$  (the last two are encompassed in term  $D_j$  according to (37)). In fact, this problem can be categorized as a *complementary geometric program* [58], a particular class of non-convex and NP-hard optimization problems. Based on this classification, we will develop a distributed, iterative approach to solve  $\mathcal{P}$  where iterative approximation of the problem in the format of a geometric program (GP) is considered.

### B. Distributed Algorithm for Data Processing/Offloading

To solve  $\mathcal{P}$ , we first make two key observations:

**Observation 1: Complementary Geometric Programming.** GP is a method for converting a non-convex optimization problem into convex form when the objective and constraints are composed of *monomials* and *posynomials*. We provide an overview of this for the interested reader in Appendix C. Although the objective in  $\mathcal{P}$  is composed of multiplications between the variables, it does not follow the format of GP: the expressions of  $\Xi$  and  $\hat{\Xi}$  consist of terms that are in the format of ratio of two posynomials, which are not posynomials (e.g.,  $\frac{\Delta_j}{\Delta_j}$ ,  $\Upsilon$ , and  $\sigma_j^{\text{F}}$ , each of which contain arithmetic relationships of  $\rho$  and  $\varrho$  in the denominators). Rather,  $\mathcal{P}$  is a complementary GP, which cannot readily be translated to

$$\bar{\Delta}_u(k) \triangleq \sum_{j \in \mathcal{W}_u} \left( \alpha_{j,1}(k) + \alpha_{j,2}(k) + \alpha_{j,3}(k) \right) \left( \sum_{i \in \mathcal{C}(u,s)} \rho_{i,j}(k) \tilde{D}_i(k) + \sum_{h \in \tilde{\mathcal{W}}_u} \sum_{i \in \mathcal{C}(u,s)} \varrho_{h,j}(k) \rho_{i,h}(k) \tilde{D}_i(k) \right) \quad (47)$$

$$\bar{\Delta}_u(k) \geq \hat{\Delta}_u(k) \triangleq \prod_{j \in \mathcal{W}_u} \left[ \prod_{i \in \mathcal{C}(u,s)} \left[ \left( \frac{\tilde{\delta}_{i,j,1}(k) [\bar{\Delta}_u(k; m)]}{\tilde{\delta}_{i,j,1}(k; m)} \right)^{\frac{\tilde{\delta}_{i,j,1}(k; m)}{\Delta_u(k; m)}} \left( \frac{\tilde{\delta}_{i,j,2}(k) [\bar{\Delta}_u(k; m)]}{\tilde{\delta}_{i,j,2}(k; m)} \right)^{\frac{\tilde{\delta}_{i,j,2}(k; m)}{\Delta_u(k; m)}} \left( \frac{\tilde{\delta}_{i,j,3}(k) [\bar{\Delta}_u(k; m)]}{\tilde{\delta}_{i,j,3}(k; m)} \right)^{\frac{\tilde{\delta}_{i,j,3}(k; m)}{\Delta_u(k; m)}} \right] \right. \\ \left. \prod_{h \in \tilde{\mathcal{W}}_u} \prod_{i \in \mathcal{C}(u,s)} \left[ \left( \frac{\delta_{j,h,i,1}(k) [\bar{\Delta}_u(k; m)]}{\delta_{j,h,i,1}(k; m)} \right)^{\frac{\delta_{j,h,i,1}(k; m)}{\Delta_u(k; m)}} \left( \frac{\delta_{j,h,i,2}(k) [\bar{\Delta}_u(k; m)]}{\delta_{j,h,i,2}(k; m)} \right)^{\frac{\delta_{j,h,i,2}(k; m)}{\Delta_u(k; m)}} \left( \frac{\delta_{j,h,i,3}(k) [\bar{\Delta}_u(k; m)]}{\delta_{j,h,i,3}(k; m)} \right)^{\frac{\delta_{j,h,i,3}(k; m)}{\Delta_u(k; m)}} \right] \right], \quad (48)$$

where

$$\tilde{\delta}_{j,i,n}(k) \triangleq \alpha_{j,n}(k) \rho_{i,j}(k) \tilde{D}_i(k), \quad \delta_{j,h,i,n}(k) \triangleq \alpha_{j,n}(k) \varrho_{h,j}(k) \rho_{i,h}(k) \tilde{D}_i(k), \quad n \in \{1, 2, 3\}. \quad (49)$$

$$D_j(k) \triangleq \sum_{i \in \mathcal{C}(u,s)} \rho_{i,j}(k) \tilde{D}_i(k) + \sum_{h \in \tilde{\mathcal{W}}_u} \sum_{i \in \mathcal{C}(u,s)} \varrho_{h,j}(k) \rho_{i,h}(k) \tilde{D}_i(k), \quad (50)$$

$$D_j(k) \geq \hat{D}_j(k) \triangleq \prod_{i \in \mathcal{C}(u,s)} \left( \frac{\tilde{\lambda}_{i,j}(k) D_j(k; m)}{\tilde{\lambda}_{i,j}(k; m)} \right)^{\frac{\tilde{\lambda}_{i,j}(k; m)}{D_j(k; m)}} \prod_{h \in \tilde{\mathcal{W}}_u} \prod_{i \in \mathcal{C}(u,s)} \left( \frac{\lambda_{h,i,j}(k) D_j(k; m)}{\lambda_{h,i,j}(k; m)} \right)^{\frac{\lambda_{h,i,j}(k; m)}{D_j(k; m)}}, \quad (51)$$

where

$$\lambda_{i,j}(k) \triangleq \rho_{i,j}(k) \tilde{D}_i(k), \quad \tilde{\lambda}_{h,i,j}(k) \triangleq \varrho_{h,j}(k) \rho_{i,h}(k) \tilde{D}_i(k). \quad (52)$$

convex form [58]. We exploit a method based on *posynomial condensation* to approximate the ratios of two posynomials appearing in the expressions of  $\Xi$  and  $\hat{\Xi}$  (via approximating  $\bar{\Delta}_u$  and  $D_j$  where needed) as the ratio between a posynomial and a monomial. Since the ratio of a posynomial and a monomial is a posynomial, we then can convert the approximations into geometric programs.

### Observation 2: Potential of Distributed Implementation.

In  $\mathcal{P}$ , all of the constraints are separable with respect to the UAV swarm index  $u$ , and the objective function (including the terms  $\Xi$  and  $\hat{\Xi}$ ) can be written as a sum of separable functions with respect to the UAV swarm index. In practice, however,  $\gamma^F$  (defined in Lemma 2) and  $\mu^F$  (defined in Proposition 1) cannot be locally and independently computed by UAV swarms  $u \in \mathcal{U}(s)$ , as it depends on the maximum over all worker UAVs in the network. We can approximate  $\gamma^F$  and  $\mu^F$  by estimating it at the core network at the instance of global aggregations, and subsequently broadcast it to the leader UAVs through the APs. With the knowledge of  $\gamma^F$  and  $\mu^F$  at the swarm leaders, the problem can then be decomposed among the local aggregation instances  $k \in \{1, \dots, K_s^L\}$  and solved distributively by each swarm  $u \in \mathcal{U}(s)$  at its leader.

**Developing the solver:** First, we must convert the ratio of posynomials in the objective of  $\mathcal{P}$  into that of a posynomial and a monomial. To do so, we iteratively approximate the posynomial denominators, which are  $\bar{\Delta}_u$  and  $D_j$  in our case, using the arithmetic-geometric mean inequality (see Lemma 5 in Appendix C). The resulting approximations for iteration  $m+1$  are given in (48) and (51), where  $m$  is the iteration index. Here, the solution to the problem at the  $m$ -th approximation iteration is denoted  $\mathbf{x}[m] = \{\varrho[m], \rho[m], \alpha[m], \mathbf{g}[m]\}$ .  $\bar{\Delta}_u(k; m)$ ,  $\delta_{j,h,i,n}(k; m)$ , and  $\tilde{\delta}_{i,j,n}(k; m)$ ,  $n \in \{1, 2, 3\}$  in (48) and  $D_j(k; m)$ ,  $\lambda_{h,i,j}(k; m)$ , and  $\tilde{\lambda}_{i,j}(k; m)$  in (51) are scalar values obtained by substituting the solution at iteration  $m$  (i.e.,  $\mathbf{x}[m]$ ) in the corresponding expressions in (47), (49), (50), and (52), respectively. It can be verified that the approximations in (48) and (51) are in fact the best local monomial approximations to their respective posynomials near the fixed point  $\mathbf{x}[m]$  in the sense of the first-order Taylor approximation.

### Algorithm 1: Distributed network-aware optimization of HN-PFL under partial global knowledge

**input** : Convergence criterion between two consecutive iterations. Estimated Lipschitz continuity factors (i.e.,  $\mu^G$ ,  $\mu^H$ , and  $\mu^F$ ), estimated data variability (i.e.,  $\sigma^H$  and  $\sigma^G$ ), and estimated data quantities (i.e.,  $D_j(k)$ ) at devices, all of which are obtained based on historical data observations.

- 1 // Procedure at the UAV swarms
- 2 for  $k' \in \{1, \dots, K_s^G\}$  do
- 3 // Procedure at the core network
- 4 for  $\ell_u \in \mathcal{L}(s)$  do
- 5 // Procedure conducted across the UAV swarms in parallel using their leader
- 6 for  $k \in \{(k' - 1)\tau_s^G + 1, \dots, k'\tau_s^G\}$  do
- 7 Initialize the iteration count  $m = 0$ .
- 8 Choose an initial feasible point
- 9  $\mathbf{x}[0] = [\rho[0], \varrho[0], \alpha[0], \mathbf{g}[0]]$  for  $\tilde{\mathcal{P}}_0$  at  $k$ .
- 10 while convergence criterion is not met OR  $m = 0$  do
- 11 Obtain the scalar values for  $\bar{\Delta}_u(k; m)$ ,  $\tilde{\delta}_{j,i,n}(k; m)$ ,  $\delta_{j,h,i,n}(k; m)$ ,  $D_j(k; m)$ , and  $\lambda_{i,j}(k; m)$ ,  $\tilde{\lambda}_{h,i,j}(k; m)$  by substituting  $\mathbf{x}[m]$  in (47), (49), (50), and (52).
- 12 Use the above scalars to obtain the monomial approximations given in (48) and (51), and replace them in  $\tilde{\mathcal{P}}_m$ .
- 13 Apply the logarithmic change of variables and take the log from the constraints of  $\tilde{\mathcal{P}}_m$  and convert it to a convex optimization problem (as in (93) in Appendix C).
- 14 Solve the resulting convex optimization problem to obtain  $\mathbf{x}[m+1]$  (e.g., using CVX [59]), and set  $m = m + 1$ .
- 15 Choose the obtained point as  $\mathbf{x}^* = \mathbf{x}[m] = [\rho^*, \varrho^*, \alpha^*, \mathbf{g}^*]$ .
- The leader broadcasts the solution  $\mathbf{x}^*$  among its constituent workers/coordinators/devices to start their respective data transfer procedures, and specifically for workers to tune their CPU cycles and mini-batch sizes.

We solve  $\mathcal{P}$  in a distributed manner at each UAV swarm through sequentially applying the above approximations to obtain problem  $\tilde{\mathcal{P}}_m$  at iteration  $m$ . In  $\tilde{\mathcal{P}}_m$ , each constraint is an inequality on posynomials, and the objective function is a sum of posynomials, admitting the GP format:

$$(\tilde{\mathcal{P}}_m) : \min_{\rho, \mathbf{g}, \alpha, \mathbf{g}} (1 - \theta) \tilde{a}_m + \theta(b) \quad \text{s.t.} \quad (25) - (46),$$

where term  $\tilde{a}_m$  is obtained from term  $(a)$  in problem  $\mathcal{P}$  by: (i) decomposing  $(a)$  into a sum of separable functions with respect to UAV swarm indexes; and then (ii) using the expressions in (48) and (51) for iteration  $m$  in  $(a)$ . Note that term  $(b)$  defined in (24) is indexed by UAV swarm  $u$ , and the constraints of  $\tilde{\mathcal{P}}$  are with respect to UAV swarm.

The pseudocode of our resulting sequential approximation method is given in Algorithm 1. The problem is solved at the beginning of each global aggregation interval  $k'$  by the leader UAVs in each active swarm. The following proposition shows that the algorithm has the most desirable convergence properties for a non-convex solver:

**Proposition 2.** *Algorithm 1 generates a sequence of improved feasible solutions for problem  $\tilde{\mathcal{P}}_m$  that converge to a point  $\mathbf{x}^*$  satisfying the Karush-Kuhn-Tucker (KKT) conditions of  $\mathcal{P}$ .*

*Sketch of Proof:* The proof uses the fact that the algorithm iteratively solves an *inner approximation* for problem  $\mathcal{P}$ , where sufficient conditions for convergence to KKT solutions expressed in [60] are satisfied. Details are in Appendix D. ■

## V. SWARM TRAJECTORY AND TEMPORAL DESIGN

Our developed HN-PFL methodology (Sec. I) and ML performance and energy optimization (Sec. II) are the fundamental components of our UAV-assisted ML methodology. In fact, in cases where the swarms are deployed and *stationary* above the clusters (e.g., [7], [8]), these two components are enough to achieve optimal ML performance and energy efficiency.

Nevertheless, we go further by generalizing our methodology to a more realistic scenario where there are more clusters than UAV swarms, which requires UAV swarms to travel among the clusters, and thus necessitates the swarm trajectory design. It is this generalization that motivates swarm trajectory and temporal (e.g., length of ML training sequence) design components (the green block of Fig. 2). Together our three components, depicted in Fig. 2 and developed in Sec. III, IV, and V, complete our holistic methodology.

Upon completion of a training sequence using our HN-PFL and performance optimization components (Sec. III and IV), the UAVs will then travel to another destination (i.e., another device cluster).<sup>3</sup> We will next design the swarm trajectories, sequence duration, and aggregation periodicity for the training sequences to maximize the ML performance.

### A. Online Model Training under Model/Concept Drift

Since we consider *online model training*, where the data distributions at the devices are time varying, the performance of the local model changes over time. To capture this effect, we introduce the notion of *model/concept drift*.

**Definition 1 (Model/Concept Drift).** *For device cluster  $c$  with local meta-loss function  $F_c$ , we denote the online model drift at time  $t$  by  $\Lambda_c(t) \in \mathbb{R}^+$ , which captures the maximum variation*

<sup>3</sup>Positioning of the UAVs, i.e., how individual UAVs are spread throughout a device cluster and their 3D positions, is not the focus of this work and can be computed apriori at the core network [57], [61].

*of the gradient for any given model parameter across two consecutive time instances; mathematically:*

$$\left\| \nabla F_c \left( \mathbf{w} \middle| \tilde{\mathcal{D}}(t) \right) - \nabla F_c \left( \mathbf{w} \middle| \tilde{\mathcal{D}}(t-1) \right) \right\|^2 \leq \Lambda_c(t), \forall \mathbf{w} \quad (53)$$

Device clusters with higher values of model drift are likely to require more frequent recalibration of their local models (achieved by revisiting with UAV swarms), as their local models become obsolete faster. In contrast, clusters with smaller model drift, i.e., small fluctuations in local gradient, may not be worth revisiting, due to marginal rewards (in terms of model performance gains) per energy consumed. Also, if clusters experience large and consistent model/concept drift, then the learning duration  $T_s$  should be smaller as the network will require swarms to re-calibrate local models more frequently. Model drift can be estimated every time a UAV swarm returns to a previously visited cluster by comparing historical meta-gradient vs. current meta-gradient computed by upon arrival.

Next, we demonstrate how model drift can be utilized to estimate local model performance given the current data distribution at a device cluster:

**Lemma 4 (Estimating online gradient via model drift).** *Let  $t_c^V$  denote a time instance when device cluster  $c$  was visited by a UAV swarm,  $\mathbf{w}_c(t_c^V)$  denote the corresponding local model, and  $\nabla F_c(\mathbf{w}_c(t_c^V) | \tilde{\mathcal{D}}_c(t_c^V))$  denote the local gradient. Consider time instance  $t \geq t_c^V + 1$ , where during the time interval  $[t_c^V + 1, t]$  cluster  $c$  remains unvisited by UAV swarms. Given the updated data at device cluster  $c$ , i.e.,  $\tilde{\mathcal{D}}_c(t)$ , the local meta gradient at the device cluster for the outdated local model is upper bounded as:*

$$\left\| \nabla F_c \left( \mathbf{w}_c(t_c^V) | \tilde{\mathcal{D}}_c(t) \right) \right\|^2 \leq \underbrace{(t - t_c^V + 1) \left\| \nabla F_c \left( \mathbf{w}_c(t_c^V) | \tilde{\mathcal{D}}_c(t_c^V) \right) \right\|^2}_{(a)} + \underbrace{(t - t_c^V + 1) \sum_{t'=t_c^V+1}^t \Lambda_c(t')}_{(b)}, \quad (54)$$

where  $\Lambda_c(\cdot)$  is defined in (53). Subsequently, assuming an upper bound on the model drift at the device cluster  $\Lambda_c(t') \leq \Lambda_c$ ,  $t' \in [t_c^V + 1, t]$ , we have:  $\left\| \nabla F_c \left( \mathbf{w}_c(t_c^V) | \tilde{\mathcal{D}}_c(t) \right) \right\|^2 \leq (t - t_c^V + 1) \left\| \nabla F_c \left( \mathbf{w}_c(t_c^V) | \tilde{\mathcal{D}}_c(t_c^V) \right) \right\|^2 + (t - t_c^V + 1)(t - t_c^V) \Lambda_c$ .

*Sketch of Proof:* The proof is carried out using the definition of model drift in (53) and applying the Cauchy-Schwarz inequality. Refer to Appendix E for the complete proof. ■

The bound in (54) demonstrates that the real-time performance of the outdated model, measured through the value of the meta gradient, becomes obsolete linearly with time (term (a)) and cumulative value of the model drift at the device cluster (term (b)). We will incorporate this result in the design of UAV swarm trajectories.

### B. Problem Formulation and DRL Characteristics

1) *Background:* In the following, we first formulate the problem of UAV swarm trajectory design and learning sequence duration. We then cast the problem as a sequential decision making problem. Subsequently, we develop a deep reinforcement learning (DRL) methodology by encoding the

real-time characteristics of our network into *states* for the DRL, defining a calculation methodology for the *actions* available for the DRL, and linking the actions to DRL *reward* calculations by embedding the optimization methodology from Section IV.

For training sequence  $s$ , let  $X_u(s)$  denote the location of UAV swarm  $u$ ,  $\Lambda_c(s)$  denote the latest estimation of the model drift of device cluster  $c$ ,  $E_u(s)$  denote the minimum remaining battery among the UAVs belong to swarm  $u$ , and  $G_c(s)$  denote the latest value of the gradient at device cluster  $c$ . Since the duration of ML model training  $T_s$ ,  $\forall s$ , is usually far smaller than the delay between consecutive visits to the same device cluster, we assume that the effect of model drift during model training is negligible, as we do so in Section III, and instead integrate the effects of model drift in our DRL design caused by delay between consecutive visits of the device cluster. For device cluster  $c$ , if it has been visited during sequence  $s$ , i.e.,  $c \in \mathcal{C}(s)$ ,  $G_c(s)$  captures its recent gradient:  $G_c(s) = \left\| \nabla F_c(\mathbf{w}_c(t_s + T_s) | \tilde{\mathcal{D}}_c(t_s + T_s)) \right\|^2$  measured at the end of the training sequence; however, if it is not visited, i.e.,  $c \in \bar{\mathcal{C}}(s)$ , then  $G_c(s) = \left\| \nabla F_c(\mathbf{w}_c(t_s^V) | \tilde{\mathcal{D}}_c(t_s)) \right\|^2$ , which is computed via the bound in (54). Also, we let  $E^M(s)$  denote the sum of energy of movement of the UAV swarms to travel to their current location in training sequence  $s$  from their previous locations in sequence  $s - 1$ , and let  $O(s)$  denote the value of the final objective function of  $\mathcal{P}$  solved in Section IV encompassing both the energy used for model training and the gradient of those devices under model training.

2) *Problem Formulation*: Given a total of  $S$  ML model training sequences, we propose the following formulation to determine the optimal trajectory design and temporal ML characteristics:

$$(\hat{\mathcal{P}}) : \min_{\left\{ \begin{array}{l} \mathcal{X}(s) \\ \mathcal{T}(s) \end{array} \right\}_{s=1}^S} \frac{1}{S} \sum_{s=1}^S \left[ c_1 E^M(s) + c_2 O(s) + c_3 \sum_{c \in \bar{\mathcal{C}}(s)} G_c(s) \right] \quad (55)$$

s.t.

$$E_u(s) \geq E^T, u \in \mathcal{U}(s), s \in \{1, \dots, S\} \quad (56)$$

$$\mathcal{T}(s) \in \mathcal{T}^F, s \in \{1, \dots, S\}, \quad (57)$$

where  $\mathcal{X}(s) \triangleq \{X_1(s), \dots, X_U(s)\}$ , and  $\mathcal{T}(s) \triangleq \{T_s \cup \tau_s^L \cup \tau_s^G\}$ . The objective function in (55) consists of three parts, the energy required for swarms to move to their next destination ( $E^M(s)$ ), the data offloading/processing objective function result ( $O(s)$  derived from  $\mathcal{P}$ ), and the estimated online gradient as a result of model drift at clusters without UAV training ( $G_c(s), c \in \bar{\mathcal{C}}(s)$ ). Constraint (56) ensures that swarms have sufficient energy  $E^T$ , at all times, to travel to a recharging station before they can no longer sustain their flight, and constraint (57) guarantees that the temporal ML characteristics  $\mathcal{T}(s) \triangleq \{T_s \cup \tau_s^L \cup \tau_s^G\}$ ,  $\forall s$ , are always within some feasible set  $\mathcal{T}^F$ . Finally,  $c_1$ ,  $c_2$ , and  $c_3$  in (55) scale the objective components.

Solving  $\hat{\mathcal{P}}$  faces the following challenges: (i) the effects of training at a previous device cluster carries over to all future training sequences, at any device cluster, (ii)  $\hat{\mathcal{P}}$  is a combinatorial problem, which suffers from the *curse of dimensionality*, since at each sequence the core network must assign the swarms to either device clusters or recharging stations, and (iii)  $\hat{\mathcal{P}}$  is defined over an unknown environment,

i.e., neither the data distributions at the device clusters nor the model/concept drift are known apriori. These facts motivate us to cast the problem as a *sequential decision making problem*, which is solved at the core network for each training sequence by encoding the network aspects as reinforcement learning objectives. Classical reinforcement learning methods rely on a pre-built Q-table to determine future actions and associated network states [62], but, due to the aforementioned challenges of our problem, in particular the curse of dimensionality, building a Q-table is infeasible. Motivated by the success that recurrent neural networks (RNN) exhibited as the deep Q-network for sequential decision making [63], [64], we adapt an RNN based DRL featuring LSTM layers.

3) *State of the DRL*: We encode the locations of the UAV swarms, the model drift and gradients at device clusters, and the temporal ML characteristics (i.e., total time, local-global aggregation periods) as the state of the DRL. Formally, we define the state at the end of training sequence  $s$ ,  $\mathcal{Z}(s)$ , as:

$$\mathcal{Z}(s) = \mathcal{U}(s) \cup \mathcal{X}(s) \cup \Lambda(s) \cup \mathcal{E}(s) \cup \mathcal{G}(s) \cup \mathcal{T}(s), \quad (58)$$

where  $\mathcal{U}(s)$  denotes the set of active UAV swarms,  $\mathcal{X}(s)$  denotes the locations of all the swarms,  $\Lambda(s) = \{\Lambda_1(s), \dots, \Lambda_C(s)\}$  are the latest model drift estimates observed at the device clusters,  $\mathcal{E}(s) = \{E_1(s), \dots, E_U(s)\}$ ,  $\mathcal{G}(s) = \{G_1(s), \dots, G_C(s)\}$ , and  $\mathcal{T}(s) = \{T_s \cup \tau_s^L \cup \tau_s^G\}$ .

4) *Action of the DRL*: The core network, as the DRL agent, determines the active UAV swarms  $\mathcal{U}(s+1)$ , their locations  $\mathcal{X}(s+1)$ , and the temporal behavior  $\mathcal{T}(s+1)$  of the next training sequence. In particular, we define the DRL action,  $\mathcal{H}(s)$ , as:

$$\mathcal{H}(s) = \mathcal{X}(s+1) \cup \mathcal{U}(s+1) \cup \mathcal{T}(s+1). \quad (59)$$

5) *Reward of the DRL*: The DRL agent aims to maximize the reward of each action  $\mathcal{H}(s)$  with respect to the current state  $\mathcal{Z}(s)$  via the objective value of  $\hat{\mathcal{P}}$ . Formally, we define the reward of the agent as:

$$V(s) = C \underbrace{\left( c_1 O(s) + c_2 \sum_{c \in \bar{\mathcal{C}}(s)} G_c(s) + c_3 E^M(s) \right)^{-1}}_{(a)} - P \underbrace{\sum_{u \in \mathcal{U}} \mathbb{1}_{\{E_u \leq E^T\}}}_{(b)} \quad (60)$$

where (a) captures the (inverse) value of the objective function of  $\hat{\mathcal{P}}$  for a particular training sequence  $s$ , and (b) is a penalty function with  $P \gg 1$ , capturing the case where UAVs' battery level drops below  $E^T$ , upon which the indicator  $\mathbb{1}_{\{E_u \leq E^T\}}$  takes the value of one for UAV swarm  $u$ .

**Main Takeaways.** Our reward function in (60) captures multiple possibly competing objectives: (i) it motivates visiting device clusters that benefit from network-aware ML model training, i.e., those that require less energy to achieve a better model, (ii) it avoids leaving clusters with larger model drifts (via  $G_c(s)$ ) unvisited for long periods of time, (iii) it promotes visiting clusters with high performance gain (via  $O(s)$ ) as compared to ML energy consumption, and (iv) it avoids situations where swarm battery levels would drop below a threshold (via term (b)).

6) *DRL Learning Architecture*: We exploit an RNN with LSTM layers to approximate the optimal action-value function based on the Bellman equation:

$$Q^*(\mathcal{Z}(s), \mathcal{H}(s)) = \mathbb{E} \left[ V(s) + \gamma \max_{\mathcal{H}(s+1)} Q^*(\mathcal{Z}(s+1), \mathcal{H}(s+1)) \mid \mathcal{Z}(s), \mathcal{H}(s) \right], \quad (61)$$

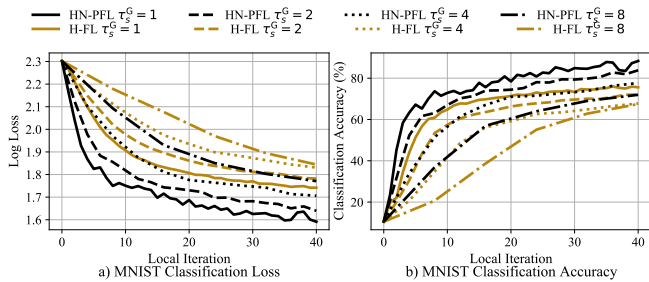


FIGURE 4: ML architecture comparisons for MNIST with fixed  $\tau_s^L = 1$ . HN-PFL demonstrates faster convergence and better final classification accuracy than H-FL for various  $\tau_s^G$ .

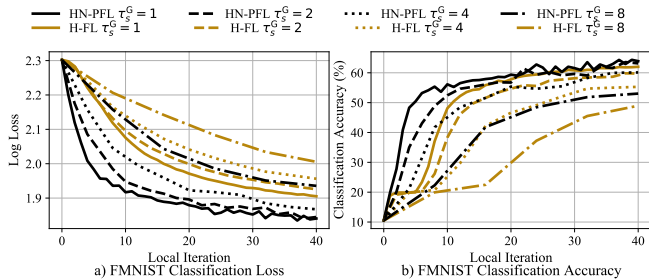


FIGURE 5: ML architecture comparisons for FMNIST with fixed  $\tau_s^L = 1$ . HN-PFL demonstrates faster convergence than H-FL for various  $\tau_s^G$  in this more challenging task.

where  $\gamma$  is the future reward discount. We use one RNN to approximate  $Q^*$  called the *train Q-network*  $Q_\theta(\mathcal{Z}(s), \mathcal{H}(s))$ , which we train by adjusting its parameters  $\theta$  to reduce the mean-squared error (MSE). Classical deep Q-network techniques determine the MSE of the train Q-network with respect to a target reward  $y(s)$  that also depends on the train Q-network's model parameters  $\theta$ . This self-coupling produces over-estimation, so we use an additional RNN called *target Q-network*  $\hat{Q}_\theta$  with parameters  $\theta$  to produce accurate loss measurements and periodically synchronize the target Q-network to the train Q-network. Furthermore, to prevent correlations in the environment observation sequence from influencing the parameters  $\theta$  in the *train Q-network*, we use *experience replay* to sample a randomized mini-batch of  $\mathcal{M}^Q$  experience tuples, each of which is of the form  $(\mathcal{Z}(s), \mathcal{H}(s), V(s), \mathcal{Z}(s+1))$ , to calculate MSE. In particular, we compute the mean-squared error as:

$$L(\theta) = \frac{1}{|\mathcal{M}^Q|} \sum_{s \in \mathcal{M}^Q} (Q_\theta(\mathcal{Z}(s), \mathcal{H}(s)) - y(s))^2, \quad (62)$$

where  $y(s) = V(s) + \gamma \max_{\mathcal{H}(s+1)} \hat{Q}_\theta(\mathcal{Z}(s+1), \mathcal{H}(s+1))$  is the target reward. Using the MSE, we then perform SGD to adjust the parameters  $\theta$ . Since this procedure requires at least  $M^Q$  previous experience tuples (saved in a deque-style buffer of size  $B^Q$ ), and each training sequence  $s$  only generates a single tuple, the RNN training requires at least  $M^Q$  training sequences before it begins. In order to generate representative experience tuples from the environment before the RNN is properly trained and to ensure that the DRL process is better able to find the global maximum (rather than getting stuck in a local maxima), we utilize an  $\epsilon$ -greedy policy [65], wherein with probability  $\epsilon$  the agent will select an action randomly and with probability  $(1 - \epsilon)$  the agent will determine the action based on the train Q-network  $Q_\theta$ . As the train Q-network improves over time,  $\epsilon$  decreases with limit  $\epsilon^{\min} \leq \epsilon$ .

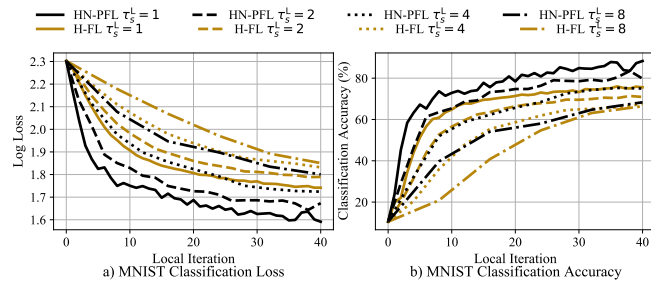


FIGURE 6: Using the same network for MNIST as Fig. 4, this experiment fixes  $\tau_s^G = 1$  to vary  $\tau_s^L$  instead. Our methodology HN-PFL continues to outperform H-FL consistently.

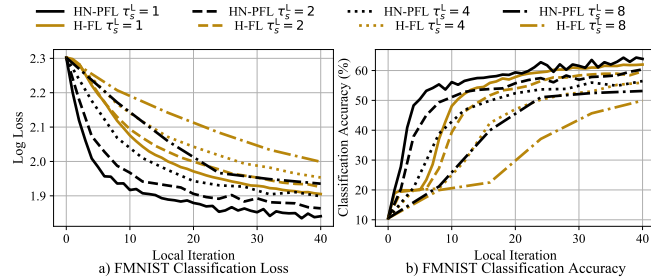


FIGURE 7: Using the same network for FMNIST as Fig. 5, this experiment fixes  $\tau_s^G = 1$  to vary  $\tau_s^L$  instead. Our methodology HN-PFL converges more rapidly than H-FL for all test cases.

### C. System Integration: A Holistic Solution for UAV-enabled Online ML Over Heterogeneous Networks

In the past few sections, we developed our methodology for network-aware UAV-enabled online model training, which comprises HN-PFL from Sec. III, the data processing/offloading optimization from Sec. IV, and the swarm trajectory and ML design from Sec. V. The interconnection between the different components is visualized in Fig. 2, which we provided a high level discussion on in Sec. II-C. Given our introduced variables and parameters in Sec. III, IV, and V, we can now further comment on the interdependence.

Specifically, the HN-PFL methodology (orange block) is implemented by the UAV swarms, and operates based on the reception of transfer/processing parameters (i.e.,  $\rho, \mathbf{g}, \alpha, \mathbf{f}$ ) from the data processing optimization at the swarm leaders (blue block). The ML training results and UAV battery statuses are embedded into network states and form the bases of our swarm trajectory (i.e.,  $\mathcal{X}(s)$ ) and temporal training decisions (i.e.,  $\mathcal{T}(s), \tau_s^L, \tau_s^G$ ) for the training sequences (green block), which is then shared from the core network to the swarm leaders. With these core network decisions, the next sequence of ML training will begin, and the cycles continues.

## VI. NUMERICAL EVALUATION AND DISCUSSION

In this section, we conduct numerical evaluations of our proposed methodology. When literature contains existing techniques, such as hierarchical federated learning (H-FL) [34], we compare our methodology against it; otherwise, we develop heuristic algorithms as baselines. For brevity, we describe the UAV network parameters and MNIST and F-MNIST datasets used for model training in Appendix F.

### A. HN-PFL Proof-of-Concept

We start by investigating the HN-PFL procedure from Sec. III, by comparing its performance (measured via clas-

TABLE II: Energy Consumption for MNIST to Reach 65% Classification Accuracy

Ratio		MNIST (kJ)			Ratio		MNIST (kJ)		
$\tau_s^L$	$\tau_s^G$	HFL	HNPFL	Savings	$\tau_s^L$	$\tau_s^G$	HFL	HNPFL	Savings
1	1	4.64	2.32	50.0%	1	1	4.64	2.32	50.0%
1	2	8.13	4.06	50.1%	2	1	9.29	4.64	50.1%
1	4	14.51	8.13	44.0%	4	1	15.10	8.13	46.2%
1	8	19.73	17.99	8.8 %	8	1	18.57	14.51	21.9%

sification accuracy, loss, and energy consumption) to that of hierarchical federated learning (H-FL) proposed in [34]. For this simulation, we consider a network composed of 4 UAV swarms with 2-3 workers, where each swarm has data from only 3 labels (thus, non-i.i.d. data distributions) and data quantity determined randomly from a Gaussian distribution:  $\mathcal{N}(2500, 250)$  for MNIST and  $\mathcal{N}(3500, 350)$  for FMNIST. As a proof-of-concept, we strictly isolate the performance of the distributed ML methodologies to the UAV layers, i.e., we assume the data has already been transferred to the worker UAVs. For a fair comparison between HN-PFL and H-FL, we ensure that both methodologies train over the same amount of data for each of their iterations by defining the batch size for H-FL as  $\alpha^{\text{HFL}}$  and setting each batch ratio for HN-PFL as  $\alpha_{j,i} \triangleq \lfloor \frac{1}{3}\alpha^{\text{HFL}} \rfloor \forall i \in \{1, 2, 3\}$ . Finally, we use the following settings for ML model training:  $\eta = \eta_1 = 10^{-3}$  and  $\eta_2 = 10^{-2}$ , where  $\eta$  is the learning rate for gradient descent in H-FL, and to avoid lengthy Hessian computations, we use the Hessian first-order approximation (see Remark 1).

Due to the hierarchical nature of HN-PFL, we investigate the impacts of local and global aggregations on the performance and efficiency of the ML training separately. We first investigate the effects of varying global aggregation period  $\tau_s^G$  from [1, 8] and fix local aggregation period (i.e.,  $\tau_s^L = 1$ ) in Fig. 4 for MNIST. We repeat this experiment with fixed  $\tau_s^G = 1$  and vary  $\tau_s^L$  from [1, 8] in Fig. 6, also for MNIST. The corresponding FMNIST experiments are in Fig. 5 and 7. Due to the non-iid and non-convex natures of our problem, the noisy convergence seen in Figs. 4-7 is expected.

For both MNIST and FMNIST, HN-PFL attains better final model accuracy and classification loss over its H-FL counterpart. For example, when  $\tau_s^L = \tau_s^G = 1$ , HN-PFL outperforms H-FL in classification accuracy by  $\sim 10\%$  for MNIST and  $\sim 3\%$  for FMNIST. When we increase the aggregation period, the model performances decrease for all test cases because the total iterations are fixed and thus longer aggregation periods result in fewer aggregations within the same timeframe. Fewer aggregations leads to worse performance as a result. Nonetheless, HN-PFL is able to maintain its advantage as  $\tau_s^G$  or  $\tau_s^L$  increases for both MNIST and FMNIST. Furthermore, HN-PFL has notably faster convergence speed than H-FL, e.g., to attain 55% accuracy for MNIST when  $\tau_s^L = 1$  and  $\tau_s^G = 2$ , HN-PFL needs only 5 iterations while H-FL uses 10 iterations. The faster convergence of HN-PFL results in less network energy expenditures in the form of flight, processing, and communication energy among UAVs in order to reach desired accuracy thresholds. We demonstrate the energy savings of HN-PFL in Table II for MNIST and Tables III for FMNIST. For each table, we selected model accuracies that are reachable for all combinations of  $\tau_s^L$  and

TABLE III: Energy Consumption for FMNIST to Reach 45% Classification Accuracy

Ratio		FMNIST (kJ)			Ratio		FMNIST (kJ)		
$\tau_s^L$	$\tau_s^G$	HFL	HNPFL	Savings	$\tau_s^L$	$\tau_s^G$	HFL	HNPFL	Savings
1	1	5.22	2.32	55.6%	1	1	5.22	2.32	55.6%
1	2	6.96	3.48	50.0%	2	1	6.96	4.06	41.7%
1	4	11.03	6.38	42.2%	4	1	11.61	7.55	35.0%
1	8	17.99	11.61	35.5%	8	1	18.57	11.61	37.5%

$\tau_s^G$ . As such, we used 65% for MNIST and 45% for FMNIST. On average, our method saves 38.7% and 42.5%, for MNIST and FMNIST respectively, of the energy used for H-FL.

### B. Data Offloading/Processing Optimization

We focus on the optimization (i.e., blue) block from Fig. 2. Note that our optimization formulation from Sec. IV adjusts the performance and energy consumption of HN-PFL and is separable with respect to each swarm. We investigate the performance of our optimization solver on a single swarm composed of two workers and two coordinators training for a device cluster composed of ten devices in Figs. 8-9, averaging over 10 experiments. In particular, Fig. 8 varies  $1-\theta$ , i.e. scaling the importance of the ML model performance in the objective of  $\mathcal{P}$ , and investigates the following optimization parameters for HN-PFL: device-to-UAV data offloading ( $\rho$ ), coordinator-to-worker data offloading ( $\varrho$ ), aggregate data processing (i.e.,  $D_j \times \alpha_j$ ,  $\alpha_j = \alpha_{j,1} + \alpha_{j,2} + \alpha_{j,3}$ ), and worker CPU frequency determination ( $g$ ). As the network operator places greater importance on ML model performance (i.e., increasing  $1-\theta$ ), our solver increases data offloading, i.e., larger average  $\rho$  in Fig. 8(a), and swarm leaders also instruct their workers to increase their CPU frequencies in Fig. 8(c). In this manner, more data is offloaded and subsequently processed within the same time frame, which increases the ML model performance. Fig. 8(b) also demonstrates that the coordinator UAVs never retain data for themselves as the average  $\varrho$  is 0.5, which implies that all the data is getting offloaded to the 2 workers. This is the case since the coordinator UAVs are only used for data relaying and do not have data processing power. The joint effect of larger average  $\rho$  and  $g$  is more average total data processed, seen in Fig. 8(d).

Next, in Fig. 9, we verify that our optimization formulation optimizes the performance of HN-PFL. As no alternative methodology for our optimization problem exists, we develop two methods, called greedy offloading (G.O.) and maximum processed (M.P.), and use them as baselines to compare the effectiveness of our data offloading/processing optimization in Fig. 9. In G.O., the devices always offload their entire datasets to the UAVs, and, in M.P., the UAVs overclock their CPU frequencies (reaching 2.3GHz for all UAVs) and maximize mini-batch ratios. Both G.O. and M.P. are determined in a fashion that adheres to the constraints in (25)-(46), and we use our solver to determine the rest of the optimization variables in each baseline. We show the percentage savings in objective function of  $\mathcal{P}$  of our method over the two baselines in Fig. 9. When the network operator places greater emphasis on energy efficiency (i.e., small  $1-\theta$ ), our joint optimization will decrease data offloading and processing to conserve energy. As a result, our method achieves over 80% decrease in objective function value

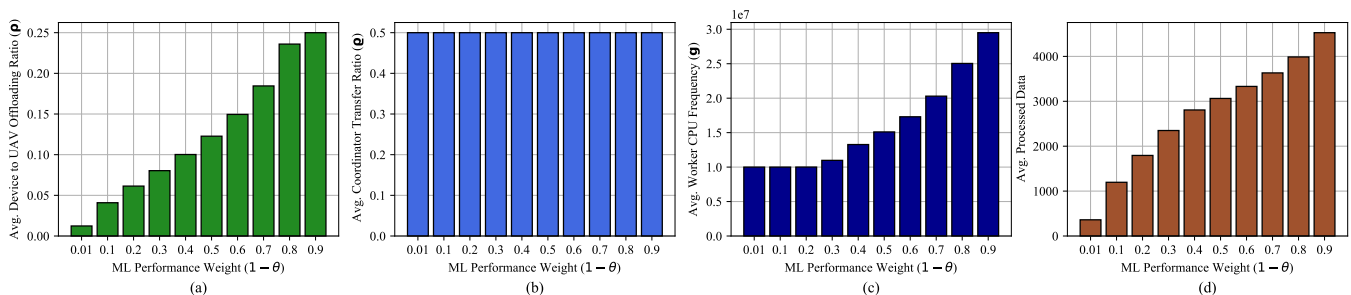


FIGURE 8: The behavior of the optimization variables:  $\rho$ ,  $\varrho$ ,  $\alpha$ ,  $g$  depends on the ML learning importance factor  $1 - \theta$  in the optimization formulation. As  $1 - \theta$  increases, i.e., the importance of ML model performance increases, the network responds by offloading more data on average, increasing the CPU frequencies of workers, and processing more data as a result.

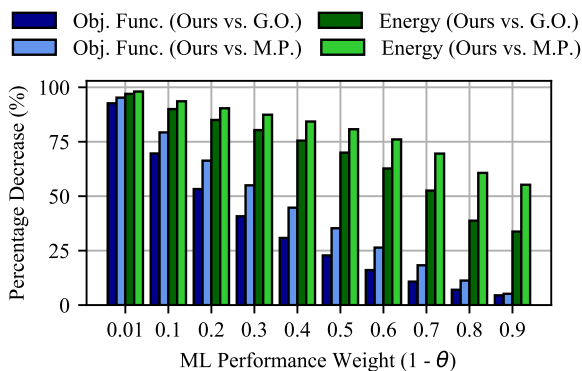


FIGURE 9: Our data offloading/processing optimization minimizes the network objective better than the two baselines, greedy offloading (G.O.) and maximum processed (M.P.). For comparison, we show the percentage decrease of energy consumption and objective function that our optimization achieves when compared to the baselines. For the baselines, M.P. outperforms G.O. as M.P. is able to schedule the data offloading more efficiently, consuming less energy and processing more data.

and energy consumption compared to either baseline when  $1 - \theta = 0.01$ . Even when  $1 - \theta = 0.9$ , i.e., the network aims to process more data in order to improve the ML component of the objective function, our method retains a roughly 6% improvement for the objective function and a 25% improvement for the energy consumption against both baselines. Fig. 9 also reveals that, between the baselines, M.P. outperforms G.O. because M.P. always processes more data and can offload data from device-to-UAV more optimally, which leads to both less energy consumption and smaller objective function value.

### C. Trajectory Optimization with Model/Concept Drift

Next, we turn to the trajectory optimization component of Sec. V (green block in Fig. 2). We consider 2 recharging stations and 8 device clusters separated by distances in  $[500, 2000]$ m, where each device cluster has  $[8, 10]$  devices. At the UAV level, we consider 3 swarms, each of which has  $[3, 5]$  workers and  $[1, 2]$  coordinators. Additionally, we will refer to the recharging stations as R:1 and R:2, and the clusters as C:1,  $\dots$ , C:8. First, we evaluate the performance of the DRL methodology by calculating the moving average reward from (60), average UAV battery levels, and learning objective (isolated to demonstrate the online ML model performance over epochs, which is sum of the objective function  $O(s)$  derived from  $\mathcal{P}$  and the estimated online gradient  $G_c(s)$  across the unvisited device clusters) for our RNN-based DRL method with  $\gamma = 0.7$  and three baselines in Fig. 10. Since existing

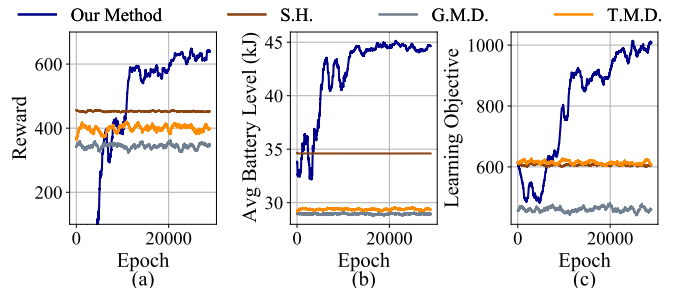


FIGURE 10: Comparison of our method for swarm trajectory and temporal ML design against several heuristic baselines. Our method gradually learns optimal patterns for efficient swarm trajectories and outperforms the baselines.

baselines for our problem do not exist, we developed three baseline algorithms: (i) sequential heuristic (S.H.), (ii) greedy minimum distance (G.M.D.), and (iii) threshold minimum distance (T.M.D.), and calculated their rewards using the reward function in (60). S.H. cycles through the sites sequentially from C:1 to R:2, in the order presented in the x-axis of Fig. 11. On the other hand, our minimum distance methods determine the next destination for a swarm based on closest proximity, with G.M.D. always selecting the minimum distance and T.M.D. choosing between a random option or the minimum distance based on a probability threshold (set at 20% probability to select the random option). Both minimum distance based methods will reroute swarms to the nearest recharging station when UAV batteries fall within the threshold. As seen in Fig. 10, the DRL agent initially undergoes a training phase to learn the optimal travel patterns to maximize the reward function and schedule optimal recharging (hence the initial lower battery). Our RNN-based DRL agent learns to schedule cluster training visits and UAV recharging so that the average reward, battery levels, and learning objectives outperform those of baseline algorithms by at least 29%.

As the other goal for our DRL-based trajectory optimization is adaptability to changing model drifts, we use the same network as that in Fig. 10 with time-varying model drifts for each device cluster, and measure the cluster visit rate per 1k epochs in Fig. 11. Each cluster has a unique affine function to model its model drift growth. Initially, the 8 clusters have scaled model drifts of  $[2, 4, 6, 8, 10, 12, 14, 16]$ , but end at  $[15, 15, 21, 11, 12, 17, 19, 17]$ . So, initially, the cluster visit rate favors C:8 and C:7, which have the highest model drifts. However, as the epochs increase, the model drift begins skewing towards C:3, and our methodology responds by increasing its

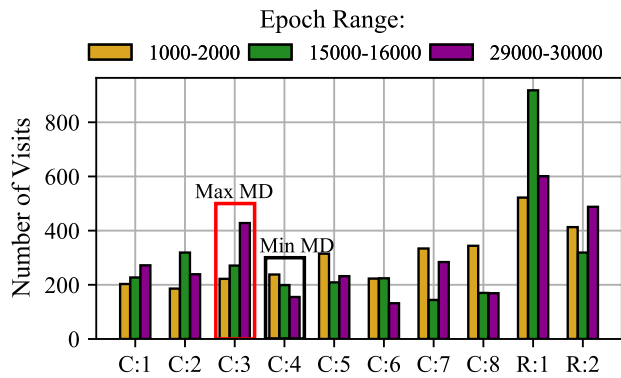


FIGURE 11: Swarm visit statistics per thousand epochs at various training progression stages. Our method learns to adjust its visit frequency to those device clusters with the largest model drift (MD), even when the model drift is time-varying. Over time, cluster C:3 has the largest model drift of 21, which our method adapts to by increasing its visit rate from 210 to 450 visits per thousand epochs. Conversely, the final model drift at cluster C:4 is only 11, and our method decreases its visit rate from 220 to 170 per thousand epochs.

visit rate from 210 to 450. Inversely, C:4 has the smallest final model drift and our method is able to adjust its visit rate from 220 to 170.

## VII. CONCLUSION

We developed a holistic framework for integrating UAV swarm networks for online distributed machine learning. This involved a number of unique modelling decisions and analysis. We proposed a swarm stratification architecture tailored for our distributed machine learning framework. Our introduced distributed machine learning architecture, hierarchical nested personalized federated learning HN-PFL, nests meta-function based gradient descent into local and global aggregations through the worker-leader-core network hierarchy, for which we characterized the performance bound. Finally, we proposed and developed a holistic framework for network-aware UAV-enabled model training, consisting of two intertwined parts: (i) data offloading and processing optimization, for which we developed a distributed algorithm with performance guarantee, and (ii) learning duration and trajectory design, for which we developed a solution based on deep reinforcement learning.

## REFERENCES

- [1] Y. Zhang, X. Ma, J. Zhang, M. S. Hossain, G. Muhammad, and S. U. Amin, "Edge intelligence in the cognitive internet of things: Improving sensitivity and interactivity," *IEEE Netw.*, vol. 33, no. 3, pp. 58–64, 2019.
- [2] Y. Xiao, G. Shi, Y. Li, W. Saad, and H. V. Poor, "Toward self-learning edge intelligence in 6g," *IEEE Commun. Mag.*, vol. 58, no. 12, pp. 34–40, 2020.
- [3] S. Hosseinalipour, C. G. Brinton, V. Aggarwal, H. Dai, and M. Chiang, "From federated to fog learning: Distributed machine learning over heterogeneous wireless networks," *IEEE Commun. Mag.*, vol. 58, no. 12, pp. 41–47, 2020.
- [4] N. H. Motlagh, T. Taleb, and O. Arouk, "Low-altitude unmanned aerial vehicles-based internet of things services: Comprehensive survey and future perspectives," *IEEE Internet Things J.*, vol. 3, no. 6, pp. 899–922, 2016.
- [5] Y. Zeng, R. Zhang, and T. J. Lim, "Wireless communications with unmanned aerial vehicles: Opportunities and challenges," *IEEE Commun. Mag.*, vol. 54, no. 5, pp. 36–42, 2016.
- [6] Q. Wu, J. Xu, Y. Zeng, D. W. K. Ng, N. Al-Dhahir, R. Schober, and A. L. Swindlehurst, "5g-and-beyond networks with UAVs: From communications to sensing and intelligence," *arXiv preprint arXiv:2010.09317*, 2020.

- [7] W. Y. B. Lim, J. Huang, Z. Xiong, J. Kang, D. Niyato, X.-S. Hua, C. Leung, and C. Miao, "Towards federated learning in UAV-enabled internet of vehicles: A multi-dimensional contract-matching approach," *arXiv preprint arXiv:2004.03877*, 2020.
- [8] T. Zeng, O. Semiari, M. Mozaffari, M. Chen, W. Saad, and M. Bennis, "Federated learning in the sky: Joint power allocation and scheduling with UAV swarms," *arXiv:2002.08196*, 2020.
- [9] H. Zhang and L. Hanzo, "Federated learning assisted multi-UAV networks," *IEEE Trans. Veh. Technol.*, vol. 69, no. 11, pp. 14 104–14 109, 2020.
- [10] H. Yang, J. Zhao, Z. Xiong, K.-Y. Lam, S. Sun, and L. Xiao, "Privacy-preserving federated learning for UAV-enabled networks: Learning-based joint scheduling and resource management," *arXiv preprint arXiv:2011.14197*, 2020.
- [11] "Amazon details its low bandwidth sidewalk neighborhood network coming to echo and tile devices soon." [Online]. Available: <https://tcn.ch/2TvJxL6>
- [12] "Amazon sidewalk a new way to stay connected." [Online]. Available: <https://blog.aboutamazon.com/devices/amazon-sidewalk-a-new-way-to-stay-connected>
- [13] R. Ciovacco, "Amazon Sidewalk Privacy and Security Whitepaper," Tech. Rep., 09 2020.
- [14] "Amazon prime air." [Online]. Available: <https://www.amazon.com/Amazon-Prime-Air/b?ie=UTF8&node=8037720011>
- [15] E. L. Piza, B. C. Welsh, D. P. Farrington, and A. L. Thomas, "Cctv surveillance for crime prevention: A 40-year systematic review with meta-analysis," *Criminology & Public Policy*, vol. 18, no. 1, pp. 135–159, 2019.
- [16] "The pentagon has a laser that can identify people from a distance by their heartbeat." [Online]. Available: <https://bit.ly/35EcS6P>
- [17] C. Benedek, B. Gálai, B. Nagy, and Z. Jankó, "Lidar-based gait analysis and activity recognition in a 4d surveillance system," *IEEE Trans. Circuits Syst. Video Technol.*, vol. 28, no. 1, pp. 101–113, 2016.
- [18] M. A. Alsheikh, S. Lin, D. Niyato, and H.-P. Tan, "Machine learning in wireless sensor networks: Algorithms, strategies, and applications," *IEEE Commun. Surveys & Tuts.*, vol. 16, no. 4, pp. 1996–2018, 2014.
- [19] M. Erdelj, E. Natalizio, K. R. Chowdhury, and I. F. Akyildiz, "Help from the sky: Leveraging UAVs for disaster management," *IEEE Pervasive Comput.*, vol. 16, no. 1, pp. 24–32, 2017.
- [20] G. Zhu, D. Liu, Y. Du, C. You, J. Zhang, and K. Huang, "Toward an intelligent edge: Wireless communication meets machine learning," *IEEE Commun. Mag.*, vol. 58, no. 1, pp. 19–25, 2020.
- [21] J. Park, S. Samarakoon, M. Bennis, and M. Debbah, "Wireless network intelligence at the edge," *Proc. IEEE*, vol. 107, no. 11, pp. 2204–2239, 2019.
- [22] C. T. Dinh, N. H. Tran, M. N. H. Nguyen, C. S. Hong, W. Bao, A. Y. Zomaya, and V. Gramoli, "Federated learning over wireless networks: Convergence analysis and resource allocation," *IEEE/ACM Trans. Netw.*, pp. 1–12, 2020.
- [23] M. M. Amiri and D. Gündüz, "Federated learning over wireless fading channels," *IEEE Trans. Wireless Commun.*, vol. 19, no. 5, pp. 3546–3557, 2020.
- [24] M. Chen, Z. Yang, W. Saad, C. Yin, H. V. Poor, and S. Cui, "A joint learning and communications framework for federated learning over wireless networks," *arXiv preprint arXiv:1909.07972*, 2019.
- [25] S. Wang, T. Tuor, T. Salonidis, K. K. Leung, C. Makaya, T. He, and K. Chan, "Adaptive federated learning in resource constrained edge computing systems," *IEEE J. Sel. Areas Commun.*, vol. 37, no. 6, pp. 1205–1221, 2019.
- [26] Z. Yang, M. Chen, W. Saad, C. S. Hong, and M. Shikh-Bahaei, "Energy efficient federated learning over wireless communication networks," *arXiv preprint arXiv:1911.02417*, 2019.
- [27] S. Wang, Y. Ruan, Y. Tu, S. Wagle, C. G. Brinton, and C. Joe-Wong, "Network-aware optimization of distributed learning for fog computing," *IEEE/ACM Transactions on Networking*, vol. 29, no. 5, pp. 2019–2032, 2021.
- [28] S. Hosseinalipour, S. Wang, N. Michelusi, V. Aggarwal, C. G. Brinton, D. J. Love, and M. Chiang, "Parallel successive learning for dynamic distributed model training over heterogeneous wireless networks," 2022.
- [29] S. Hosseinalipour, S. Azam, C. Brinton, N. Michelusi, V. Aggarwal, D. Love, and H. Dai, "Multi-stage hybrid federated learning over large-scale D2D-enabled fog networks," *arXiv preprint arXiv:2007.09511*, 2020.
- [30] K. Yang, T. Jiang, Y. Shi, and Z. Ding, "Federated learning via over-the-air computation," *IEEE Trans. Wireless Commun.*, vol. 19, no. 3, pp. 2022–2035, 2020.

- [31] V. Smith, C.-K. Chiang, M. Sanjabi, and A. S. Talwalkar, "Federated multi-task learning," in *Adv. Neural Inf. Process. Syst.*, 2017, pp. 4424–4434.
- [32] R. Li, F. Ma, W. Jiang, and J. Gao, "Online federated multitask learning," in *IEEE Int. Conf. Big Data (Big Data)*, 2019, pp. 215–220.
- [33] A. Fallah, A. Mokhtari, and A. Ozdaglar, "Personalized federated learning: A meta-learning approach," *arXiv preprint arXiv:2002.07948*, 2020.
- [34] L. Liu, J. Zhang, S. Song, and K. B. Letaief, "Client-edge-cloud hierarchical federated learning," in *IEEE Int. Conf. Commun. (ICC)*. IEEE, 2020, pp. 1–6.
- [35] Y. Sun, M. Peng, Y. Zhou, Y. Huang, and S. Mao, "Application of machine learning in wireless networks: Key techniques and open issues," *IEEE Commun. Surveys & Tuts.*, vol. 21, no. 4, pp. 3072–3108, 2019.
- [36] F. B. Mismar, B. L. Evans, and A. Alkhateeb, "Deep reinforcement learning for 5G networks: Joint beamforming, power control, and interference coordination," *IEEE Trans. Commun.*, vol. 68, no. 3, pp. 1581–1592, 2019.
- [37] Y. Wei, F. R. Yu, M. Song, and Z. Han, "User scheduling and resource allocation in hetnets with hybrid energy supply: An actor-critic reinforcement learning approach," *IEEE Trans. Wireless Commun.*, vol. 17, no. 1, pp. 680–692, 2017.
- [38] X. Liu, Y. Liu, Y. Chen, and L. Hanzo, "Trajectory design and power control for multi-UAV assisted wireless networks: A machine learning approach," *IEEE Trans. Veh. Technol.*, vol. 68, no. 8, pp. 7957–7969, 2019.
- [39] N. Zhao, Z. Liu, and Y. Cheng, "Multi-agent deep reinforcement learning for trajectory design and power allocation in multi-UAV networks," *IEEE Access*, vol. 8, pp. 139 670–139 679, 2020.
- [40] Y. Zhang, Z. Mou, F. Gao, J. Jiang, R. Ding, and Z. Han, "UAV-enabled secure communications by multi-agent deep reinforcement learning," *IEEE Trans. Veh. Technol.*, vol. 69, no. 10, pp. 11 599–11 611, 2020.
- [41] J. Cui, Y. Liu, and A. Nallanathan, "Multi-agent reinforcement learning-based resource allocation for UAV networks," *IEEE Trans. Wireless Commun.*, vol. 19, no. 2, pp. 729–743, 2020.
- [42] "Collaborating with UAVTEK to develop nano 'bug' drone." [Online]. Available: <https://www.baesystems.com/en/collaborating-with-uavtek-to-develop-nano-bug-drone>
- [43] K. Lu, J. Xie, Y. Wan, and S. Fu, "Toward UAV-based airborne computing," *IEEE Wireless Commun.*, vol. 26, no. 6, pp. 172–179, 2019.
- [44] C. H. Liu, Z. Chen, J. Tang, J. Xu, and C. Piao, "Energy-efficient UAV control for effective and fair communication coverage: A deep reinforcement learning approach," *IEEE J. Sel. Areas Commun.*, vol. 36, no. 9, pp. 2059–2070, 2018.
- [45] A. V. Savkin and H. Huang, "Asymptotically optimal deployment of drones for surveillance and monitoring," *Sensors*, vol. 19, no. 9, p. 2068, 2019.
- [46] M. Won, "UBAT: On jointly optimizing UAV trajectories and placement of battery swap stations," 2020.
- [47] C. H. Choi, H. J. Jang, S. G. Lim, H. C. Lim, S. H. Cho, and I. Gaponov, "Automatic wireless drone charging station creating essential environment for continuous drone operation," in *Int. Conf. Control, Autom. Inf. Sci. (ICCAIS)*, 2016, pp. 132–136.
- [48] H. B. McMahan, E. Moore, D. Ramage, S. Hampson, and B. A. y Arcas, "Communication-Efficient Learning of Deep Networks from Decentralized Data," in *Proc. Int. Conf. Artif. Intell. Stat. (AISTATS)*, 2017.
- [49] C. Finn, P. Abbeel, and S. Levine, "Model-agnostic meta-learning for fast adaptation of deep networks," *arXiv:1703.03400*, 2017.
- [50] S. Wang, M. Lee, S. Hosseinipour, R. Morabito, M. Chiang, and C. G. Brinton, "Device sampling for heterogeneous federated learning: Theory, algorithms, and implementation," *arXiv preprint arXiv:2101.00787*, 2021.
- [51] A. Fallah, A. Mokhtari, and A. Ozdaglar, "On the convergence theory of gradient-based model-agnostic meta-learning algorithms," in *Int. Conf. Artificial Intell. Stat.* PMLR, 2020, pp. 1082–1092.
- [52] C. T. Dinh, N. H. Tran, and T. D. Nguyen, "Personalized federated learning with moreau envelopes," *arXiv:2006.08848*, 2020.
- [53] A. Al-Hourani, S. Kandeepan, and A. Jamalipour, "Modeling air-to-ground path loss for low altitude platforms in urban environments," in *Proc. of IEEE Global Commun. Conf. (GLOBECOM)*, pp. 2898–2904, Austin, TX, USA, Dec. 2014.
- [54] M. Mozaffari, W. Saad, M. Bennis, and M. Debbah, "Mobile unmanned aerial vehicles (UAVs) for energy-efficient internet of things communications," *IEEE Trans. Wireless Commun.*, vol. 16, no. 11, pp. 7574–7589, 2017.
- [55] V. Vahidi and E. Saberinia, "Orthogonal frequency division multiplexing and channel models for payload communications of unmanned aerial systems," in *Int. Conf. Unmanned Aircraft Syst. (ICUAS)*, 2016, pp. 1156–1161.
- [56] Y. Zeng and R. Zhang, "Energy-efficient UAV communication with trajectory optimization," *IEEE Trans. Wireless Commun.*, vol. 16, no. 6, pp. 3747–3760, June 2017.
- [57] Y. Zeng, J. Xu, and R. Zhang, "Energy minimization for wireless communication with rotary-wing UAV," *IEEE Trans. Wireless Commun.*, vol. 18, no. 4, pp. 2329–2345, 2019.
- [58] M. Chiang, C. W. Tan, D. P. Palomar, D. O'neill, and D. Julian, "Power control by geometric programming," *IEEE Trans. Wireless Commun.*, vol. 6, no. 7, pp. 2640–2651, 2007.
- [59] S. Diamond and S. Boyd, "CVXPY: A Python-embedded modeling language for convex optimization," *J. Machine Learn. Research*, vol. 17, no. 83, pp. 1–5, 2016.
- [60] B. R. Marks and G. P. Wright, "A general inner approximation algorithm for nonconvex mathematical programs," *Oper. Res.*, vol. 26, no. 4, pp. 681–683, 1978.
- [61] Y. Zeng and R. Zhang, "Energy-efficient UAV communication with trajectory optimization," *IEEE Trans. Wireless Commun.*, vol. 16, no. 6, pp. 3747–3760, 2017.
- [62] V. Mnih, K. Kavukcuoglu, D. Silver, A. A. Rusu, J. Veness, M. G. Bellemare, A. Graves, M. Riedmiller, A. K. Fidjeland, G. Ostrovski *et al.*, "Human-level control through deep reinforcement learning," *nature*, vol. 518, no. 7540, pp. 529–533, 2015.
- [63] A. Doshi, S. Yerramalli, L. Ferrari, T. Yoo, and J. G. Andrews, "A deep reinforcement learning framework for contention-based spectrum sharing," *IEEE Journal on Selected Areas in Communications*, vol. 39, no. 8, pp. 2526–2540, 2021.
- [64] M. Tang and V. W. Wong, "Deep reinforcement learning for task offloading in mobile edge computing systems," *IEEE Transactions on Mobile Computing*, pp. 1–1, 2020.
- [65] B. C. Stadie, S. Levine, and P. Abbeel, "Incentivizing exploration in reinforcement learning with deep predictive models," *arXiv preprint arXiv:1507.00814*, 2015.
- [66] S. Boyd, S.-J. Kim, L. Vandenberghe, and A. Hassibi, "A tutorial on geometric programming," *Opt. Eng.*, vol. 8, no. 1, p. 67, 2007.



**Su Wang** is a PhD student in ECE at Purdue University. He received his BS in Electrical Engineering from Purdue in 2018.



**Seyyedali Hosseinipour** received his Ph.D. in EE from NCSU in 2020. He was the recipient of the 2020 ECE Doctoral Scholar of the Year Award and 2021 ECE Distinguished Dissertation Award at NC State University. He is currently a postdoctoral researcher at Purdue University.



**Maria Gorlatova** is a Nortel Networks Assistant Professor of ECE at Duke University. She received her PhD from Columbia University in 2013. She won the NSF CAREER Award, the ACM/IEEE IPSN Best Research Artifact Award, and the IEEE Communications Society Young Author Best Paper Award.



**Christopher G. Brinton** is an assistant professor of ECE at Purdue University. He received his Ph.D. in EE from Princeton University in 2016. He is the recipient of a 2022 NSF CAREER Award and a 2022 ONR Young Investigator Program Award.



**Mung Chiang** is the John A. Edwardson Dean of the College of Engineering and executive vice president at Purdue University. Previously, he was the Arthur LeGrand Doty Professor of EE at Princeton University. He received his Ph.D. from Stanford University in 2003. He won the 2013 Alan T. Waterman Award, the highest honor to U.S. young scientists and engineers.

APPENDIX A  
PROOF OF PROPOSITION 1

*Proof.* To bound

$$\mathbb{E} \left[ \left\| \frac{1}{U(s)} \sum_{u \in \mathcal{U}(s)} \sum_{j \in \mathcal{W}_u} \frac{\Delta_j(k' \tau_s^G)}{\Delta_u(k' \tau_s^G)} \left( \mathbf{w}_j(t) - \bar{\mathbf{w}}(t) \right) \right\|^2 \right], \quad (63)$$

where  $t = t_s^G(k') = t_s + k' \tau_s^L \tau_s^G$ , we introduce  $\bar{\mathbf{w}}_u(t)$  and omit the  $t_s$  aspect of  $t_s^G(k')$ , i.e., ignoring the starting time of the sequence  $t_s$  in all the derivations since it is just a constant, to obtain:

$$\begin{aligned} & \mathbb{E} \left[ \left\| \frac{1}{U(s)} \sum_{u \in \mathcal{U}(s)} \sum_{j \in \mathcal{W}_u} \frac{\Delta_j(k' \tau_s^G)}{\Delta_u(k' \tau_s^G)} \left( \mathbf{w}_j(\tau_s^L \tau_s^G k') - \bar{\mathbf{w}}_u(\tau_s^L \tau_s^G k') + \bar{\mathbf{w}}_u(\tau_s^L \tau_s^G k') - \bar{\mathbf{w}}(\tau_s^L \tau_s^G k') \right) \right\|^2 \right] \\ & \leq 2 \underbrace{\frac{1}{U(s)} \sum_{u \in \mathcal{U}(s)} \sum_{j \in \mathcal{W}_u} \frac{\Delta_j(k' \tau_s^G)}{\Delta_u(k' \tau_s^G)} \mathbb{E} [\| \mathbf{w}_j(\tau_s^L \tau_s^G k') - \bar{\mathbf{w}}_u(\tau_s^L \tau_s^G k') \|^2]}_{(i)} + 2 \underbrace{\frac{1}{U(s)} \sum_{u \in \mathcal{U}(s)} \mathbb{E} [\| \bar{\mathbf{w}}_u(\tau_s^L \tau_s^G k') - \bar{\mathbf{w}}(\tau_s^L \tau_s^G k') \|^2]}_{(ii)}, \end{aligned} \quad (64)$$

where the inequality is due to Jensen's inequality and  $\|a + b\|^2 \leq 2(\|a\|^2 + \|b\|^2)$ . We first upper bound (64)(i), omitting the summations for simplicity:

$$\begin{aligned} & 2 \mathbb{E} [\| \mathbf{w}_j(\tau_s^L \tau_s^G k') - \bar{\mathbf{w}}_u(\tau_s^L \tau_s^G k') \|^2] \stackrel{(a)}{=} 2 \mathbb{E} \left[ \left\| \mathbf{w}_j(\tau_s^L \tau_s^G k') - \sum_{\hat{j} \in \mathcal{W}_u} \frac{\Delta_{\hat{j}}(k' \tau_s^G)}{\Delta_u(k' \tau_s^G)} \mathbf{w}_{\hat{j}}(\tau_s^L \tau_s^G k') \right\|^2 \right] \\ & \stackrel{(b)}{=} 2 \mathbb{E} \left[ \left\| \mathbf{w}_j(\tau_s^L \tau_s^G k' - 1) - \eta_2 \nabla \tilde{F}_j(\mathbf{w}_j(\tau_s^L \tau_s^G k' - 1)) - \sum_{\hat{j} \in \mathcal{W}_u} \frac{\Delta_{\hat{j}}(k' \tau_s^G)}{\Delta_u(k' \tau_s^G)} \left( \mathbf{w}_{\hat{j}}(\tau_s^L \tau_s^G k' - 1) - \eta_2 \nabla \tilde{F}_{\hat{j}}(\mathbf{w}_{\hat{j}}(\tau_s^L \tau_s^G k' - 1)) \right) \right\|^2 \right] \\ & \stackrel{(c)}{\leq} \underbrace{8 \mathbb{E} [\| \mathbf{w}_j(\tau_s^L \tau_s^G k' - 1) - \bar{\mathbf{w}}_u(\tau_s^L \tau_s^G k' - 1) \|^2]}_{(i)} + \underbrace{8 \eta_2^2 \mathbb{E} [\| \nabla F_j(\mathbf{w}_j(\tau_s^L \tau_s^G k' - 1)) - \nabla \tilde{F}_j(\mathbf{w}_j(\tau_s^L \tau_s^G k' - 1)) \|^2]}_{(ii)} \\ & + \underbrace{8 \eta_2^2 \mathbb{E} \left[ \left\| \sum_{\hat{j} \in \mathcal{W}_u} \frac{\Delta_{\hat{j}}(k' \tau_s^G)}{\Delta_u(k' \tau_s^G)} \left( \nabla \tilde{F}_{\hat{j}}(\mathbf{w}_{\hat{j}}(\tau_s^L \tau_s^G k' - 1)) - \nabla F_{\hat{j}}(\mathbf{w}_{\hat{j}}(\tau_s^L \tau_s^G k' - 1)) \right) \right\|^2 \right]}_{(iii)} \\ & + \underbrace{8 \eta_2^2 \mathbb{E} \left[ \left\| \nabla F_j(\mathbf{w}_j(\tau_s^L \tau_s^G k' - 1)) - \sum_{\hat{j} \in \mathcal{W}_u} \frac{\Delta_{\hat{j}}(k' \tau_s^G)}{\Delta_u(k' \tau_s^G)} \nabla F_{\hat{j}}(\mathbf{w}_{\hat{j}}(\tau_s^L \tau_s^G k' - 1)) \right\|^2 \right]}_{(iv)}, \end{aligned} \quad (65)$$

where (a) is the aggregation rule of  $\bar{\mathbf{w}}_u$ , (b) uses the gradient update from (1), and (c) introduces  $\eta_2 \nabla F_j$  and  $\eta_2 \nabla \tilde{F}_u$  terms and then applies Cauchy-Schwarz, i.e.,  $(\sum_i^n a_i)^2 \leq n(\sum_i^n a_i^2)$ . The bounds for (65)(ii) and (65)(iii) follow immediately from Lemma 1, and we analyze (65)(iv), while recalling the summations from (64) as follows:

$$\begin{aligned} & 8 \eta_2^2 \frac{1}{U(s)} \sum_{u \in \mathcal{U}(s)} \sum_{j \in \mathcal{W}_u} \frac{\Delta_j(k' \tau_s^G)}{\Delta_u(k' \tau_s^G)} \mathbb{E} \left[ \left\| \nabla F_j(\mathbf{w}_j(\tau_s^L \tau_s^G k' - 1)) - \sum_{\hat{j} \in \mathcal{W}_u} \frac{\Delta_{\hat{j}}(k' \tau_s^G)}{\Delta_u(k' \tau_s^G)} \nabla F_{\hat{j}}(\mathbf{w}_{\hat{j}}(\tau_s^L \tau_s^G k' - 1)) \right\|^2 \right] \\ & \stackrel{(a)}{=} 8 \eta_2^2 \frac{1}{U(s)} \sum_{u \in \mathcal{U}(s)} \sum_{j \in \mathcal{W}_u} \frac{\Delta_j(k' \tau_s^G)}{\Delta_u(k' \tau_s^G)} \mathbb{E} \left[ \left\| \nabla F_j(\mathbf{w}_j(\tau_s^L \tau_s^G k' - 1)) - \nabla F_j(\bar{\mathbf{w}}_u(\tau_s^L \tau_s^G k' - 1)) + \nabla F_j(\bar{\mathbf{w}}_u(\tau_s^L \tau_s^G k' - 1)) \right. \right. \\ & \quad \left. \left. - \sum_{\hat{j} \in \mathcal{W}_u} \frac{\Delta_{\hat{j}}(k' \tau_s^G)}{\Delta_u(k' \tau_s^G)} \left( \nabla F_{\hat{j}}(\mathbf{w}_{\hat{j}}(\tau_s^L \tau_s^G k' - 1)) + \nabla F_{\hat{j}}(\bar{\mathbf{w}}_u(\tau_s^L \tau_s^G k' - 1)) - \nabla F_{\hat{j}}(\bar{\mathbf{w}}_u(\tau_s^L \tau_s^G k' - 1)) \right) \right\|^2 \right] \\ & \stackrel{(b)}{\leq} 24 \eta_2^2 \frac{1}{U(s)} \sum_{u \in \mathcal{U}(s)} \sum_{j \in \mathcal{W}_u} \frac{\Delta_j(k' \tau_s^G)}{\Delta_u(k' \tau_s^G)} \mathbb{E} [\| \nabla F_j(\mathbf{w}_j(\tau_s^L \tau_s^G k' - 1)) - \nabla F_j(\bar{\mathbf{w}}_u(\tau_s^L \tau_s^G k' - 1)) \|^2] \\ & + 24 \eta_2^2 \frac{1}{U(s)} \sum_{u \in \mathcal{U}(s)} \sum_{j \in \mathcal{W}_u} \frac{\Delta_j(k' \tau_s^G)}{\Delta_u(k' \tau_s^G)} \mathbb{E} \left[ \left\| \sum_{\hat{j} \in \mathcal{W}_u} \frac{\Delta_{\hat{j}}(k' \tau_s^G)}{\Delta_u(k' \tau_s^G)} \left( \nabla F_{\hat{j}}(\bar{\mathbf{w}}_u(\tau_s^L \tau_s^G k' - 1)) - \nabla F_{\hat{j}}(\mathbf{w}_{\hat{j}}(\tau_s^L \tau_s^G k' - 1)) \right) \right\|^2 \right] \\ & + 24 \eta_2^2 \frac{1}{U(s)} \sum_{u \in \mathcal{U}(s)} \sum_{j \in \mathcal{W}_u} \frac{\Delta_j(k' \tau_s^G)}{\Delta_u(k' \tau_s^G)} \mathbb{E} \left[ \left\| \nabla F_j(\bar{\mathbf{w}}_u(\tau_s^L \tau_s^G k' - 1)) - \sum_{\hat{j} \in \mathcal{W}_u} \frac{\Delta_{\hat{j}}(k' \tau_s^G)}{\Delta_u(k' \tau_s^G)} \nabla F_{\hat{j}}(\bar{\mathbf{w}}_u(\tau_s^L \tau_s^G k' - 1)) \right\|^2 \right] \end{aligned} \quad (66)$$

$$\begin{aligned}
&\stackrel{(c)}{\leq} 24\eta_2^2 \frac{1}{U(s)} \sum_{u \in \mathcal{U}(s)} \sum_{j \in \mathcal{W}_u} \frac{\Delta_j(k' \tau_s^G)}{\Delta_u(k' \tau_s^G)} \mathbb{E}[\|\nabla F_j(\mathbf{w}_j(\tau_s^L \tau_s^G k' - 1)) - \nabla F_j(\bar{\mathbf{w}}_u(\tau_s^L \tau_s^G k' - 1))\|^2] \\
&+ 24\eta_2^2 \frac{1}{U(s)} \sum_{u \in \mathcal{U}(s)} \sum_{j \in \mathcal{W}_u} \frac{\Delta_j(k' \tau_s^G)}{\Delta_u(k' \tau_s^G)} \sum_{\hat{j} \in \mathcal{W}_u} \frac{\Delta_{\hat{j}}(k' \tau_s^G)}{\Delta_u(k' \tau_s^G)} \mathbb{E}\left[\left\|\nabla F_{\hat{j}}(\bar{\mathbf{w}}_u(\tau_s^L \tau_s^G k' - 1)) - \nabla F_{\hat{j}}(\mathbf{w}_{\hat{j}}(\tau_s^L \tau_s^G k' - 1))\right\|^2\right] \\
&+ 24\eta_2^2 \frac{1}{U(s)} \sum_{u \in \mathcal{U}(s)} \sum_{j \in \mathcal{W}_u} \frac{\Delta_j(k' \tau_s^G)}{\Delta_u(k' \tau_s^G)} \mathbb{E}\left[\left\|\nabla F_j(\bar{\mathbf{w}}_u(\tau_s^L \tau_s^G k' - 1)) - \nabla \bar{F}_u(\bar{\mathbf{w}}_u(\tau_s^L \tau_s^G k' - 1))\right\|^2\right] \\
&\stackrel{(d)}{\leq} 24\eta_2^2 \frac{1}{U(s)} \sum_{u \in \mathcal{U}(s)} \sum_{j \in \mathcal{W}_u} \frac{\Delta_j(k' \tau_s^G)}{\Delta_u(k' \tau_s^G)} \mu_F^2 \mathbb{E}[\|\mathbf{w}_j(\tau_s^L \tau_s^G k' - 1) - \bar{\mathbf{w}}_u(\tau_s^L \tau_s^G k' - 1)\|^2] \\
&+ 24\eta_2^2 \frac{1}{U(s)} \sum_{u \in \mathcal{U}(s)} \sum_{\hat{j} \in \mathcal{W}_u} \frac{\Delta_{\hat{j}}(k' \tau_s^G)}{\Delta_u(k' \tau_s^G)} \mu_F^2 \mathbb{E}[\|\bar{\mathbf{w}}_u(\tau_s^L \tau_s^G k' - 1) - \mathbf{w}_{\hat{j}}(\tau_s^L \tau_s^G k' - 1)\|^2] \\
&+ 24\eta_2^2 \frac{1}{U(s)} \sum_{u \in \mathcal{U}(s)} \sum_{j \in \mathcal{W}_u} \frac{\Delta_j(k' \tau_s^G)}{\Delta_u(k' \tau_s^G)} \mathbb{E}\left[\left\|\nabla F_j(\bar{\mathbf{w}}_u(\tau_s^L \tau_s^G k' - 1)) - \nabla \bar{F}_u(\bar{\mathbf{w}}_u(\tau_s^L \tau_s^G k' - 1))\right\|^2\right] \\
&\stackrel{(e)}{\leq} 48\mu_F^2 \eta_2^2 \frac{1}{U(s)} \sum_{u \in \mathcal{U}(s)} \sum_{j \in \mathcal{W}_u} \frac{\Delta_j(k' \tau_s^G)}{\Delta_u(k' \tau_s^G)} \mathbb{E}[\|\mathbf{w}_j(\tau_s^L \tau_s^G k' - 1) - \bar{\mathbf{w}}_u(\tau_s^L \tau_s^G k' - 1)\|^2] + 24\eta_2^2 \frac{1}{U(s)} \sum_{u \in \mathcal{U}(s)} (\gamma_F^u)^2,
\end{aligned}$$

where (a) introduces  $\nabla F_j(\bar{\mathbf{w}}_u)$  and  $\nabla F_{\hat{j}}(\bar{\mathbf{w}}_u)$ , (b) applies Jensen's inequality, (c) recalls the aggregation rule of  $\nabla \bar{F}_u$  and applies Jensen's inequality, (d) uses  $\mu_F$ -smoothness (i.e.,  $\|\nabla F_j(\mathbf{w}) - \nabla F_j(\mathbf{w}')\| \leq \mu_F \|\mathbf{w} - \mathbf{w}'\| \forall i \in \cup_{u \in \mathcal{U}(s)} \mathcal{W}_u$ ), and (e) leverages Lemma 2. Combining (65) and (66) yields:

$$\begin{aligned}
&2 \frac{1}{U(s)} \sum_{u \in \mathcal{U}(s)} \sum_{j \in \mathcal{W}_u} \frac{\Delta_j(k' \tau_s^G)}{\Delta_u(k' \tau_s^G)} \mathbb{E}[\|\mathbf{w}_j(\tau_s^L \tau_s^G k' - 1) - \bar{\mathbf{w}}_u(\tau_s^L \tau_s^G k' - 1)\|^2] \tag{67} \\
&\stackrel{(a)}{\leq} 8 \frac{1}{U(s)} \sum_{u \in \mathcal{U}(s)} \sum_{j \in \mathcal{W}_u} \frac{\Delta_j(k' \tau_s^G)}{\Delta_u(k' \tau_s^G)} \mathbb{E}[\|\mathbf{w}_j(\tau_s^L \tau_s^G k' - 1) - \bar{\mathbf{w}}_u(\tau_s^L \tau_s^G k' - 1)\|^2] \\
&+ 8\eta_2^2 \frac{1}{U(s)} \sum_{u \in \mathcal{U}(s)} \sum_{j \in \mathcal{W}_u} \frac{\Delta_j(k' \tau_s^G)}{\Delta_u(k' \tau_s^G)} \mathbb{E}[\|\nabla F_j(\mathbf{w}_j(\tau_s^L \tau_s^G k' - 1)) - \nabla \tilde{F}_j(\mathbf{w}_j(\tau_s^L \tau_s^G k' - 1))\|^2] \\
&+ 8\eta_2^2 \frac{1}{U(s)} \sum_{u \in \mathcal{U}(s)} \sum_{j \in \mathcal{W}_u} \frac{\Delta_j(k' \tau_s^G)}{\Delta_u(k' \tau_s^G)} \mathbb{E}\left[\left\|\sum_{\hat{j} \in \mathcal{W}_u} \frac{\Delta_{\hat{j}}(k' \tau_s^G)}{\Delta_u(k' \tau_s^G)} \left(\nabla \tilde{F}_{\hat{j}}(\mathbf{w}_{\hat{j}}(\tau_s^L \tau_s^G k' - 1)) - \nabla F_{\hat{j}}(\mathbf{w}_{\hat{j}}(\tau_s^L \tau_s^G k' - 1))\right)\right\|^2\right] \\
&+ 8\eta_2^2 \frac{1}{U(s)} \sum_{u \in \mathcal{U}(s)} \sum_{j \in \mathcal{W}_u} \frac{\Delta_j(k' \tau_s^G)}{\Delta_u(k' \tau_s^G)} \mathbb{E}\left[\left\|\nabla F_j(\mathbf{w}_j(\tau_s^L \tau_s^G k' - 1)) - \sum_{\hat{j} \in \mathcal{W}_u} \frac{\Delta_{\hat{j}}(k' \tau_s^G)}{\Delta_u(k' \tau_s^G)} \nabla F_{\hat{j}}(\mathbf{w}_{\hat{j}}(\tau_s^L \tau_s^G k' - 1))\right\|^2\right] \\
&\stackrel{(b)}{\leq} 8 \frac{1}{U(s)} \sum_{u \in \mathcal{U}(s)} \sum_{j \in \mathcal{W}_u} \frac{\Delta_j(k' \tau_s^G)}{\Delta_u(k' \tau_s^G)} \mathbb{E}[\|\mathbf{w}_j(\tau_s^L \tau_s^G k' - 1) - \bar{\mathbf{w}}_u(\tau_s^L \tau_s^G k' - 1)\|^2] + 16\eta_2^2 \frac{1}{U(s)} \sum_{u \in \mathcal{U}(s)} \sum_{j \in \mathcal{W}_u} \frac{\Delta_j(k' \tau_s^G)}{\Delta_u(k' \tau_s^G)} (\sigma_j^F(\tau_s^L \tau_s^G k' - 1))^2 \\
&+ 8\eta_2^2 \frac{1}{U(s)} \sum_{u \in \mathcal{U}(s)} \sum_{j \in \mathcal{W}_u} \frac{\Delta_j(k' \tau_s^G)}{\Delta_u(k' \tau_s^G)} \mathbb{E}\left[\left\|\nabla F_j(\mathbf{w}_j(\tau_s^L \tau_s^G k' - 1)) - \sum_{\hat{j} \in \mathcal{W}_u} \frac{\Delta_{\hat{j}}(k' \tau_s^G)}{\Delta_u(k' \tau_s^G)} \nabla F_{\hat{j}}(\mathbf{w}_{\hat{j}}(\tau_s^L \tau_s^G k' - 1))\right\|^2\right] \\
&\stackrel{(c)}{\leq} (8 + 48\eta_2^2 \mu_F^2) \frac{1}{U(s)} \sum_{u \in \mathcal{U}(s)} \sum_{j \in \mathcal{W}_u} \frac{\Delta_j(k' \tau_s^G)}{\Delta_u(k' \tau_s^G)} \mathbb{E}[\|\mathbf{w}_j(\tau_s^L \tau_s^G k' - 1) - \bar{\mathbf{w}}_u(\tau_s^L \tau_s^G k' - 1)\|^2] \\
&+ 16\eta_2^2 \frac{1}{U(s)} \sum_{u \in \mathcal{U}(s)} \sum_{j \in \mathcal{W}_u} \frac{\Delta_j(k' \tau_s^G)}{\Delta_u(k' \tau_s^G)} (\sigma_j^F(\tau_s^L \tau_s^G k' - 1))^2 + 24\eta_2^2 \frac{1}{U(s)} \sum_{u \in \mathcal{U}(s)} (\gamma_F^u)^2,
\end{aligned}$$

where (a) restates (65) with the previously omitted summations, (b) applies Jensen's inequality and Lemma 1, and (c) uses the result in (66). Solving (67) recursively yields:

$$\begin{aligned}
&2 \frac{1}{U(s)} \sum_{u \in \mathcal{U}(s)} \sum_{j \in \mathcal{W}_u} \frac{\Delta_j(k' \tau_s^G)}{\Delta_u(k' \tau_s^G)} \mathbb{E}[\|\mathbf{w}_j(\tau_s^L \tau_s^G k' - 1) - \bar{\mathbf{w}}_u(\tau_s^L \tau_s^G k' - 1)\|^2] \tag{68} \\
&\stackrel{(a)}{\leq} 16\eta_2^2 \frac{1}{U(s)} \sum_{u \in \mathcal{U}(s)} \sum_{j \in \mathcal{W}_u} \frac{\Delta_j(k' \tau_s^G)}{\Delta_u(k' \tau_s^G)} \left( \sum_{y=0}^{\tau_s^L - 1} (\sigma_j^F(\tau_s^L \tau_s^G k' - 1 - y))^2 (8 + 48\eta_2^2 \mu_F^2)^y \right) + 24\eta_2^2 \frac{1}{U(s)} \sum_{u \in \mathcal{U}(s)} (\gamma_F^u)^2 \frac{1 - (8 + 48\eta_2^2 \mu_F^2)^{\tau_s^L}}{1 - (8 + 48\eta_2^2 \mu_F^2)} \tag{69}
\end{aligned}$$

$$\stackrel{(b)}{\leq} \left( 16\eta_2^2 \frac{1}{U(s)} \sum_{u \in \mathcal{U}(s)} \sum_{j \in \mathcal{W}_u} \frac{\Delta_j(k' \tau_s^G)}{\Delta_u(k' \tau_s^G)} \sum_{y=0}^{\tau_s^L - 1} (\sigma_j^F(\tau_s^L \tau_s^G k' - 1 - y))^2 + 24\eta_2^2 \frac{1}{U(s)} \sum_{u \in \mathcal{U}(s)} (\gamma_F^u)^2 \right) \frac{1 - (8 + 48\eta_2^2 \mu_F^2)^{\tau_s^L}}{1 - (8 + 48\eta_2^2 \mu_F^2)}, \quad (70)$$

where (a) is the result of recursion and the finite sum of geometric series, and (b) uses  $\sum_i a_i b_i \leq \sum_i a_i \sum_i b_i \forall a_i, b_i \geq 0$ . Next, we bound (64)(ii) as follows:

$$\begin{aligned} & 2 \frac{1}{U(s)} \sum_{u \in \mathcal{U}(s)} \mathbb{E} \left[ \left\| \bar{\mathbf{w}}_u(\tau_s^L \tau_s^G k') - \bar{\mathbf{w}}(\tau_s^L \tau_s^G k') \right\|^2 \right] \stackrel{(a)}{=} 2 \frac{1}{U(s)} \sum_{u \in \mathcal{U}(s)} \mathbb{E} \left[ \left\| \bar{\mathbf{w}}_u(\tau_s^L \tau_s^G k') - \frac{1}{U(s)} \sum_{\hat{u} \in \mathcal{U}(s)} \bar{\mathbf{w}}_{\hat{u}}(\tau_s^L \tau_s^G k') \right\|^2 \right] \\ & \stackrel{(b)}{=} 2 \frac{1}{U(s)} \sum_{u \in \mathcal{U}(s)} \mathbb{E} \left[ \left\| \bar{\mathbf{w}}_u(\tau_s^L \tau_s^G k' - 1) - \eta_2 \nabla \tilde{F}_u(\bar{\mathbf{w}}_u(\tau_s^L \tau_s^G k' - 1)) - \frac{1}{U(s)} \sum_{\hat{u} \in \mathcal{U}(s)} \left( \bar{\mathbf{w}}_{\hat{u}}(\tau_s^L \tau_s^G k' - 1) - \eta_2 \nabla \tilde{F}_{\hat{u}}(\bar{\mathbf{w}}_{\hat{u}}(\tau_s^L \tau_s^G k' - 1)) \right) \right\|^2 \right] \\ & \stackrel{(c)}{=} 2 \frac{1}{U(s)} \sum_{u \in \mathcal{U}(s)} \mathbb{E} \left[ \left\| \bar{\mathbf{w}}_u(\tau_s^L \tau_s^G k' - 1) - \eta_2 \nabla \tilde{F}_u(\bar{\mathbf{w}}_u(\tau_s^L \tau_s^G k' - 1)) + \eta_2 \nabla \bar{F}_u(\bar{\mathbf{w}}_u(\tau_s^L \tau_s^G k' - 1)) - \eta_2 \nabla \bar{F}_u(\bar{\mathbf{w}}_u(\tau_s^L \tau_s^G k' - 1)) \right. \right. \\ & \quad \left. \left. - \frac{1}{U(s)} \sum_{\hat{u} \in \mathcal{U}(s)} \left( \bar{\mathbf{w}}_{\hat{u}}(\tau_s^L \tau_s^G k' - 1) - \eta_2 \nabla \tilde{F}_{\hat{u}}(\bar{\mathbf{w}}_{\hat{u}}(\tau_s^L \tau_s^G k' - 1)) + \eta_2 \nabla \bar{F}_{\hat{u}}(\bar{\mathbf{w}}_{\hat{u}}(\tau_s^L \tau_s^G k' - 1)) - \eta_2 \nabla \bar{F}_{\hat{u}}(\bar{\mathbf{w}}_{\hat{u}}(\tau_s^L \tau_s^G k' - 1)) \right) \right\|^2 \right] \\ & \stackrel{(d)}{\leq} 8 \frac{1}{U(s)} \sum_{u \in \mathcal{U}(s)} \mathbb{E} \left[ \underbrace{\left\| \bar{\mathbf{w}}_u(\tau_s^L \tau_s^G k' - 1) - \frac{1}{U(s)} \sum_{\hat{u} \in \mathcal{U}(s)} \bar{\mathbf{w}}_{\hat{u}}(\tau_s^L \tau_s^G k' - 1) \right\|^2}_{(i)} \right] \\ & \quad + 8\eta_2^2 \frac{1}{U(s)} \sum_{u \in \mathcal{U}(s)} \mathbb{E} \left[ \underbrace{\left\| \nabla \bar{F}_u(\bar{\mathbf{w}}_u(\tau_s^L \tau_s^G k' - 1)) - \nabla \tilde{F}_u(\bar{\mathbf{w}}_u(\tau_s^L \tau_s^G k' - 1)) \right\|^2}_{(ii)} \right] \\ & \quad + 8\eta_2^2 \frac{1}{U(s)} \sum_{u \in \mathcal{U}(s)} \mathbb{E} \left[ \underbrace{\left\| \frac{1}{U(s)} \sum_{\hat{u} \in \mathcal{U}(s)} \left( \nabla \tilde{F}_{\hat{u}}(\bar{\mathbf{w}}_{\hat{u}}(\tau_s^L \tau_s^G k' - 1)) - \nabla \bar{F}_{\hat{u}}(\bar{\mathbf{w}}_{\hat{u}}(\tau_s^L \tau_s^G k' - 1)) \right) \right\|^2}_{(iii)} \right] \\ & \quad + 8\eta_2^2 \frac{1}{U(s)} \sum_{u \in \mathcal{U}(s)} \mathbb{E} \left[ \underbrace{\left\| \frac{1}{U(s)} \sum_{\hat{u} \in \mathcal{U}(s)} \nabla \bar{F}_{\hat{u}}(\bar{\mathbf{w}}_{\hat{u}}(\tau_s^L \tau_s^G k' - 1)) - \nabla \bar{F}_u(\bar{\mathbf{w}}_u(\tau_s^L \tau_s^G k' - 1)) \right\|^2}_{(iv)} \right], \end{aligned} \quad (71)$$

where (a) uses the definition of  $\bar{\mathbf{w}}$  from (7), (b) is the global parameter update rule with  $\tilde{F}_u$  using an approximation  $\tilde{F}$  of  $F$  in (6) (the same applies for  $\bar{F}$ ), (c) introduces  $\eta_2 \nabla \tilde{F}_u(\bar{\mathbf{w}}_u)$  and  $\eta_2 \nabla \tilde{F}_{\hat{u}}(\bar{\mathbf{w}}_{\hat{u}})$ , and (d) follows from Cauchy-Schwarz inequality. Upper bounds for (71)(ii) and (71)(iii) follow immediately from Lemma 1, and we bound (71)(iv) as follows:

$$\begin{aligned} & 8\eta_2^2 \frac{1}{U(s)} \sum_{u \in \mathcal{U}(s)} \mathbb{E} \left[ \left\| \frac{1}{U(s)} \sum_{\hat{u} \in \mathcal{U}(s)} \nabla \bar{F}_{\hat{u}}(\bar{\mathbf{w}}_{\hat{u}}(\tau_s^L \tau_s^G k' - 1)) - \nabla \bar{F}_u(\bar{\mathbf{w}}_u(\tau_s^L \tau_s^G k' - 1)) \right\|^2 \right] \\ & \stackrel{(a)}{=} 8\eta_2^2 \frac{1}{U(s)} \sum_{u \in \mathcal{U}(s)} \mathbb{E} \left[ \left\| \frac{1}{U(s)} \sum_{\hat{u} \in \mathcal{U}(s)} \left( \nabla \bar{F}_{\hat{u}}(\bar{\mathbf{w}}_{\hat{u}}(\tau_s^L \tau_s^G k' - 1)) - \nabla \bar{F}_{\hat{u}}(\bar{\mathbf{w}}(\tau_s^L \tau_s^G k' - 1)) + \nabla \bar{F}_{\hat{u}}(\bar{\mathbf{w}}(\tau_s^L \tau_s^G k' - 1)) \right. \right. \right. \\ & \quad \left. \left. - \nabla \bar{F}_u(\bar{\mathbf{w}}_u(\tau_s^L \tau_s^G k' - 1)) + \nabla \bar{F}_u(\bar{\mathbf{w}}(\tau_s^L \tau_s^G k' - 1)) - \nabla \bar{F}_u(\bar{\mathbf{w}}(\tau_s^L \tau_s^G k' - 1)) \right) \right\|^2 \right] \\ & \stackrel{(b)}{\leq} 24\eta_2^2 \frac{1}{U(s)} \sum_{u \in \mathcal{U}(s)} \mathbb{E} \left[ \left\| \frac{1}{U(s)} \sum_{\hat{u} \in \mathcal{U}(s)} \sum_{j \in \mathcal{W}_{\hat{u}}} \frac{\Delta_j(k' \tau_s^G)}{\Delta_{\hat{u}}(k' \tau_s^G)} \left( \nabla F_j(\bar{\mathbf{w}}_{\hat{u}}(\tau_s^L \tau_s^G k' - 1)) - \nabla F_j(\bar{\mathbf{w}}(\tau_s^L \tau_s^G k' - 1)) \right) \right\|^2 \right] \\ & \quad + 24\eta_2^2 \frac{1}{U(s)} \sum_{u \in \mathcal{U}(s)} \mathbb{E} \left[ \left\| \sum_{j \in \mathcal{W}_{\hat{u}}} \frac{\Delta_j(k' \tau_s^G)}{\Delta_{\hat{u}}(k' \tau_s^G)} \left( \nabla F_j(\bar{\mathbf{w}}(\tau_s^L \tau_s^G k' - 1)) - \nabla F_j(\bar{\mathbf{w}}_u(\tau_s^L \tau_s^G k' - 1)) \right) \right\|^2 \right] \\ & \quad + 24\eta_2^2 \frac{1}{U(s)} \sum_{u \in \mathcal{U}(s)} \mathbb{E} \left[ \left\| \nabla \bar{F}(\bar{\mathbf{w}}(\tau_s^L \tau_s^G k' - 1)) - \nabla \bar{F}_u(\bar{\mathbf{w}}(\tau_s^L \tau_s^G k' - 1)) \right\|^2 \right] \\ & \stackrel{(c)}{\leq} 24\eta_2^2 \frac{1}{U(s)} \sum_{u \in \mathcal{U}(s)} \frac{1}{U(s)} \sum_{\hat{u} \in \mathcal{U}(s)} \sum_{j \in \mathcal{W}_{\hat{u}}} \frac{\Delta_j(k' \tau_s^G)}{\Delta_{\hat{u}}(k' \tau_s^G)} \mathbb{E} \left[ \left\| \nabla F_j(\bar{\mathbf{w}}_{\hat{u}}(\tau_s^L \tau_s^G k' - 1)) - \nabla F_j(\bar{\mathbf{w}}(\tau_s^L \tau_s^G k' - 1)) \right\|^2 \right] \end{aligned}$$

$$\begin{aligned}
& + 24\eta_2^2 \frac{1}{U(s)} \sum_{u \in \mathcal{U}(s)} \sum_{j \in \mathcal{W}_u} \frac{\Delta_j(k' \tau_s^G)}{\Delta_u(k' \tau_s^G)} \mathbb{E} \left[ \left\| \nabla F_j(\bar{\mathbf{w}}(\tau_s^L \tau_s^G k' - 1)) - \nabla F_j(\bar{\mathbf{w}}_u(\tau_s^L \tau_s^G k' - 1)) \right\|^2 \right] \\
& + 24\eta_2^2 \frac{1}{U(s)} \sum_{u \in \mathcal{U}(s)} \mathbb{E} [\| \nabla \bar{F}(\bar{\mathbf{w}}(\tau_s^L \tau_s^G k' - 1)) - \nabla \bar{F}_u(\bar{\mathbf{w}}(\tau_s^L \tau_s^G k' - 1)) \|^2] \\
& \stackrel{(d)}{\leq} 24\eta_2^2 \mu_F^2 \frac{1}{U(s)} \sum_{u \in \mathcal{U}(s)} \frac{1}{U(s)} \sum_{\hat{u} \in \mathcal{U}(s)} \sum_{j \in \mathcal{W}_{\hat{u}}} \frac{\Delta_j(k' \tau_s^G)}{\Delta_{\hat{u}}(k' \tau_s^G)} \mathbb{E} [\| \bar{\mathbf{w}}_{\hat{u}}(\tau_s^L \tau_s^G k' - 1) - \bar{\mathbf{w}}(\tau_s^L \tau_s^G k' - 1) \|^2] \\
& + 24\eta_2^2 \mu_F^2 \frac{1}{U(s)} \sum_{u \in \mathcal{U}(s)} \sum_{j \in \mathcal{W}_u} \frac{\Delta_j(k' \tau_s^G)}{\Delta_u(k' \tau_s^G)} \mathbb{E} [\| \bar{\mathbf{w}}(\tau_s^L \tau_s^G k' - 1) - \bar{\mathbf{w}}_u(\tau_s^L \tau_s^G k' - 1) \|^2] \\
& + 24\eta_2^2 \frac{1}{U(s)} \sum_{u \in \mathcal{U}(s)} \mathbb{E} [\| \nabla \bar{F}(\bar{\mathbf{w}}(\tau_s^L \tau_s^G k' - 1)) - \nabla \bar{F}_u(\bar{\mathbf{w}}(\tau_s^L \tau_s^G k' - 1)) \|^2] \\
& \stackrel{(e)}{\leq} 48\eta_2^2 \mu_F^2 \frac{1}{U(s)} \sum_{u \in \mathcal{U}(s)} \mathbb{E} [\| \bar{\mathbf{w}}_{\hat{u}}(\tau_s^L \tau_s^G k' - 1) - \bar{\mathbf{w}}(\tau_s^L \tau_s^G k' - 1) \|^2] + 24\eta_2^2 \gamma_F^2, \tag{72}
\end{aligned}$$

where (a) introduces  $\nabla \bar{F}_{\hat{u}}(\mathbf{w})$  and  $\nabla \bar{F}_u(\mathbf{w})$  terms, (b) uses the Cauchy-Schwarz followed by the swarm-wide meta-gradient definition from (6), (c) applies Jensen's inequality to the expectations, (d) recalls the  $\mu_F$ -smoothness property of  $\nabla F_j$ , and (e) uses the result of Lemma 2. Combining (71) and (72) yields:

$$\begin{aligned}
& 2 \frac{1}{U(s)} \sum_{u \in \mathcal{U}(s)} \mathbb{E} [\| \bar{\mathbf{w}}_u(\tau_s^L \tau_s^G k') - \bar{\mathbf{w}}(\tau_s^L \tau_s^G k') \|^2] \\
& \stackrel{(a)}{\leq} 8 \frac{1}{U(s)} \sum_{u \in \mathcal{U}(s)} \mathbb{E} \left[ \left\| \bar{\mathbf{w}}_u(\tau_s^L \tau_s^G k' - 1) - \frac{1}{U(s)} \sum_{\hat{u} \in \mathcal{U}(s)} \bar{\mathbf{w}}_{\hat{u}}(\tau_s^L \tau_s^G k' - 1) \right\|^2 \right] \\
& + 8\eta_2^2 \frac{1}{U(s)} \sum_{u \in \mathcal{U}(s)} \mathbb{E} [\| \nabla \bar{F}_u(\bar{\mathbf{w}}_u(\tau_s^L \tau_s^G k' - 1)) - \nabla \tilde{\bar{F}}_u(\bar{\mathbf{w}}_u(\tau_s^L \tau_s^G k' - 1)) \|^2] \\
& + 8\eta_2^2 \frac{1}{U(s)} \sum_{u \in \mathcal{U}(s)} \mathbb{E} \left[ \left\| \frac{1}{U(s)} \sum_{\hat{u} \in \mathcal{U}(s)} \left( \nabla \tilde{\bar{F}}_{\hat{u}}(\bar{\mathbf{w}}_{\hat{u}}(\tau_s^L \tau_s^G k' - 1)) - \nabla \bar{F}_{\hat{u}}(\bar{\mathbf{w}}_{\hat{u}}(\tau_s^L \tau_s^G k' - 1)) \right) \right\|^2 \right] \\
& + 48\eta_2^2 \mu_F^2 \frac{1}{U(s)} \sum_{u \in \mathcal{U}(s)} \mathbb{E} [\| \bar{\mathbf{w}}_{\hat{u}}(\tau_s^L \tau_s^G k' - 1) - \bar{\mathbf{w}}(\tau_s^L \tau_s^G k' - 1) \|^2] + 24\eta_2^2 \gamma_F^2 \\
& \stackrel{(b)}{\leq} (8 + 48\eta_2^2 \mu_F^2) \frac{1}{U(s)} \sum_{u \in \mathcal{U}(s)} \mathbb{E} \left[ \left\| \bar{\mathbf{w}}_u(\tau_s^L \tau_s^G k' - 1) - \frac{1}{U(s)} \sum_{\hat{u} \in \mathcal{U}(s)} \bar{\mathbf{w}}_{\hat{u}}(\tau_s^L \tau_s^G k' - 1) \right\|^2 \right] + 24\eta_2^2 \gamma_F^2 \\
& + 8\eta_2^2 \frac{1}{U(s)} \sum_{u \in \mathcal{U}(s)} \mathbb{E} \left[ \left\| \sum_{j \in \mathcal{W}_u} \frac{\Delta_j(k' \tau_s^G)}{\Delta_u(k' \tau_s^G)} \left( \nabla F_j(\bar{\mathbf{w}}_u(\tau_s^L \tau_s^G k' - 1)) - \nabla \tilde{F}_j(\bar{\mathbf{w}}_u(\tau_s^L \tau_s^G k' - 1)) \right) \right\|^2 \right] \\
& + 8\eta_2^2 \frac{1}{U(s)} \sum_{u \in \mathcal{U}(s)} \mathbb{E} \left[ \left\| \frac{1}{U(s)} \sum_{\hat{u} \in \mathcal{U}(s)} \sum_{j \in \mathcal{W}_u} \frac{\Delta_j(k' \tau_s^G)}{\Delta_u(k' \tau_s^G)} \left( \nabla \tilde{F}_j(\bar{\mathbf{w}}_{\hat{u}}(\tau_s^L \tau_s^G k' - 1)) - \nabla F_j(\bar{\mathbf{w}}_{\hat{u}}(\tau_s^L \tau_s^G k' - 1)) \right) \right\|^2 \right] \\
& \stackrel{(c)}{\leq} (8 + 48\eta_2^2 \mu_F^2) \frac{1}{U(s)} \sum_{u \in \mathcal{U}(s)} \mathbb{E} [\| \bar{\mathbf{w}}_u(\tau_s^L \tau_s^G k' - 1) - \bar{\mathbf{w}}(\tau_s^L \tau_s^G k' - 1) \|^2] + 24\eta_2^2 \gamma_F^2 \\
& + 16\eta_2^2 \frac{1}{U(s)} \sum_{u \in \mathcal{U}(s)} \sum_{j \in \mathcal{W}_u} \frac{\Delta_j(k' \tau_s^G)}{\Delta_u(k' \tau_s^G)} (\sigma_F^j(\tau_s^L \tau_s^G k' - 1))^2, \tag{73}
\end{aligned}$$

where (a) combines (71) and (72), (b) applies definition of  $\nabla \bar{F}_u$  from (6), (c) uses Jensen's inequality followed by Lemma 1 and the definition of  $\bar{\mathbf{w}}$  from (7). Solving (73) recursively yields:

$$2 \frac{1}{U(s)} \sum_{u \in \mathcal{U}(s)} \mathbb{E} [\| \bar{\mathbf{w}}_u(\tau_s^L \tau_s^G k') - \bar{\mathbf{w}}(\tau_s^L \tau_s^G k') \|^2] \tag{74}$$

$$\stackrel{(a)}{\leq} 16\eta_2^2 \frac{1}{U(s)} \sum_{u \in \mathcal{U}(s)} \sum_{j \in \mathcal{W}_u} \frac{\Delta_j(k' \tau_s^G)}{\Delta_u(k' \tau_s^G)} \left( \sum_{y=0}^{\tau_s^L \tau_s^G - 1} (\sigma_F^j(\tau_s^L \tau_s^G k' - 1 - y))^2 (8 + 48\eta_2^2 \mu_F^2)^y \right) + 24\eta_2^2 \gamma_F^2 \frac{1 - (8 + 48\eta_2^2 \mu_F^2)^{\tau_s^L \tau_s^G}}{1 - (8 + 48\eta_2^2 \mu_F^2)} \tag{75}$$

$$\stackrel{(b)}{\leq} \left( 16\eta_2^2 \frac{1}{U(s)} \sum_{u \in \mathcal{U}(s)} \sum_{j \in \mathcal{W}_u} \frac{\Delta_j(k' \tau_s^G)}{\bar{\Delta}_u(k' \tau_s^G)} \sum_{y=0}^{\tau_s^L \tau_s^G - 1} (\sigma_j^F(\tau_s^L \tau_s^G k' - 1 - y))^2 + 24\eta_2^2 \gamma_F^2 \right) \frac{1 - (8 + 48\eta_2^2 \mu_F^2)^{\tau_s^L \tau_s^G}}{1 - (8 + 48\eta_2^2 \mu_F^2)}, \quad (76)$$

where (a) is the result of recursion and the finite sum of geometric series, and (b) uses  $\sum_i a_i b_i \leq \sum_i a_i \sum_i b_i \forall a_i, b_i \geq 0$ . Combining the results of (68) and (74) in (64) yields:

$$\begin{aligned} & 2 \frac{1}{U(s)} \sum_{u \in \mathcal{U}(s)} \sum_{j \in \mathcal{W}_u} \frac{\Delta_j(k' \tau_s^G)}{\bar{\Delta}_u(k' \tau_s^G)} \left( \mathbb{E}[\|\mathbf{w}_j(\tau_s^L \tau_s^G k') - \bar{\mathbf{w}}_u(\tau_s^L \tau_s^G k')\|^2] + \mathbb{E}[\|\bar{\mathbf{w}}_u(\tau_s^L \tau_s^G k') - \bar{\mathbf{w}}(\tau_s^L \tau_s^G k')\|^2] \right) \\ & \leq \left( 16\eta_2^2 \frac{1}{U(s)} \sum_{u \in \mathcal{U}(s)} \sum_{j \in \mathcal{W}_u} \frac{\Delta_j(k' \tau_s^G)}{\bar{\Delta}_u(k' \tau_s^G)} \sum_{y=1}^{\tau_s^L} (\sigma_j^F(\tau_s^L \tau_s^G k' - y))^2 + 24\eta_2^2 \frac{1}{U(s)} \sum_{u \in \mathcal{U}(s)} (\gamma_F^u)^2 \right) \frac{1 - (8 + 48\eta_2^2 \mu_F^2)^{\tau_s^L}}{1 - (8 + 48\eta_2^2 \mu_F^2)} \\ & \quad + \left( 16\eta_2^2 \frac{1}{U(s)} \sum_{u \in \mathcal{U}(s)} \sum_{j \in \mathcal{W}_u} \frac{\Delta_j(k' \tau_s^G)}{\bar{\Delta}_u(k' \tau_s^G)} \sum_{y=1}^{\tau_s^L \tau_s^G} (\sigma_j^F(\tau_s^L \tau_s^G k' - y))^2 + 24\eta_2^2 \gamma_F^2 \right) \frac{1 - (8 + 48\eta_2^2 \mu_F^2)^{\tau_s^L \tau_s^G}}{1 - (8 + 48\eta_2^2 \mu_F^2)}, \end{aligned} \quad (77)$$

with the summation shifted from  $y = 0$  to  $y = 1$ . ■

APPENDIX B  
PROOF OF THEOREM 1

*Proof.* First, from Assumption 1, we see that  $F_j(t)$ ,  $F_u(t)$ , and  $F(t)$  are all  $\mu_F$ -smooth where  $\mu_F = 4\mu^G + \eta_1\mu^H B$  (result follows immediately from [33] upon using triangle inequality). In order to bound the first-order stationary point,  $\mathbb{E}[\|\nabla\bar{F}(\bar{\mathbf{w}})\|^2]$ , we start with

$$\begin{aligned}
\bar{F}(\bar{\mathbf{w}}(\tau_s^L \tau_s^G k')) &\stackrel{(a)}{\leq} \bar{F}(\bar{\mathbf{w}}(\tau_s^L \tau_s^G k' - 1)) + \nabla\bar{F}(\bar{\mathbf{w}}(\tau_s^L \tau_s^G k' - 1))^T (\bar{\mathbf{w}}(\tau_s^L \tau_s^G k') - \bar{\mathbf{w}}(\tau_s^L \tau_s^G k' - 1)) + \frac{\mu_F}{2} \|\bar{\mathbf{w}}(\tau_s^L \tau_s^G k') - \bar{\mathbf{w}}(\tau_s^L \tau_s^G k' - 1)\|^2 \\
&\stackrel{(b)}{=} \bar{F}(\bar{\mathbf{w}}(\tau_s^L \tau_s^G k' - 1)) - \eta_2 \nabla\bar{F}(\bar{\mathbf{w}}(\tau_s^L \tau_s^G k' - 1))^T \left( \frac{1}{U(s)} \sum_{u \in \mathcal{U}(s)} \sum_{j \in \mathcal{W}_u} \frac{\Delta_j(k' \tau_s^G)}{\Delta_u(k' \tau_s^G)} \nabla\tilde{F}_j(\mathbf{w}_j(\tau_s^L \tau_s^G k' - 1)) \right) \\
&\quad + \frac{\mu_F}{2} \left\| -\eta_2 \frac{1}{U(s)} \sum_{u \in \mathcal{U}(s)} \sum_{j \in \mathcal{W}_u} \frac{\Delta_j(k' \tau_s^G)}{\Delta_u(k' \tau_s^G)} \nabla\tilde{F}_j(\mathbf{w}_j(\tau_s^L \tau_s^G k' - 1)) \right\|^2 \\
&\stackrel{(c)}{=} \bar{F}(\bar{\mathbf{w}}(\tau_s^L \tau_s^G k' - 1)) - \eta_2 \nabla\bar{F}(\bar{\mathbf{w}}(\tau_s^L \tau_s^G k' - 1))^T \left( \frac{1}{U(s)} \sum_{u \in \mathcal{U}(s)} \sum_{j \in \mathcal{W}_u} \frac{\Delta_j(k' \tau_s^G)}{\Delta_u(k' \tau_s^G)} \nabla\tilde{F}_j(\mathbf{w}_j(\tau_s^L \tau_s^G k' - 1)) \right) \\
&\quad + \eta_2^2 \frac{\mu_F}{2} \left\| \frac{1}{U(s)} \sum_{u \in \mathcal{U}(s)} \sum_{j \in \mathcal{W}_u} \frac{\Delta_j(k' \tau_s^G)}{\Delta_u(k' \tau_s^G)} \nabla\tilde{F}_j(\mathbf{w}_j(\tau_s^L \tau_s^G k' - 1)) \right\|^2,
\end{aligned} \tag{78}$$

where (a) follows from the  $\mu_F$ -smoothness property of  $F$ ,  $F_u$ , and  $F_j$ , (b) uses the meta-gradient update procedure from (1) and the definition of  $\bar{\mathbf{w}}$  from (7), and (c) simplifies the algebra. Taking the expectation of both sides of (78) yields:

$$\begin{aligned}
&\mathbb{E}[\bar{F}(\bar{\mathbf{w}}(\tau_s^L \tau_s^G k'))] - \mathbb{E}[\bar{F}(\bar{\mathbf{w}}(\tau_s^L \tau_s^G k' - 1))] \leq \\
&\quad \underbrace{-\eta_2 \mathbb{E} \left[ \nabla\bar{F}(\bar{\mathbf{w}}(\tau_s^L \tau_s^G k' - 1))^T \left( \frac{1}{U(s)} \sum_{u \in \mathcal{U}(s)} \sum_{j \in \mathcal{W}_u} \frac{\Delta_j(k' \tau_s^G)}{\Delta_u(k' \tau_s^G)} \nabla\tilde{F}_j(\mathbf{w}_j(\tau_s^L \tau_s^G k' - 1)) \right) \right]}_{(i)} \\
&\quad + \underbrace{\eta_2^2 \frac{\mu_F}{2} \mathbb{E} \left[ \left\| \frac{1}{U(s)} \sum_{u \in \mathcal{U}(s)} \sum_{j \in \mathcal{W}_u} \frac{\Delta_j(k' \tau_s^G)}{\Delta_u(k' \tau_s^G)} \nabla\tilde{F}_j(\mathbf{w}_j(\tau_s^L \tau_s^G k' - 1)) \right\|^2 \right]}_{(ii)}.
\end{aligned} \tag{79}$$

Before we bound (79)(i) and (79)(ii), we first analyze

$$\begin{aligned}
&\frac{1}{U(s)} \sum_{u \in \mathcal{U}(s)} \sum_{j \in \mathcal{W}_u} \frac{\Delta_j(k' \tau_s^G)}{\Delta_u(k' \tau_s^G)} \nabla\tilde{F}_j(\mathbf{w}_j(\tau_s^L \tau_s^G k' - 1)) \\
&= X + Y + \frac{1}{U(s)} \sum_{u \in \mathcal{U}(s)} \sum_{j \in \mathcal{W}_u} \frac{\Delta_j(k' \tau_s^G)}{\Delta_u(k' \tau_s^G)} \nabla F_j(\bar{\mathbf{w}}(\tau_s^L \tau_s^G k' - 1)),
\end{aligned} \tag{80}$$

where:

$$\begin{aligned}
X &\triangleq \frac{1}{U(s)} \sum_{u \in \mathcal{U}(s)} \sum_{j \in \mathcal{W}_u} \frac{\Delta_j(k' \tau_s^G)}{\Delta_u(k' \tau_s^G)} \left[ \nabla\tilde{F}_j(\mathbf{w}_j(\tau_s^L \tau_s^G k' - 1)) - \nabla F_j(\mathbf{w}_j(\tau_s^L \tau_s^G k' - 1)) \right] \\
Y &\triangleq \frac{1}{U(s)} \sum_{u \in \mathcal{U}(s)} \sum_{j \in \mathcal{W}_u} \frac{\Delta_j(k' \tau_s^G)}{\Delta_u(k' \tau_s^G)} \left[ \nabla F_j(\mathbf{w}_j(\tau_s^L \tau_s^G k' - 1)) - \nabla F_j(\bar{\mathbf{w}}(\tau_s^L \tau_s^G k' - 1)) \right].
\end{aligned} \tag{81}$$

We now bound  $\|X\|^2$  as follows:

$$\begin{aligned}
\mathbb{E}[\|X\|^2] &= \mathbb{E} \left[ \left\| \frac{1}{U(s)} \sum_{u \in \mathcal{U}(s)} \sum_{j \in \mathcal{W}_u} \frac{\Delta_j(k' \tau_s^G)}{\Delta_u(k' \tau_s^G)} \left( \nabla\tilde{F}_j(\mathbf{w}_j(\tau_s^L \tau_s^G k' - 1)) - \nabla F_j(\mathbf{w}_j(\tau_s^L \tau_s^G k' - 1)) \right) \right\|^2 \right] \\
&\stackrel{(a)}{\leq} \frac{1}{U(s)} \sum_{u \in \mathcal{U}(s)} \sum_{j \in \mathcal{W}_u} \frac{\Delta_j(k' \tau_s^G)}{\Delta_u(k' \tau_s^G)} \mathbb{E}[\|\nabla\tilde{F}_j(\mathbf{w}_j(\tau_s^L \tau_s^G k' - 1)) - \nabla F_j(\mathbf{w}_j(\tau_s^L \tau_s^G k' - 1))\|^2] \\
&\stackrel{(b)}{\leq} \frac{1}{U(s)} \sum_{u \in \mathcal{U}(s)} \sum_{j \in \mathcal{W}_u} \frac{\Delta_j(k' \tau_s^G)}{\Delta_u(k' \tau_s^G)} (\sigma_j^F(\tau_s^L \tau_s^G k' - 1))^2,
\end{aligned} \tag{82}$$

using (a) Jensen's inequality, and (b) Lemma 1. Next, we bound  $\|Y\|^2$  as follows:

$$\begin{aligned} \mathbb{E}[\|Y\|^2] &= \mathbb{E}\left[\left\|\frac{1}{U(s)} \sum_{u \in \mathcal{U}(s)} \sum_{j \in \mathcal{W}_u} \frac{\Delta_j(k' \tau_s^G)}{\Delta_u(k' \tau_s^G)} \left( \nabla F_j(\mathbf{w}_j(\tau_s^L \tau_s^G k' - 1)) - \nabla F_j(\bar{\mathbf{w}}(\tau_s^L \tau_s^G k' - 1)) \right)\right\|^2\right] \\ &\stackrel{(a)}{\leq} \mu_F^2 \mathbb{E}\left[\left\|\frac{1}{U(s)} \sum_{u \in \mathcal{U}(s)} \sum_{j \in \mathcal{W}_u} \frac{\Delta_j(k' \tau_s^G)}{\Delta_u(k' \tau_s^G)} \left( \mathbf{w}_j(\tau_s^L \tau_s^G k' - 1) - \bar{\mathbf{w}}(\tau_s^L \tau_s^G k' - 1) \right)\right\|^2\right] \\ &\stackrel{(b)}{\leq} \mu_F^2 \Upsilon(k' \tau_s^L \tau_s^G), \end{aligned} \quad (83)$$

where (a) uses  $\mu_F$ -Lipschitz gradient property of  $F_j$ , and (b) follows from Proposition 1, note that the recursion step which bounds  $\mathbf{w}_j(t) - \bar{\mathbf{w}}(t)$  in Proposition 1 also bounds  $\mathbf{w}_j(t-1) - \bar{\mathbf{w}}(t-1)$ . Using these results, we first analyze (79)(i) as follows:

$$\begin{aligned} & -\eta_2 \mathbb{E}\left[\nabla \bar{F}(\bar{\mathbf{w}}(\tau_s^L \tau_s^G k' - 1))^T \left( \frac{1}{U(s)} \sum_{u \in \mathcal{U}(s)} \sum_{j \in \mathcal{W}_u} \frac{\Delta_j(k' \tau_s^G)}{\Delta_u(k' \tau_s^G)} \nabla \tilde{F}_j(\mathbf{w}_j(\tau_s^L \tau_s^G k' - 1)) \right)\right] \\ &\stackrel{(a)}{=} -\eta_2 \mathbb{E}\left[\nabla \bar{F}(\bar{\mathbf{w}}(\tau_s^L \tau_s^G k' - 1))^T \left( X + Y + \frac{1}{U(s)} \sum_{u \in \mathcal{U}(s)} \sum_{j \in \mathcal{W}_u} \frac{\Delta_j(k' \tau_s^G)}{\Delta_u(k' \tau_s^G)} \nabla F_j(\bar{\mathbf{w}}(\tau_s^L \tau_s^G k' - 1)) \right)\right] \\ &\stackrel{(b)}{=} -\eta_2 \mathbb{E}\left[\nabla \bar{F}(\bar{\mathbf{w}}(\tau_s^L \tau_s^G k' - 1))^T \left( X + Y + \nabla \bar{F}(\bar{\mathbf{w}}(\tau_s^L \tau_s^G k' - 1)) \right)\right] \\ &\stackrel{(c)}{=} -\eta_2 \left( \mathbb{E}[\nabla \bar{F}(\bar{\mathbf{w}}(\tau_s^L \tau_s^G k' - 1))^T (X + Y)] + \mathbb{E}[\|\nabla \bar{F}(\bar{\mathbf{w}}(\tau_s^L \tau_s^G k' - 1))\|^2] \right) \\ &\stackrel{(d)}{\leq} \frac{-\eta_2}{2} \mathbb{E}[\|\nabla \bar{F}(\bar{\mathbf{w}}(\tau_s^L \tau_s^G k' - 1))\|^2] + \eta_2 \left( \mathbb{E}[\|X\|^2] + \mathbb{E}[\|Y\|^2] \right) \\ &\stackrel{(e)}{\leq} \frac{-\eta_2}{2} \mathbb{E}[\|\nabla \bar{F}(\bar{\mathbf{w}}(\tau_s^L \tau_s^G k' - 1))\|^2] + \eta_2 \left( \frac{1}{U(s)} \sum_{u \in \mathcal{U}(s)} \sum_{j \in \mathcal{W}_u} \frac{\Delta_j(k' \tau_s^G)}{\Delta_u(k' \tau_s^G)} (\sigma_j^F(\tau_s^L \tau_s^G k' - 1))^2 + \mu_F^2 \Upsilon(k', \tau_s^L, \tau_s^G) \right), \end{aligned} \quad (84)$$

where (a) comes from introducing  $\nabla F_j(\mathbf{w}_j)$  and  $\nabla F_j(\bar{\mathbf{w}})$  terms, (b) is the definition of  $\nabla \bar{F}$ , (c) follows from linearity of expectation, (d) is due to

$$\begin{aligned} & -\eta_2 \mathbb{E}[\nabla \bar{F}(\bar{\mathbf{w}}(\tau_s^L \tau_s^G k' - 1))^T (X + Y)] \leq \frac{1}{2} \eta_2 \mathbb{E}[\|\nabla \bar{F}(\bar{\mathbf{w}}(\tau_s^L \tau_s^G k' - 1))\|^2] + \frac{1}{2} \mathbb{E}[\|X + Y\|^2] \\ &\leq \frac{1}{2} \eta_2 \mathbb{E}[\|\nabla \bar{F}(\bar{\mathbf{w}}(\tau_s^L \tau_s^G k' - 1))\|^2] + \eta_2 \mathbb{E}[\|X\|^2] + \eta_2 \mathbb{E}[\|Y\|^2] \end{aligned} \quad (85)$$

(i.e.,  $(A + B)^2 \geq 0$  and Cauchy-Schwarz), and (e) applies the results of (82) and (83). Next, we analyze (79)(ii) as follows:

$$\begin{aligned} & \mathbb{E}\left[\left\|\frac{1}{U(s)} \sum_{u \in \mathcal{U}(s)} \sum_{j \in \mathcal{W}_u} \frac{\Delta_j(k' \tau_s^G)}{\Delta_u(k' \tau_s^G)} \nabla \tilde{F}_j(\mathbf{w}_j(\tau_s^L \tau_s^G k' - 1))\right\|^2\right] \\ &\stackrel{(a)}{\leq} \mathbb{E}\left[\left\|X + Y + \frac{1}{U(s)} \sum_{u \in \mathcal{U}(s)} \sum_{j \in \mathcal{W}_u} \frac{\Delta_j(k' \tau_s^G)}{\Delta_u(k' \tau_s^G)} \nabla F_j(\bar{\mathbf{w}}(\tau_s^L \tau_s^G k' - 1))\right\|^2\right] \\ &\stackrel{(b)}{\leq} 3\mathbb{E}[\|X\|^2] + 3\mathbb{E}[\|Y\|^2] + 3\mathbb{E}\left[\left\|\frac{1}{U(s)} \sum_{u \in \mathcal{U}(s)} \sum_{j \in \mathcal{W}_u} \frac{\Delta_j(k' \tau_s^G)}{\Delta_u(k' \tau_s^G)} \nabla F_j(\bar{\mathbf{w}}(\tau_s^L \tau_s^G k' - 1))\right\|^2\right] \\ &\stackrel{(c)}{\leq} 3 \frac{1}{U(s)} \sum_{u \in \mathcal{U}(s)} \sum_{j \in \mathcal{W}_u} \frac{\Delta_j(k' \tau_s^G)}{\Delta_u(k' \tau_s^G)} (\sigma_j^F(\tau_s^L \tau_s^G k' - 1))^2 + 3\mu_F^2 \Upsilon(k' \tau_s^L \tau_s^G) \\ &+ 3\mathbb{E}\left[\left\|\frac{1}{U(s)} \sum_{u \in \mathcal{U}(s)} \sum_{j \in \mathcal{W}_u} \frac{\Delta_j(k' \tau_s^G)}{\Delta_u(k' \tau_s^G)} \nabla F_j(\bar{\mathbf{w}}(\tau_s^L \tau_s^G k' - 1))\right\|^2\right] \\ &\stackrel{(d)}{\leq} 3 \frac{1}{U(s)} \sum_{u \in \mathcal{U}(s)} \sum_{j \in \mathcal{W}_u} \frac{\Delta_j(k' \tau_s^G)}{\Delta_u(k' \tau_s^G)} (\sigma_j^F(\tau_s^L \tau_s^G k' - 1))^2 + 3\mu_F^2 \Upsilon(k' \tau_s^L \tau_s^G) \\ &+ 3\mathbb{E}\left[\left\|\frac{1}{U(s)} \sum_{u \in \mathcal{U}(s)} \sum_{j \in \mathcal{W}_u} \frac{\Delta_j(k' \tau_s^G)}{\Delta_u(k' \tau_s^G)} \left( \nabla F_j(\bar{\mathbf{w}}(\tau_s^L \tau_s^G k' - 1)) - \nabla \bar{F}(\bar{\mathbf{w}}(\tau_s^L \tau_s^G k' - 1)) + \nabla \bar{F}(\bar{\mathbf{w}}(\tau_s^L \tau_s^G k' - 1)) \right)\right\|^2\right] \\ &\stackrel{(e)}{\leq} 3 \frac{1}{U(s)} \sum_{u \in \mathcal{U}(s)} \sum_{j \in \mathcal{W}_u} \frac{\Delta_j(k' \tau_s^G)}{\Delta_u(k' \tau_s^G)} (\sigma_j^F(\tau_s^L \tau_s^G k' - 1))^2 + 3\mu_F^2 \Upsilon(k' \tau_s^L \tau_s^G) \end{aligned} \quad (86)$$

$$\begin{aligned}
& + 6\mathbb{E} \left[ \left\| \frac{1}{U(s)} \sum_{u \in \mathcal{U}(s)} \left( \sum_{j \in \mathcal{W}_u} \frac{\Delta_j(k' \tau_s^G)}{\Delta_u(k' \tau_s^G)} \nabla F_j(\bar{\mathbf{w}}(\tau_s^L \tau_s^G k' - 1)) - \nabla F_u(\bar{\mathbf{w}}(\tau_s^L \tau_s^G k' - 1)) \right) \right\|^2 \right] + 6\mathbb{E} \left[ \left\| \nabla \bar{F}(\bar{\mathbf{w}}(\tau_s^L \tau_s^G k' - 1)) \right\|^2 \right] \\
& \stackrel{(f)}{\leq} 6\mathbb{E} \left[ \left\| \nabla \bar{F}(\bar{\mathbf{w}}(\tau_s^L \tau_s^G k' - 1)) \right\|^2 \right] + 3 \frac{1}{U(s)} \sum_{u \in \mathcal{U}(s)} \sum_{j \in \mathcal{W}_u} \frac{\Delta_j(k' \tau_s^G)}{\Delta_u(k' \tau_s^G)} (\sigma_j^F(\tau_s^L \tau_s^G k' - 1))^2 + 3\mu_F^2 \Upsilon(k' \tau_s^L \tau_s^G) + 6 \frac{1}{U(s)} \sum_{u \in \mathcal{U}(s)} (\gamma_F^u)^2,
\end{aligned}$$

where, we (a) substitute the result from (80), (b) apply  $(\sum_i^n a_i)^2 \leq n(\sum_i a_i^2)$ , (c) combine the results of (82) and (83), (d) introduce the global gradient  $\nabla \bar{F}$ , (e) recall that  $\nabla \bar{F} = \frac{1}{U(s)} \sum_{u \in \mathcal{U}(s)} \nabla \bar{F}_u$  and use  $(\sum_i^n a_i)^2 \leq n(\sum_i a_i^2)$ , and (f) apply Jensen's inequality and Lemma 2. Combining the results of (84) and (86) in (79) yields:

$$\begin{aligned}
& \mathbb{E}[\bar{F}(\bar{\mathbf{w}}(\tau_s^L \tau_s^G k'))] - \mathbb{E}[\bar{F}(\bar{\mathbf{w}}(\tau_s^L \tau_s^G k' - 1))] \\
& \leq -\frac{\eta_2}{2} \mathbb{E} \left[ \left\| \nabla \bar{F}(\bar{\mathbf{w}}(\tau_s^L \tau_s^G k' - 1)) \right\|^2 \right] + \eta_2 \left( \frac{1}{U(s)} \sum_{u \in \mathcal{U}(s)} \sum_{j \in \mathcal{W}_u} \frac{\Delta_j(k' \tau_s^G)}{\Delta_u(k' \tau_s^G)} (\sigma_j^F(\tau_s^L \tau_s^G k' - 1))^2 + \mu_F^2 \Upsilon(k' \tau_s^L \tau_s^G) \right) \\
& + \eta_2^2 \frac{\mu_F}{2} \left( 6\mathbb{E} \left[ \left\| \nabla \bar{F}(\bar{\mathbf{w}}(\tau_s^L \tau_s^G k' - 1)) \right\|^2 \right] + 3 \frac{1}{U(s)} \sum_{u \in \mathcal{U}(s)} \sum_{j \in \mathcal{W}_u} \frac{\Delta_j(k' \tau_s^G)}{\Delta_u(k' \tau_s^G)} (\sigma_j^F(\tau_s^L \tau_s^G k' - 1))^2 + 3\mu_F^2 \Upsilon(k' \tau_s^L \tau_s^G) + 6 \frac{1}{U(s)} \sum_{u \in \mathcal{U}(s)} (\gamma_F^u)^2 \right). \tag{87}
\end{aligned}$$

With some algebra, we obtain:

$$\begin{aligned}
& \mathbb{E}[\bar{F}(\bar{\mathbf{w}}(\tau_s^L \tau_s^G k'))] - \mathbb{E}[\bar{F}(\bar{\mathbf{w}}(\tau_s^L \tau_s^G k' - 1))] \leq (6\eta_2^2 \frac{\mu_F}{2} - \frac{\eta_2}{2}) \mathbb{E} \left[ \left\| \nabla \bar{F}(\bar{\mathbf{w}}(\tau_s^L \tau_s^G k' - 1)) \right\|^2 \right] \\
& + (3\eta_2^2 \frac{\mu_F}{2} + \eta_2) \left( \frac{1}{U(s)} \sum_{u \in \mathcal{U}(s)} \sum_{j \in \mathcal{W}_u} \frac{\Delta_j(k' \tau_s^G)}{\Delta_u(k' \tau_s^G)} (\sigma_j^F(\tau_s^L \tau_s^G k' - 1))^2 + \mu_F^2 \Upsilon(k' \tau_s^L \tau_s^G) \right) + 3\eta_2^2 \mu_F \frac{1}{U(s)} \sum_{u \in \mathcal{U}(s)} (\gamma_F^u)^2. \tag{88}
\end{aligned}$$

Since our goal from the beginning was to find an upper bound for the first-order stationary point,  $\mathbb{E} \left[ \left\| \nabla \bar{F}(\bar{\mathbf{w}}(t)) \right\|^2 \right]$ , we now take the average of (88) over all time  $t$ , which yields:

$$\begin{aligned}
& \frac{1}{\tau_s^L \tau_s^G K_s^G} \sum_{k'=1}^{K_s^G} \sum_{k=(k'-1)\tau_s^G+1}^{\tau_s^G k'} \sum_{t=(k-1)\tau_s^L+1}^{\tau_s^L k} \mathbb{E}[\bar{F}(\bar{\mathbf{w}}(t))] - \mathbb{E}[\bar{F}(\bar{\mathbf{w}}(t-1))] = \frac{1}{\tau_s^L \tau_s^G K_s^G} (\mathbb{E}[\bar{F}(\bar{\mathbf{w}}(\tau_s^L \tau_s^G K_s^G))] - \mathbb{E}[\bar{F}(\bar{\mathbf{w}}(0))]) \\
& \leq \frac{1}{\tau_s^L \tau_s^G K_s^G} \sum_{k'=1}^{K_s^G} \sum_{k=(k'-1)\tau_s^G+1}^{\tau_s^G k'} \sum_{t=(k-1)\tau_s^L+1}^{\tau_s^L k} \left[ (6\eta_2^2 \frac{\mu_F}{2} - \frac{\eta_2}{2}) \mathbb{E} \left[ \left\| \nabla \bar{F}(\bar{\mathbf{w}}(t-1)) \right\|^2 \right] \right. \\
& \left. + (3\eta_2^2 \frac{\mu_F}{2} + \eta_2) \left( \frac{1}{U(s)} \sum_{u \in \mathcal{U}(s)} \sum_{j \in \mathcal{W}_u} \frac{\Delta_j(k' \tau_s^G)}{\Delta_u(k' \tau_s^G)} (\sigma_j^F(t-1))^2 + \mu_F^2 \Upsilon(k' \tau_s^L \tau_s^G) \right) + 3\eta_2^2 \mu_F \frac{1}{U(s)} \sum_{u \in \mathcal{U}(s)} (\gamma_F^u)^2 \right]. \tag{89}
\end{aligned}$$

We set  $\eta_2 < \frac{1}{6\mu_F}$  and obtain:

$$\begin{aligned}
& - \frac{6\eta_2^2 \frac{\mu_F}{2} - \frac{\eta_2}{2}}{\tau_s^L \tau_s^G K_s^G} \sum_{k'=1}^{K_s^G} \sum_{k=\tau_s^G(k'-1)+1}^{\tau_s^G k'} \sum_{t=\tau_s^L(k-1)+1}^{\tau_s^L k} \mathbb{E} \left[ \left\| \nabla \bar{F}(\bar{\mathbf{w}}(t-1)) \right\|^2 \right] \\
& \leq \frac{1}{\tau_s^L \tau_s^G K_s^G} \left( \mathbb{E}[\bar{F}(\bar{\mathbf{w}}(0))] - \mathbb{E}[\bar{F}(\bar{\mathbf{w}}(\tau_s^L \tau_s^G K_s^G))] + \sum_{k'=1}^{K_s^G} \sum_{k=\tau_s^G(k'-1)+1}^{\tau_s^G k'} \sum_{t=\tau_s^L(k-1)+1}^{\tau_s^L k} \right. \\
& \left. \left[ (3\eta_2^2 \frac{\mu_F}{2} + \eta_2) \left( \frac{1}{U(s)} \sum_{u \in \mathcal{U}(s)} \sum_{j \in \mathcal{W}_u} \frac{\Delta_j(k' \tau_s^G)}{\Delta_u(k' \tau_s^G)} (\sigma_j^F(t-1))^2 + \mu_F^2 \Upsilon(k', \tau_s^L, \tau_s^G) \right) + 3\eta_2^2 \mu_F \frac{1}{U(s)} \sum_{u \in \mathcal{U}(s)} (\gamma_F^u)^2 \right] \right). \tag{90}
\end{aligned}$$

Finally, noting that  $\mathbb{E}[\bar{F}(\bar{\mathbf{w}}(0))] = \bar{F}(\bar{\mathbf{w}}(0))$  and that  $-\mathbb{E}[\bar{F}(\bar{\mathbf{w}}(\tau_s^L \tau_s^G K_s^G))] \leq -F^*$ , we have the result:

$$\begin{aligned}
& \frac{1}{\tau_s^L \tau_s^G K_s^G} \sum_{k'=1}^{K_s^G} \sum_{k=(k'-1)\tau_s^G+1}^{\tau_s^G k'} \sum_{t=(k-1)\tau_s^L+1}^{\tau_s^L k} \mathbb{E} \left[ \left\| \nabla \bar{F}(\bar{\mathbf{w}}(t-1)) \right\|^2 \right] \leq \frac{1}{\eta_2 - 6\eta_2^2 \frac{\mu_F}{2}} \frac{1}{\tau_s^L \tau_s^G K_s^G} \left[ \bar{F}(\bar{\mathbf{w}}(0)) - F^* + \sum_{k'=1}^{K_s^G} \sum_{k=(k'-1)\tau_s^G+1}^{\tau_s^G k'} \right. \\
& \left. \sum_{t=(k-1)\tau_s^L+1}^{\tau_s^L k} \left[ (3\eta_2^2 \frac{\mu_F}{2} + \eta_2) \left( \frac{1}{U(s)} \sum_{u \in \mathcal{U}(s)} \sum_{j \in \mathcal{W}_u} \frac{\Delta_j(k' \tau_s^G)}{\Delta_u(k' \tau_s^G)} (\sigma_j^F(t-1))^2 + \mu_F^2 \Upsilon(k' \tau_s^L \tau_s^G) \right) + 3\eta_2^2 \mu_F \frac{1}{U(s)} \sum_{u \in \mathcal{U}(s)} (\gamma_F^u)^2 \right] \right]. \tag{91}
\end{aligned}$$

■

APPENDIX C  
AN OVERVIEW OF GEOMETRIC PROGRAMMING

A prerequisite to geometric programming (GP) is the notion of *monomials* and *posynomials*, which we provide below.

**Definition 2.** A *monomial* is a function  $f : \mathbb{R}_{++}^n \rightarrow \mathbb{R}$ :  $f(\mathbf{y}) = d y_1^{a_1} y_2^{a_2} \cdots y_n^{a_n}$ , with  $d \geq 0$ ,  $\mathbf{y} = [y_1, \cdots, y_n]$ , and  $a_j \in \mathbb{R}$ ,  $\forall j$ , where  $\mathbb{R}_{++}^n$  denotes the strictly positive quadrant of  $n$ -dimensional Euclidean space. Also, a *posynomial*  $g$  is a sum of monomials:

$$g(\mathbf{y}) = \sum_{m=1}^M d_m y_1^{\alpha_m^{(1)}} \cdots y_n^{\alpha_m^{(n)}}.$$

A standard GP is a non-convex problem formulated as minimizing a posynomial under posynomial inequality constraints and monomial equality constraints [58], [66]:

$$\begin{aligned} & \min_{\mathbf{y}} g_0(\mathbf{y}) \\ & \text{s.t.} \\ & g_i(\mathbf{y}) \leq 1, \quad i = 1, \cdots, I, \\ & f_\ell(\mathbf{y}) = 1, \quad \ell = 1, \cdots, L, \end{aligned} \tag{92}$$

where  $g_i(\mathbf{y}) = \sum_{m=1}^{M_i} d_{i,m} y_1^{a_{i,m}^{(1)}} \cdots y_n^{a_{i,m}^{(n)}}$ ,  $\forall i$ , and  $f_\ell(\mathbf{y}) = d_\ell y_1^{a_\ell^{(1)}} \cdots y_n^{a_\ell^{(n)}}$ ,  $\forall \ell$ . Since the log-sum-exp function  $f(\mathbf{y}) = \log \sum_{j=1}^n e^{y_j}$  is convex, where log denotes the natural logarithm, with logarithmic change of variables and constants  $z_i = \log(y_i)$ ,  $b_{i,k} = \log(d_{i,k})$ ,  $b_\ell = \log(d_\ell)$ , and applying the log on the objective and constrains of (92), the GP in its standard format can be transformed to the following convex programming formulation:

$$\begin{aligned} & \min_{\mathbf{z}} \log \sum_{m=1}^{M_0} e^{(\mathbf{a}_{0,m}^\top \mathbf{z} + b_{0,m})} \\ & \text{s.t.} \log \sum_{m=1}^{M_i} e^{(\mathbf{a}_{i,m}^\top \mathbf{z} + b_{i,m})} \leq 0, \quad i = 1, \cdots, I, \\ & \quad \mathbf{a}_\ell^\top \mathbf{z} + b_\ell = 0, \quad \ell = 1, \cdots, L, \end{aligned} \tag{93}$$

where  $\mathbf{z} = [z_1, \cdots, z_n]^\top$ ,  $\mathbf{a}_{i,m} = [a_{i,m}^{(1)}, \cdots, a_{i,m}^{(n)}]^\top$ ,  $\forall i, m$ , and  $\mathbf{a}_\ell = [a_\ell^{(1)}, \cdots, a_\ell^{(n)}]^\top$ ,  $\forall \ell$ .

As can be seen, in  $\mathcal{P}$ , there are multiple terms in the objective function (in the upper bound of convergence of the ML model) that are in the format of ratio between two posynomials, which are not posynomial. We thus aim to transform a ratio of two posynomials to a ratio between a posynomial (in the numerator) and a monomial (in the denominator). Given the fact that the ratio between a posynomial and a monomial is a posynomial, we then aim to transform the problem to the standard GP format. To carry out this transformation, we exploit arithmetic-geometric mean inequality which lower bounds a posynomial with a monomial.

**Lemma 5 (Arithmetic-geometric mean inequality [58]).** A posynomial  $g(\mathbf{x}) = \sum_{k=1}^K u_k(\mathbf{x})$ , where  $u_k(\mathbf{x})$  is a monomial,  $\forall k$ , can be lower-bounded via a monomial as follows:

$$g(\mathbf{x}) \geq \hat{g}(\mathbf{x}) \triangleq \prod_{k=1}^K \left( \frac{u_k(\mathbf{x})}{a_k(\mathbf{y})} \right)^{a_k(\mathbf{y})}, \tag{94}$$

where  $a_k(\mathbf{y}) = u_k(\mathbf{y})/g(\mathbf{y})$ ,  $\forall k$ , and  $\mathbf{y} > 0$  is a fixed point.

APPENDIX D  
PROOF OF PROPOSITION 2

Let us first rewrite problem  $(\mathcal{P})$  in its equivalent form as follows:

$$(\mathcal{P}) : \min_{\rho, \varrho, \alpha, g, \Omega} \Omega \quad (95)$$

$$\text{s.t.} \quad (96)$$

$$(25) - (46), \quad (97)$$

$$(1 - \theta)(a) + \theta(b) \leq \Omega, \quad \Omega \geq 0, \quad (98)$$

where  $\Omega \in \mathbb{R}^+$  is an auxiliary variable used to move the objective function into the constraints, and  $(a)$ , and  $(b)$  are those introduced in (24). The corresponding approximated problem can also be expressed as follows:

$$(\widehat{\mathcal{P}}_m) : \min_{\rho, \varrho, \alpha, g, \Omega} \Omega \quad \text{s.t.} \quad (25) - (46), \quad (1 - \theta)(\widetilde{a})_m + \theta(b) \leq \Omega, \quad \Omega \geq 0, \quad (99)$$

where  $\theta(\widetilde{a})$  follows from the procedure outlined to obtain  $\widetilde{\mathcal{P}}_m$  in the main text, i.e., applying the posynomial condensation technique. It is easy to verify that the solution of  $\widetilde{\mathcal{P}}_m$  coincides with that of  $\widehat{\mathcal{P}}_m$ . Thus to prove the proposition, it is enough to prove that solving  $\widehat{\mathcal{P}}_m$  generates a sequence of improved feasible solutions for problem  $\widehat{\mathcal{P}}_m$  that converge to a point  $x^*$  satisfying the Karush-Kuhn-Tucker (KKT) conditions of  $\mathcal{P}$ . Note that  $\widehat{\mathcal{P}}_m$  can be solved using the procedure Algorithm 1.

Following the justifications in **Observation 2** in Sec. IV-B, the constraints of  $\widehat{\mathcal{P}}_m$  are separable with respect to each individual UAV swam. Thus, the performance of the distributed algorithm proposed to solve  $\widehat{\mathcal{P}}_m$  distributedly at each UAV swarm coincides with that of the centralized one for a fixed set of estimated parameters. Under the approximations described in (48) and (51), the algorithm in fact solves an *inner approximation* of problem  $\mathcal{P}$  [60]. Hence, it is sufficient to prove the following three conditions for the sequence of generated solutions by the algorithm [60]:

- 1) *The approximations used in problem  $\widehat{\mathcal{P}}_m$  should tighten the constraints of problem  $\mathcal{P}$ :* Since the constraints (25)-(46) are common to both Problems  $(\mathcal{P})$  and  $\widehat{\mathcal{P}}_m$ , it is enough to show that  $(1 - \theta)(a) + \theta(b) \leq (1 - \theta)(\widetilde{a}) + \theta(b)$  for the approximated constraint, assuming some solution  $x[m]$  ( $x$  is the solution vector defined in Algorithm 1). Equivalently, it is sufficient to show that  $(a) \leq (\widetilde{a})$  for  $x[m]$ .

To show this, it is sufficient to show (i)  $\Xi(s) \leq \widetilde{\Xi}(s)$ , and (ii)  $\widehat{\Xi}(k) \leq \widetilde{\Xi}(k)$ ,  $\forall k$ , where  $\Xi(s), \widehat{\Xi}(k)$  are the two terms in  $(a)$  (see (24)) and  $\widetilde{\Xi}(s)$  and  $\widetilde{\Xi}(k)$  are their respective approximations obtained via (48) and (51). Condition (i) holds since  $\overline{\Delta}_u(k) \geq \widehat{\Delta}_u(k)$ , and condition (ii) also holds since  $D_j(k) \geq \widehat{D}_j(k) \forall k$ , as in equations (48) and (51).<sup>4</sup>

- 2) *Upon convergence, the value of each approximated constraint in problem  $\widehat{\mathcal{P}}_m$  should coincide with that of the corresponding original constraint in  $\mathcal{P}$ :* Since the constraints (25)-(46) are common in problems  $(\mathcal{P})$  and  $(\widehat{\mathcal{P}})$ , we need to show  $(1 - \theta)(a) + \theta(b) = (1 - \theta)(\widetilde{a}) + \theta(b)$  for the approximated constraint upon convergence. Note that when the algorithm converges we have

$$\widetilde{\delta}_{j,i,n}(k) = \widetilde{\delta}_{j,i,n}(k; m), \quad \delta_{j,h,i,n}(k) = \delta_{j,h,i,n}(k; m), \quad n \in \{1, 2, 3\}, \quad (100)$$

where  $\widetilde{\delta}_{j,i,n}(k; m)$  and  $\delta_{j,h,i,n}(k; m)$  are the approximations used in (48) (see (49) for the definition of  $\widetilde{\delta}_{j,i,n}(k)$  and  $\delta_{j,h,i,n}(k)$ ). Also, upon convergence, we have:

$$\lambda_{i,j}(k) = \lambda_{i,j}(k; m), \quad \widetilde{\lambda}_{h,i,j}(k) = \widetilde{\lambda}_{h,i,j}(k; m), \quad (101)$$

where  $\lambda_{i,j}(k; m), \widetilde{\lambda}_{h,i,j}(k; m)$  are the approximations used in (51) (see (52) for the definition of  $\lambda_{i,j}(k), \widetilde{\lambda}_{h,i,j}(k)$ ).

Considering the terms inside (a), we need to show that upon convergence (i)  $\Xi(s) = \widetilde{\Xi}(s)$ , and (ii)  $\widehat{\Xi}(k) = \widetilde{\Xi}(k)$ . To demonstrate that (i) holds, it is sufficient to show that  $\overline{\Delta}_u(k) = \widehat{\Delta}_u(k)$ , and  $D_j(k) = \widehat{D}_j(k)$ , upon convergence. In the following, we demonstrate that  $\overline{\Delta}_u(k) = \widehat{\Delta}_u(k)$  upon convergence:

$$\begin{aligned} \widehat{\Delta}_u(k) \Big|_{(100),(101)} &= \prod_{j \in \mathcal{W}_u} \left[ \prod_{i \in \mathcal{C}(u,s)} \left[ \left( \frac{\widetilde{\delta}_{i,j,1}(k; m) [\overline{\Delta}_u(k; m)]}{\widetilde{\delta}_{i,j,1}(k; m)} \right)^{\frac{\widetilde{\delta}_{i,j,1}(k; m)}{\overline{\Delta}_u(k; m)}} \right. \right. \\ &\times \left. \left( \frac{\widetilde{\delta}_{i,j,2}(k; m) [\overline{\Delta}_u(k; m)]}{\widetilde{\delta}_{i,j,2}(k; m)} \right)^{\frac{\widetilde{\delta}_{i,j,2}(k; m)}{\overline{\Delta}_u(k; m)}} \times \left. \left( \frac{\widetilde{\delta}_{i,j,3}(k; m) [\overline{\Delta}_u(k; m)]}{\widetilde{\delta}_{i,j,3}(k; m)} \right)^{\frac{\widetilde{\delta}_{i,j,3}(k; m)}{\overline{\Delta}_u(k; m)}} \right] \end{aligned}$$

<sup>4</sup>Note that we replace  $\overline{\Delta}_u(k)$  and  $D_j(k)$  with their approximated versions in (48) and (51) only when they appear in the denominator of the terms in (a). Thus lower bounding these terms result in upper bounding (a) as desired.

$$\begin{aligned}
& \times \prod_{h \in \widehat{\mathcal{W}}_u} \prod_{i \in \mathcal{C}(u,s)} \left[ \left( \frac{\delta_{j,h,i,1}(k;m) [\overline{\Delta}_u(k;m)]}{\delta_{j,h,i,1}(k;m)} \right)^{\frac{\delta_{j,h,i,1}(k;m)}{\Delta_u(k;m)}} \right. \\
& \left. \left( \frac{\delta_{j,h,i,2}(k;m) [\overline{\Delta}_u(k;m)]}{\delta_{j,h,i,2}(k;m)} \right)^{\frac{\delta_{j,h,i,2}(k;m)}{\Delta_u(k;m)}} \times \left( \frac{\delta_{j,h,i,3}(k;m) [\overline{\Delta}_u(k;m)]}{\delta_{j,h,i,3}(k;m)} \right)^{\frac{\delta_{j,h,i,3}(k;m)}{\Delta_u(k;m)}} \right] \\
& = \prod_{j \in \mathcal{W}_u} \left[ \prod_{i \in \mathcal{C}(u,s)} \left[ \left( [\overline{\Delta}_u(k;m)] \right)^{\frac{\delta_{i,j,1}(k;m)}{\Delta_u(k;m)}} \right. \right. \\
& \times \left. \left( [\overline{\Delta}_u(k;m)] \right)^{\frac{\delta_{i,j,2}(k;m)}{\Delta_u(k;m)}} \times \left. \left( [\overline{\Delta}_u(k;m)] \right)^{\frac{\delta_{i,j,3}(k;m)}{\Delta_u(k;m)}} \right] \right] \\
& \times \prod_{h \in \widehat{\mathcal{W}}_u} \prod_{i \in \mathcal{C}(u,s)} \left[ \left( [\overline{\Delta}_u(k;m)] \right)^{\frac{\delta_{j,h,i,1}(k;m)}{\Delta_u(k;m)}} \left( [\overline{\Delta}_u(k;m)] \right)^{\frac{\delta_{j,h,i,2}(k;m)}{\Delta_u(k;m)}} \right. \\
& \left. \times \left( [\overline{\Delta}_u(k;m)] \right)^{\frac{\delta_{j,h,i,3}(k;m)}{\Delta_u(k;m)}} \right] \\
& = \overline{\Delta}_u(k) \left( \frac{\sum_{j \in \mathcal{W}_u} \sum_{i \in \mathcal{C}(u,s)} \delta_{i,j,1}(k;m) + \delta_{i,j,2}(k;m) + \delta_{i,j,3}(k;m)}{\Delta_u(k;m)} \right) \\
& \times \overline{\Delta}_u(k) \left( \frac{\sum_{j \in \mathcal{W}_u} \sum_{h \in \widehat{\mathcal{W}}_u} \sum_{i \in \mathcal{C}(u,s)} \delta_{j,h,i,1}(k;m) + \delta_{j,h,i,2}(k;m) + \delta_{j,h,i,3}(k;m)}{\Delta_u(k;m)} \right) \\
& = \overline{\Delta}_u(k) \left( \frac{\overline{\Delta}_u(k;m)}{\Delta_u(k;m)} \right) = \overline{\Delta}_u(k) \Big|_{(100),(101)}.
\end{aligned} \tag{102}$$

Using a similar technique, it can be shown that  $D_j(k) = \widehat{D}_j(k)$ , upon convergence, and thus (i) holds. The proof for (ii) is similar, which is omitted for brevity.

- 3) *The KKT conditions of  $\mathcal{P}$  should be satisfied after the series of approximations converges in problem  $\widehat{\mathcal{P}}_m$ :* Since the constraints (25)-(46) are common in problems ( $\mathcal{P}$ ) and ( $\widehat{\mathcal{P}}$ ), for the approximated constraint we should have  $\nabla(1 - \theta)((a) + \theta(b)) = \nabla((1 - \theta)(\widetilde{a}) + \theta(b))$ , upon convergence ( $\nabla$  denotes the gradient sign). Note that (a) involves the product between two ratios of posynomials (as can be seen from (18), one is  $\frac{\Delta_j(k)}{\Delta_u(k)}$ , where both the numerator and denominator are posynomial with respect to the optimization variables according to (37), and the other one is  $\sigma_j^F$ , which can be written as ratio of two posynomials according to (12)), where we approximate the denominator of each ratio via a monomial in  $(\widetilde{a})$ . For compactness, let us define (a)  $\triangleq \frac{A_1(\mathbf{x})A_2(\mathbf{x})}{B_1(\mathbf{x})B_2(\mathbf{x})}$ , where  $A_1(\mathbf{x})$  and  $B_1(\mathbf{x})$  are posynomials corresponding to the numerator and denominator of  $\frac{\Delta_j(k)}{\Delta_u(k)}$  (encompassing all the coefficients) and  $A_2(\mathbf{x})$  and  $B_2(\mathbf{x})$  are posynomials corresponding to the numerator and denominator of  $\sigma_j^F$  ( $\mathbf{x}$  denotes the set of optimization variables). We provide the proof for the general case. In general, the posynomials in the denominators can be described as  $B_1(\mathbf{x}) = \sum_{k=1}^{K_1} u_k^{(1)}(\mathbf{x})$  and  $B_2(\mathbf{x}) = \sum_{k=1}^{K_2} u_k^{(2)}(\mathbf{x})$ , where  $u_k^{(1)}$ -s and  $u_k^{(2)}$ -s are monomial functions. Accordingly, we can write  $(\widetilde{a})$  as  $(\widetilde{a}) = \frac{A_1(\mathbf{x})A_2(\mathbf{x})}{\widetilde{B}_1(\mathbf{x})\widetilde{B}_2(\mathbf{x})}$ , where  $\widetilde{B}_1(\mathbf{x}) = \prod_{k=1}^{K_1} \left( \frac{u_k^{(1)}(\mathbf{x})}{a_k^{(1)}(\mathbf{y})} \right)^{\alpha_k^{(1)}(\mathbf{y})}$  and  $\widetilde{B}_2(\mathbf{x}) = \prod_{k=1}^{K_2} \left( \frac{u_k^{(2)}(\mathbf{x})}{a_k^{(2)}(\mathbf{y})} \right)^{\alpha_k^{(2)}(\mathbf{y})}$  are the monomial approximation of  $B_1(\mathbf{x})$  and  $B_2(\mathbf{x})$  obtained according to (94) (equivalent to the condensations carried out in (48) and (51)). In the following, we show that the desired result holds for partial derivative with respect to an arbitrary element  $x_i$  considering  $\mathbf{x} = [x_1, \dots, x_i, \dots, x_n]$  (note that upon convergence  $\mathbf{x} = \mathbf{y}$  in (94), which in our problem translates to the equalities in (100),(101)):

$$\begin{aligned}
& \frac{\partial \left( \frac{A_1(\mathbf{x})A_2(\mathbf{x})}{B_1(\mathbf{x})B_2(\mathbf{x})} \right)}{\partial x_i} \Big|_{\mathbf{x}=\mathbf{y}} = \frac{\frac{\partial A_1(\mathbf{x})A_2(\mathbf{x})}{\partial x_i} \widetilde{B}_1(\mathbf{y})\widetilde{B}_2(\mathbf{y}) - \frac{\partial \widetilde{B}_1(\mathbf{x})\widetilde{B}_2(\mathbf{x})}{\partial x_i} A_1(\mathbf{y})A_2(\mathbf{y})}{\left( \widetilde{B}_1(\mathbf{y})\widetilde{B}_2(\mathbf{y}) \right)^2} \Big|_{\mathbf{x}=\mathbf{y}} \\
& \frac{\partial A_1(\mathbf{x})A_2(\mathbf{x})}{\partial x_i} \Big|_{\mathbf{x}=\mathbf{y}} = \frac{\partial \prod_{k=1}^{K_1} \left( \frac{u_k^{(1)}(\mathbf{x})}{a_k^{(1)}(\mathbf{y})} \right)^{\alpha_k^{(1)}(\mathbf{y})}}{\partial x_i} \Big|_{\mathbf{x}=\mathbf{y}} = \frac{\partial \prod_{k=1}^{K_1} \left( \frac{u_k^{(1)}(\mathbf{x})}{a_k^{(1)}(\mathbf{y})} \right)^{\alpha_k^{(1)}(\mathbf{y})}}{\partial x_i} \Big|_{\mathbf{x}=\mathbf{y}} B_2(\mathbf{y})A_1(\mathbf{y})A_2(\mathbf{y}) \\
& \underline{(a)} \frac{\partial A_1(\mathbf{x})A_2(\mathbf{x})}{\partial x_i} \Big|_{\mathbf{x}=\mathbf{y}} = \frac{B_2(\mathbf{y})A_1(\mathbf{y})A_2(\mathbf{y})}{(B_1(\mathbf{y})B_2(\mathbf{y}))^2}
\end{aligned}$$

$$\begin{aligned}
& + \frac{\partial \prod_{k=1}^{K_2} \left( \frac{u_k^{(2)}(\mathbf{x})}{a_k^{(2)}(\mathbf{y})} \right)^{a_k^{(2)}(\mathbf{y})}}{\partial x_i} \Big|_{\mathbf{x}=\mathbf{y}} \frac{B_1(\mathbf{y})A_1(\mathbf{y})A_2(\mathbf{y})}{(B_1(\mathbf{y})B_2(\mathbf{y}))^2} \\
& = \frac{\frac{\partial A_1(\mathbf{x})A_2(\mathbf{x})}{\partial x_i} \Big|_{\mathbf{x}=\mathbf{y}} B_1(\mathbf{y})B_2(\mathbf{y})}{(B_1(\mathbf{y})B_2(\mathbf{y}))^2} \\
& \quad + \frac{-\sum_{n=1}^{K_1} \frac{\partial u_n^{(1)}(\mathbf{x})}{\partial x_i} \Big|_{\mathbf{x}=\mathbf{y}} \left( \frac{u_n^{(1)}(\mathbf{y})}{\alpha_n^{(1)}(\mathbf{y})} \right)^{\alpha_n^{(1)}(\mathbf{y})-1} \left( \prod_{k=1, k \neq n}^{K_1} \left( \frac{u_k^{(1)}(\mathbf{y})}{\alpha_k^{(1)}(\mathbf{y})} \right)^{\alpha_k^{(1)}(\mathbf{y})} \right) B_2(\mathbf{y})A_1(\mathbf{y})A_2(\mathbf{y})}{(B_1(\mathbf{y})B_2(\mathbf{y}))^2} \\
& \quad + \frac{-\sum_{n=1}^{K_2} \frac{\partial u_n^{(2)}(\mathbf{x})}{\partial x_i} \Big|_{\mathbf{x}=\mathbf{y}} \left( \frac{u_n^{(2)}(\mathbf{y})}{a_n^{(2)}(\mathbf{y})} \right)^{a_n^{(2)}(\mathbf{y})-1} \left( \prod_{k=1, k \neq n}^{K_2} \left( \frac{u_k^{(2)}(\mathbf{y})}{a_k^{(2)}(\mathbf{y})} \right)^{a_k^{(2)}(\mathbf{y})} \right) B_1(\mathbf{y})A_1(\mathbf{y})A_2(\mathbf{y})}{(B_1(\mathbf{y})B_2(\mathbf{y}))^2} \\
& \stackrel{(b)}{=} \frac{\frac{\partial A_1(\mathbf{y})A_2(\mathbf{y})}{\partial x_i} \Big|_{\mathbf{x}=\mathbf{y}} B_1(\mathbf{y})B_2(\mathbf{y})}{(B_1(\mathbf{y})B_2(\mathbf{y}))^2} \\
& \quad + \frac{-\sum_{n=1}^{K_1} \frac{\partial u_n^{(1)}(\mathbf{x})}{\partial x_i} \Big|_{\mathbf{x}=\mathbf{y}} B_1(\mathbf{y})^{\alpha_n^{(1)}(\mathbf{y})-1} \left( B_1(\mathbf{y})^{\sum_{k=1, k \neq n}^{K_1} \alpha_k^{(1)}(\mathbf{y})} \right) B_2(\mathbf{y})A_1(\mathbf{y})A_2(\mathbf{y})}{(B_1(\mathbf{y})B_2(\mathbf{y}))^2} \\
& \quad + \frac{-\sum_{n=1}^{K_2} \frac{\partial u_n^{(2)}(\mathbf{x})}{\partial x_i} \Big|_{\mathbf{x}=\mathbf{y}} B_2(\mathbf{y})^{a_n^{(2)}(\mathbf{y})-1} \left( B_2(\mathbf{y})^{\sum_{k=1, k \neq n}^{K_2} a_k^{(2)}(\mathbf{y})} \right) B_1(\mathbf{y})A_1(\mathbf{y})A_2(\mathbf{y})}{(B_1(\mathbf{y})B_2(\mathbf{y}))^2} \\
& \stackrel{(c)}{=} \frac{\frac{\partial A_1(\mathbf{y})A_2(\mathbf{y})}{\partial x_i} \Big|_{\mathbf{x}=\mathbf{y}} B_1(\mathbf{y})B_2(\mathbf{y})}{(B_1(\mathbf{y})B_2(\mathbf{y}))^2} \\
& \quad + \frac{-\sum_{n=1}^K \frac{\partial u_n^{(1)}(\mathbf{x})}{\partial x_i} \Big|_{\mathbf{x}=\mathbf{y}} B_2(\mathbf{y})A_1(\mathbf{y})A_2(\mathbf{y}) - \sum_{n=1}^K \frac{\partial u_n^{(2)}(\mathbf{x})}{\partial x_i} \Big|_{\mathbf{x}=\mathbf{y}} B_1(\mathbf{y})A_1(\mathbf{y})A_2(\mathbf{y})}{(B_1(\mathbf{y})B_2(\mathbf{y}))^2} \\
& = \frac{\frac{\partial A_1(\mathbf{x})A_2(\mathbf{x})}{\partial x_i} \Big|_{\mathbf{x}=\mathbf{y}} B_1(\mathbf{y})B_2(\mathbf{y}) - \frac{\partial B_1(\mathbf{x})}{\partial x_i} \Big|_{\mathbf{x}=\mathbf{y}} A_1(\mathbf{y})A_2(\mathbf{y})B_2(\mathbf{y}) - \frac{\partial B_2(\mathbf{x})}{\partial x_i} \Big|_{\mathbf{x}=\mathbf{y}} A_1(\mathbf{y})A_2(\mathbf{y})B_1(\mathbf{y})}{(B_1(\mathbf{y})B_2(\mathbf{y}))^2} \\
& = \frac{\partial \left( \frac{A_1(\mathbf{x})A_2(\mathbf{x})}{B_1(\mathbf{x})B_2(\mathbf{x})} \right)}{\partial x_i} \Big|_{\mathbf{x}=\mathbf{y}}. \tag{103}
\end{aligned}$$

In (a), we used the fact that  $B_1(\mathbf{y}) = \tilde{B}_1(\mathbf{y})$  and  $B_2(\mathbf{y}) = \tilde{B}_2(\mathbf{y})$  (this is the equality of monomial approximation with the original posynomial upon convergence that we showed in bullet point 2 above). In (b), we used the fact that (see (94))  $a_k^{(1)}(\mathbf{y}) = u_k^{(1)}(\mathbf{y})/B_1(\mathbf{y})$  and  $a_k^{(2)}(\mathbf{y}) = u_k^{(2)}(\mathbf{y})/B_2(\mathbf{y})$ ,  $\forall k$ . Also, in (c) we use the fact that  $\sum_{k=1}^{K_1} \alpha_k^{(1)}(\mathbf{y}) = 1$  and  $\sum_{k=1}^{K_2} a_k^{(2)}(\mathbf{y}) = 1$ . The proof for the rest of partial derivatives, and thus the gradient, is similar.

Verification of the three aforementioned bullet points results in the conclusion of the proof.

APPENDIX E  
PROOF OF LEMMA 4

Given the previous computed gradient for the local model at the device cluster, i.e.,  $\nabla F_c(\mathbf{w}_c(t_c^V)|\tilde{\mathcal{D}}_c(t_c^V))$ , the value of the local gradient given the outdated model  $\mathbf{w}_c(t_c^V)$  for the recent data distribution  $\tilde{\mathcal{D}}_c(t)$  at time  $t$  can be expressed as follows:

$$\begin{aligned}
\left\| \nabla F_c(\mathbf{w}_c(t_c^V)|\tilde{\mathcal{D}}_c(t)) \right\|^2 &= \left\| \nabla F_c(\mathbf{w}_c(t_c^V)|\tilde{\mathcal{D}}_c(t)) - \nabla F_c(\mathbf{w}_c(t_c^V)|\tilde{\mathcal{D}}_c(t-1)) + \nabla F_c(\mathbf{w}_c(t_c^V)|\tilde{\mathcal{D}}_c(t-1)) \right. \\
&\quad \left. - \nabla F_c(\mathbf{w}_c(t_c^V)|\tilde{\mathcal{D}}_c(t-2)) + \nabla F_c(\mathbf{w}_c(t_c^V)|\tilde{\mathcal{D}}_c(t-2)) - \dots \right. \\
&\quad \left. - \nabla F_c(\mathbf{w}_c(t_c^V)|\tilde{\mathcal{D}}_c(t_c^V)) + \nabla F_c(\mathbf{w}_c(t_c^V)|\tilde{\mathcal{D}}_c(t_c^V)) \right\|^2 \\
&\stackrel{(a)}{\leq} \left( \left\| \nabla F_c(\mathbf{w}_c(t_c^V)|\tilde{\mathcal{D}}_c(t)) - \nabla F_c(\mathbf{w}_c(t_c^V)|\tilde{\mathcal{D}}_c(t-1)) \right\| + \left\| \nabla F_c(\mathbf{w}_c(t_c^V)|\tilde{\mathcal{D}}_c(t-1)) \right. \right. \\
&\quad \left. \left. - \nabla F_c(\mathbf{w}_c(t_c^V)|\tilde{\mathcal{D}}_c(t-2)) \right\| + \left\| \nabla F_c(\mathbf{w}_c(t_c^V)|\tilde{\mathcal{D}}_c(t-2)) - \nabla F_c(\mathbf{w}_c(t_c^V)|\tilde{\mathcal{D}}_c(t-3)) \right\| + \dots + \right. \\
&\quad \left. \left\| \nabla F_c(\mathbf{w}_c(t_c^V)|\tilde{\mathcal{D}}_c(t_c^V+1)) - \nabla F_c(\mathbf{w}_c(t_c^V)|\tilde{\mathcal{D}}_c(t_c^V)) \right\| + \left\| \nabla F_c(\mathbf{w}_c(t_c^V)|\tilde{\mathcal{D}}_c(t_c^V)) \right\| \right)^2 \\
&\stackrel{(b)}{\leq} (t - t_c^V + 1) \left\| \nabla F_c(\mathbf{w}_c(t_c^V)|\tilde{\mathcal{D}}_c(t_c^V)) \right\|^2 + (t - t_c^V + 1) \sum_{t'=t_c^V+1}^t \Lambda_c(t'), \tag{104}
\end{aligned}$$

where in (a) we used triangle inequality, and (b) is the result of Cauchy–Schwarz inequality (i.e, for any  $N$  numbers  $A_1, \dots, A_N$ , we have  $(\sum_{i=1}^N A_i)^2 \leq N \sum_{i=1}^N (A_i)^2$ ).

APPENDIX F  
SIMULATION SETTINGS

**Network Characteristics and Parameters.** To calculate data rates among pairs of networked devices/UAVs, i.e., (21), (22), we use the following set of values [54]:  $N_0 = -174\text{dBm/Hz}$ ,  $\alpha^{\text{PL}} = 2$ ,  $\eta^{\text{LoS}} = 3\text{dB}$ ,  $\eta^{\text{NLoS}} = 23\text{dB}$ ,  $f = 2\text{GHz}$ ,  $\psi = 11.95$ ,  $\beta = 0.14$ ,  $B = 2\text{MHz}$ . We set the transmit power of the devices in the range  $[23, 25]\text{dBm}$  and the transmit power of UAVs to  $20\text{dBm}$ . The UAVs' altitude are also selected from  $[25, 30]\text{m}$ .

**Datasets.** We consider the MNIST (<http://yann.lecun.com/exdb/mnist/>) and Fashion-MNIST (FMNIST) datasets (<https://github.com/zalandoresearch/fashion-mnist>). Each dataset contains 70K images (60K for training, 10K for testing), where each image belongs to one of 10 labels of hand-written digits and fashion products, respectively. FMNIST can be considered as a harder classification task as compared to MNIST due to its more complex images.

**Reinforcement Learning Integration and Training.** To ensure that our reinforcement learning training is based on the results of the optimization of  $\text{HN-PFL}$ , we simulate and then store the results of various configurations of our optimization formulation  $\mathcal{P}$ . For each unique configuration (e.g.,  $T_s = 100$ ,  $\tau_s^{\text{L}} = \tau_s^{\text{G}} = 2$ ), we save the ML model performance result as the learning reward  $O(s)$ , and utilize the energy consumed to complete training to update the minimum UAV battery levels  $E_u(s)$  for a swarm. In this way, when we start training the RNN-based deep reinforcement learning agent, the agent determines the optimal swarm trajectories and temporal ML characteristics based on the results of  $\text{HN-PFL}$  and our optimization formulation  $\mathcal{P}$ .

To train the DRL agent, we use train-target DQNs with an update period of 20 epochs and an experience replay deque of size 20. As the experience replay storage is initially empty, we initialize the training by running 20 random instances to fill the experience replay deque with the swarm trajectories and temporal decisions for  $\text{HN-PFL}$  and their associated reward. Thereafter, we train/update our DQN parameters after every epoch by calculating the mean square error (i.e., the loss) between the train and target network outputs, and then use gradient descent with learning rate 0.001 to update the train DQN's parameters. After every 20 epochs of training, we re-synchronize the train and target DQNs' model parameters.

At this point, our methodology will select subsequent swarm trajectory and temporal decisions for  $\text{HN-PFL}$  based on an epsilon-greedy policy, with  $\epsilon = 0.7$ . An epsilon-greedy policy means that, with probability  $1 - \epsilon$ , the DQN is used to determine the next swarm trajectory and temporal decisions. As our  $\epsilon$  is linearly decaying with the number of training epochs, reaching a minimum of 0.005, our DQN is initially trained by biasing against random results, and, eventually when the DQN is well trained, our methodology will primarily adjust the DQN based on its own decisions.

Our swarm/UAV flight and communication characteristics used for the reinforcement learning training are the same as those used in Fig. 4- 7. For the additional reward coefficients found in (60), we use:  $C = 10^5$ ,  $c_1 = 0.2$ ,  $c_2 = 0.25$ , and  $c_3 = 0.005$ .